

**SALTWATER INTRUSION AND TRACE ELEMENT CONTAMINATIONS
AT THE COASTAL AQUIFERS OF THE GANGES DELTA**

by

Nur Ahmed

A thesis submitted to the Graduate Faculty of
Auburn University
in partial fulfillment of the
requirements for the Degree of
Master of Science

Auburn, Alabama
December 10, 2016

Keyword: Saltwater intrusion, Coastal aquifer, Ganges delta, Solute transport modeling, Trace element geochemistry, Geochemical modeling

Copyright 2016 by Nur Ahmed

Approved by

Ashraf Uddin, Chair, Professor of Geosciences
Ming-Kuo Lee, Professor of Geosciences
James A. Saunders, Professor of Geosciences

ABSTRACT

The coastal area of Bangladesh has a low topography lying at the confluence of the Ganges and Brahmaputra river systems in the Bengal Basin. The distribution of aquifer sediments in the subsurface is very complex where aquifer and aquitard beds show crossing one another even within a short distance. Commonly, three aquifer layers are encountered within 350 m depth. Hydrochemical analyses effectively distinguish between groundwater in the three aquifers, and also distinguish saline groundwater from seawater. Trends in major ion chemistry in the coastal aquifer system, particularly Na/Cl and Ca/Cl ratios, indicate some degree of ion exchange accompanying seawater intrusion. Mineral dissolution and major ion chemistry clearly identify solute flux trends in the coastal aquifer system. Lateral saltwater intrusion models were constructed for the sea level rise scenarios which show a saltwater wedge consistent with the shape predicted by the Ghyben-Herzberg relation. Sensitivity analysis for these models shows that saltwater intrusion can be limited by an increase in the hydraulic gradients of fresh groundwater in the southern (downgradient) direction or by the presence of a confining clay layer in the coastal region. Vertical saltwater infiltration models show that small tidal channels have a local effect with a infiltration of saline surface water into the shallow layers, whereas larger tidal channels affect a larger area which can reach the deeper and main aquifer. Trace element concentrations were compared to Cl⁻ concentrations which showed either no or to a moderate positive correlation. Although the pH or salinity effect may cause additional mobilization of trace element in this area, geochemical data show that the elevated

concentrations of Fe, Mn, Sr and As can be correlated with high pH and HCO_3 . These geochemical correlations suggest that elevated metal concentrations may be caused by bacterial iron and manganese reduction. Furthermore, bacterial sulfate reduction may also affect either major and minor trace element mobilization or removal, but the pH effect could become problematic in the future should seawater intrusion continue to drive up pH and salinity in the aquifers.

ACKNOWLEDGMENTS

It is a great honor to thank the people who made this thesis possible. This work would not have been a successful study of geoscience without the enthusiastic support of my thesis advisor, Dr. Ashraf Uddin. He has been actively involved in my research and brought the best out of me in my work. I show my immense gratitude and respect to Dr. Uddin for his constant support and inspiration that has brought me many awards throughout the period I have been at Auburn University.

I would also like to express my gratitude to Drs. Ming-Kuo Lee and James Saunders for their guidance and support. My knowledge in aqueous geochemistry has significantly improved because of Dr. Lee. I thank Dr. Lee for being very supportive in every aspect of my research. Discussions with Dr. Saunders on geochemistry and bio-mineralization were very educational. This research was possible for financial support from the Auburn University Geosciences Advisory Board, Geological Society of America, Alabama Academy of Sciences, and Auburn University Graduate School Research Grant. I thank the Department of Geosciences of Auburn University for providing me support through graduate teaching and research assistantships. I am grateful to departmental staff at Auburn University for their friendly support.

Most importantly, I wish to thank and express my devotion to my parents. I greatly recognize their support and inspiration in every step of my research and graduate study. Finally, I dedicate this thesis to my beloved parents.

TABLE OF CONTENTS

| | |
|---|------|
| ABSTRACT..... | iii |
| ACKNOWLEDGMENTS | ivv |
| LIST OF FIGURES | viii |
| LIST OF TABLES..... | xi |
| Chapter 1. Geochemical dynamics of saltwater intrusion at the coastal aquifers of the Ganges delta..... | 2 |
| Abstract..... | 4 |
| Introduction..... | 5 |
| Study area and hydrogeology | 9 |
| Methods | 12 |
| Groundwater chemistry..... | 12 |
| Numerical modeling | 13 |
| Results and discussion | 15 |
| Geochemistry of saltwater intrusion | 15 |
| Stable isotopes | 20 |
| Saturation Indices..... | 23 |
| Hydrochemical facies analysis | 27 |
| Geochemical model of fluid mixing | 29 |
| Solute transport modeling..... | 32 |

| | |
|--|----|
| Lateral seawater intrusion model | 35 |
| Vertical seawater infiltration model | 41 |
| Conclusions..... | 46 |
| Acknowledgments | 47 |
| References..... | 48 |
| Chapter 2. Trace element reactions in the groundwater flow system of coastal aquifers of the Ganges delta..... | 62 |
| Abstract..... | 63 |
| Introduction..... | 64 |
| Geology and hydrogeology..... | 67 |
| Methods | 69 |
| Groundwater chemistry | 69 |
| Sediment chemistry | 70 |
| Sediment petrography..... | 71 |
| Reaction path modeling..... | 71 |
| Results and discussion | 70 |
| Major ion and trace element geochemistry..... | 73 |
| Carbon isotope compositions of groundwater | 77 |
| Sediment and groundwater chemistry..... | 79 |
| Biomineralization of sediments..... | 86 |
| Bacterial reduction of Fe(III) and Mn(IV) oxides | 91 |

| | |
|-------------------|-----|
| Conclusions..... | 99 |
| References..... | 101 |
| CONCLUSIONS | 107 |

LIST OF FIGURES

Chapter 1

- Figure 1. Map showing well locations in the study area. Ganges, Brahmaputra, and Meghna are the major rivers in Bangal Basin, which formed one of the largest delta systems in the world called Ganges delta. Transect lines shown on this map corresponding to hydrostratigraphic cross-sections as shown in Fig. 16 and 18..... 7
- Figure 2. General hydrostratigraphic units in the N-S transect used in the regional groundwater and solute transport modeling. Transect and well locations are shown in Fig 1. 10
- Figure 3. General hydrostratigraphic units in the E-W transect used in the regional groundwater and solute transport modeling. Transect and well locations are shown in Fig 1. 11
- Figure 4. Plots of Na^+ , Ca^{2+} , Mg^{2+} , K^+ and H^+ vs Cl^- in the coastal aquifers of Ganges delta. ... 17
- Figure 5. Plots of $\log(\Delta\text{H}^+)$ vs. $\log(\Delta\text{Ca}^{2+})$ of groundwater in the coastal aquifers of Ganges delta. Representative Cl^- concentrations of most groundwater are shown with numbers. The delta (Δ) sign represents the amount of enrichment (or depletion) of each species relative to the conservative mixing line. 18
- Figure 6. Plot of $\Delta\text{Ca}^{2+}/\Delta\text{Na}^+$ vs. Cl^- of groundwater. Ion-exchange between clay and groundwater is represented by a horizontal line intercepting the y axis at -0.5. The negative sign indicates that Na^+ is depleted in the groundwater..... 20
- Figure 7. Relationship between $\delta^{18}\text{O}$ and $\delta^2\text{H}$ (Data Source: BGS and DPHE, 2001)..... 21
- Figure 8. Plot showing the enrichment of HCO_3^- is plotted versus the depletion of SO_4^{2-} 22
- Figure 9. Plot of DOC and $\delta^{13}\text{C}$ (Data Source: BGS and DPHE, 2001). 22
- Figure 10. Plots of gypsum (a), calcite (b) and dolomite (c) saturation indices vs Salinity.. 25
- Figure 11. Plot of $\Delta\text{Mg}^{2+}/\Delta\text{Ca}^{2+}$ vs. Cl^- of groundwater..... 26
- Figure 12. Hydrochemical facies evolution diagram (HFE-D) showing the main process occurring in intrusion and freshening stages. 27

Figure 13. Piper diagram showing different hydrochemical facies from the coastal aquifers in the Ganges delta. Groundwater mixes with seawater exhibit higher proportions of Na^+ and Cl^- 29

Figure 14. Predicted sequence of mineralogical reactions resulting from seawater is diluted by fresh groundwater in coastal aquifers of the Ganges delta. The plot shows changes in mineral volume as fresh groundwater is titrated into the saline groundwater. Mineral precipitation and dissolution is influenced by dilution effects. Model was created using GWB. 30

Figure 15. Solubility diagram for dissolution of microcline in a closed system at 25°C. The reaction trace of geochemical mixing in Fig. 14 is projected as open squares onto the diagram. The reaction trace shows the sequence of mineral forms during freshwater and seawater mixing. Model was created using GWB. 31

Figure 16. Predicted groundwater flow and salinity distribution along N-S cross-section. Color map concentration of groundwater shows spatial distribution of Cl. Arrows show magnitude and flow direction; (a) Lateral intrusion model with 1000 ppm salinity contour, 0.5 meter sea level rise; (b) Lateral intrusion model with 1000 ppm salinity contour, 1 meter sea level rise; (c) Lateral intrusion model with 1000 ppm salinity contour, 1.5 meter sea level rise; (d) Sensitivity analysis for lateral intrusion model was performed during 1 meter sea level rise by increasing freshwater flux in upstream area ; (e) Lateral intrusion model at 1 meter sea level rise with confining clay..... 39

Figure 17. Spatial distribution of electrical conductivity (EC) in the deep aquifer (>250 m depth) of the study area showing lesser salt content in groundwater in the northern side. The southwestern areas show higher contents of salt which are migrating landward. 40

Figure 18. Predicted groundwater flow and salinity distribution along E-W cross-section. Color map concentration of groundwater shows spatial distribution of Cl. Arrows show magnitude and flow direction; (a) Vertical infiltration model in study area; (b) Sensitivity analysis for vertical infiltration model with confining clay. 42

Figure 19. Spatial distribution of electrical conductivity (EC) in the shallow aquifer or upper aquifer (20-150m depth) of the study area. This shows that most shallow aquifers are contaminated with surface seawater by vertical infiltration from intertidal channels. 43

Figure 20. Groundwater Cl^- concentration as a function of depth in study area..... 44

Chapter 2

- Figure 1. Map showing well locations in the study area. Ganges, Brahmaputra, and Meghna are the major rivers in Bangal Basin, which formed one of the largest delta systems in the world called Ganges Delta. N-S transect line shown on this map corresponding to hydrostratigraphic cross-sections is shown in Figure 2.....66
- Figure 2. General N-S hydrostratigraphic cross section in study area is showing the Quaternary stratigraphic units. Transect line is shown in Figure 1. The cross section is constructed based on lithostratigraphic data from (BWDB, 2014).....67
- Figure 3. (a) As, Fe, Mn, and Sr concentrations of groundwater samples at various distances from updip along the NS transect (Fig. 1) in central Ganges delta (b) HCO₃ and pH along the same transect.....74
- Figure 4. Concentrations of dissolved Ca, Mg, K, and Na in the coastal aquifer as function of distance along a flow path in central Ganges delta.....76
- Figure 5. The $\delta^{13}\text{C}$ ratios of coastal groundwater as a function of distance along a flow path in the Ganges delta. Dash line indicates missing data.....78
- Figure 6. Eh-pH diagram calculated for average geochemical conditions in C-H-O system and Activity of dissolved species: C = 10^{-10} mol. This activity diagram was generated by the Geochemist' Workbench.....78
- Figure 7. Concentrations of selected trace metals in sediments of study area in wells LKLN2 and SPNA as a function of depth.....81
- Figure 8. Calculated average aluminum-normalized enrichment factors of various elements in LKLN2 well sediments.....82
- Figure 9. Calculated average aluminum-normalized enrichment factors of various elements in SPNA well sediments82
- Figure 10. Diagram showing trace element concentrations of Fe, Mn and As both in groundwater and sediment as a function of depth in study area. Concentrations of elements in groundwater roughly match that of sediments with depth. Stratigraphic columns (LKLN2 and SPNA wells) are also shown with depths (m) which show dominance of very fine to fine sand. Both wells record higher concentration of all three elements down to 100m depth.85
- Figure 11. Representative photomicrographs of minerals from Ganges delta sediments. Thin sections of (a) biogenic siderite (Sid) (cross polar) surrounded with rim (SPNA 301-304 m), (b)

SPNA 198-201m and (c) LKLN2 54-57 m) framboidal pyrite (Py) (transmitted and reflected light) and pyrite formed by replacement of a biotite grain in (d) reflected light with varied polarization.....87

Figure 12. SEM images of authogenic minerals form in sediment. (a) Biogenic pyrite texture (SPNA, 301-304 m); (b) Pyrite nucleating between biotite layers (LKLN2, 198-201m); (c) Siderite spheroid in well SPNA 301-304m.88

Figure 13. SEM images of microbial features in iron sulfide formation.....90

Figure 14. Predicted sequence of mineralogical reactions resulting from bacteria reduction of Fe and Mn oxides in equilibrium with coastal groundwater. The plot shows changes in mineral volume as organic carbon is titrated into the system and Eh decreases with time. Positive changes indicate precipitation, and negative changes show dissolution; (b) Calculated Fe and Mn species concentrations in fluid predicted by the same reaction path model.....94

Figure 15. Eh-pH diagram calculated for average geochemical conditions in (a) Mn-HCO₃-H₂O and (b) Fe-HCO₃-H₂O systems. Activity of dissolved species: Fe²⁺ = 10⁻², Mn²⁺ = 10^{-2.5}, SO₄²⁻ = 10⁻³, and HCO₃⁻ = 10⁻² mol. The reaction trace of bacterial Mn and Fe reduction in Figure 14 is projected as open squares onto the diagram. The reaction trace shows the sequence of mineral reactions during the reductive dissolution of Mn and Fe oxides as Eh decreases. This activity diagrams were generated by the Geochemist' Workbench.....95

Figure 16. Conceptual model of trace element and biominerals precipitation reactions in groundwater flow system in the Ganges delta.....98

LIST OF TABLES

Chapter 1

| | |
|--|----|
| Table 1. Groundwater chemistry in study area | 15 |
| Table 2. Correlations used in the hydrologic simulations to calculate porosity and permeability of Basin strata in the Ganges delta aquifers. | 33 |

Chapter 2

| | |
|--|----|
| Table 1. Groundwater chemistry in study area. Well ID locations are also shown in Figure 1...73 | |
| Table 2. Concentrations of major, minor and trace elements in sediment samples (total digestion) from the LKLN2 and SPNA wells from the study area | 80 |

LIST OF APPENDIX

Chapter 1

Appendix 1. Groundwater chemistry in study area.....109

Style manual or journal used: Journal of Contaminant Hydrology

Computer software used: Adobe Illustrator, ArcGIS, Basin2, Microsoft Excel, Microsoft Word, Arc GIS, Geochemist's workbench, Rockware AqQA

CHAPTER 1

**GEOCHEMICAL DYNAMICS OF SALTWATER INTRUSION AT THE
COASTAL AQUIFERS OF THE GANGES DELTA**

ABSTRACT

Saltwater intrusion into groundwater can result in the formation of a salt water wedge progressing inland that may induce geochemical changes in coastal aquifers. Hydrological and geochemical data collected from the Ganges Delta study area indicate a significant degree of mixing of seawater and freshwater in coastal aquifers. The main hydrochemical facies of groundwater in the coastal aquifers is a Na-Cl-Ca-HCO₃ type that is enriched in Na, K, Ca, Mg, and HCO₃ (relative to the conservative mixing line of seawater and dilute groundwater). Major ion compositions and $\delta^{18}\text{O}$ and $\delta^2\text{H}$ values are used to determine the source of salinity and the nature of mixing of different groundwaters. Three water types were identified; these include carbonate groundwater, seawater mixed with freshwater, and groundwater of meteoric origin. Geochemical model of fluid mixing suggests mineral precipitation and dissolution are influenced by dilution effects of seawater and fresh groundwater. To simulate saltwater intrusion in the Ganges delta, a numerical model coupling the flow and solute transport process was used to account for permeability variation in space and flow driven by hydraulic potential (topographic relief) and density (salinity) gradient. Hydrogeological modeling and historical water-table data from the coastal aquifers show a general north to south flow trend. These results also suggest that the shallow groundwater flow is controlled by local topography causing undulations in the water table. The modeling results are consistent with O/H isotope signatures, which indicate that high salinity groundwaters are present in shallow aquifers, suggesting that shallow aquifers may be

contaminated by downward infiltration of saline tidal channel surface seawater. The less saline groundwater present in the deeper aquifers may be derived from lateral saltwater intrusion from the ocean. The hydrologic model is consistent with the hydrochemical facies evolution in the coastal aquifers. The field data and modeling efforts in the coastal regions of the Ganges delta could prove to be useful in predicting other coastal areas of the world which are susceptible to deteriorating water quality resulting from increasing sea level rise and saltwater intrusion.

INTRODUCTION

Identifying the source of salinity and chemical change in coastal aquifer groundwater remains one of the most difficult problems in hydrogeology. Rising sea-level is contributing to seawater intrusion or inundation of coastal freshwater resources, particularly in shallow aquifer systems along low-lying coastal areas of the Ganges delta. Soil chemistry from the Ganges delta shows an increase in salinity over time as a result of seawater inundation, tidal flooding, saline groundwater flow, and groundwater withdrawal (Rashid and Islam 1995; LGED and BRGM 2005). In 2006, Ministry of Environment and Forest of the Government of Bangladesh reported estuarine modeling work demonstrating that rising sea-level will result in the increase of surface salinity. Cyclones and their associated storm surges can also increase the severity of salinity in the coastal zone of Bangladesh (Ali 1996). According to an estimate of the Master Plan Organization (MPO 1987) about 14,000 km² of coastal and offshore areas have saline soils that are susceptible to tidal flooding. If some 16,000 km² of coastal land is lost due to a 45 cm rise in sea level, the salinity front would be pushed further inland. Possible salinization processes in the coastal aquifers are varied and include natural saline groundwater, halite dissolution, and presence of paleo-brackish water and seawater intrusion (MPO 1987). Among these processes, seawater intrusion is the most common and widespread phenomenon in coastal areas. In

addition, the threat of saltwater intrusion in coastal areas has increased with the onset of urbanization (Cooper et al. 1964; Smith 1988; Lacombe and Carleton 1992). Increased development causes these areas to extract greater amounts of groundwater from local aquifer systems, and excessive pumping has triggered the landward migration of saline water into the coastal areas.

Physical processes at the seawater-freshwater interface have been studied extensively, with respect to the flow and transport of miscible fluids of different densities (Bear 1972; Todd 1980; Reilly and Goodman 1985; Bear et al. 1999). However, much less attention has been given to the chemical processes. Often investigations have focused on the origin of the seawater, whether it is derived from sources such as deep brines and dissolution of evaporates (Howard and Lloyd 1983; Howard and Mullings 1996; Giménez and Morell 1997; Xue et al. 2000; Schmerge 2001; Kim et al. 2003). Studies of the seawater-freshwater interface have focused on ion exchange processes, and on using the resulting water composition as an indicator for changes in the seawater-freshwater interface position (Mercado 1985; Beekman 1991; Stuyfzand 1993; Appelo 1994; 1996). A study of the chemical mechanism by Appelo(1996) suggested that changes in the position of the seawater-freshwater interface trigger ion exchange redox and dissolution-precipitation reactions. Beekman (1991) interpreted the evolution in water quality along a freshening flow path as a coupled effect of cation exchange, mineral dissolution-precipitation, and de-dolomitization.

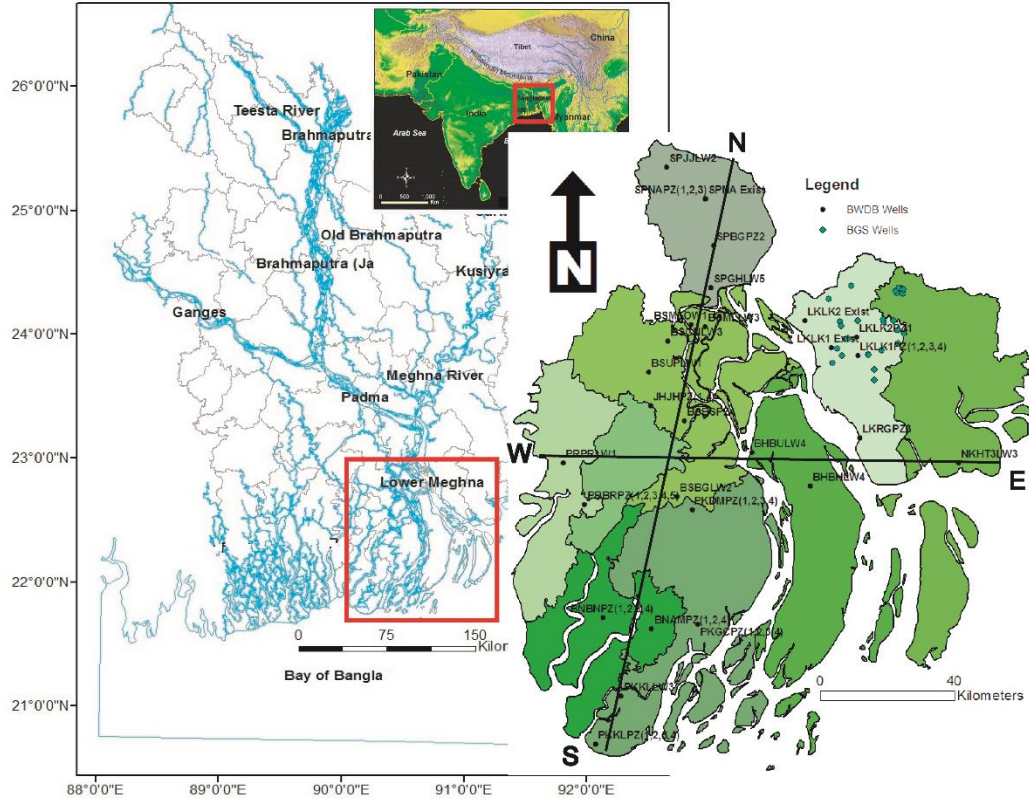


Fig.1. Map showing well locations in the study area. Ganges, Brahmaputra, and Meghna are the major rivers in Bangal Basin, which formed one of the largest delta systems in the world called Ganges delta. Transect lines shown on this map corresponding to hydrostratigraphic cross-sections as shown in Fig. 16 and 18.

Groundwater modeling studies for the Bengal Basin have not yet been carried out in any significant detail and the few studies completed to date were mainly on the upper aquifers at small scale (Harvey et al. 2002; Rahman and Ravenscroft 2003). To develop models of groundwater flow, salinity distribution, and water-sediment interaction in coastal aquifers of the Ganges delta, computer modeling techniques have been integrated with field observations and groundwater data. In addition, geochemical modeling techniques have been employed to evaluate the chemical effects of saltwater intrusion and the chemical processes which may be occurring as a result of water-sediment interaction. For example, a study by Lee et al. (2013) suggested that high sea-level stand may lead to desorption of metals from surface of hydrous

oxides due to pH effects and ionic competition for mineral sorbing sites. Research by Werner and Lockington, (2006); Badaruddin et al., (2015) have shown that seawater intrusion induces water table salinization within unconfined aquifer. This occurs when seawater intrusion causes salinization of the saturated profile of the aquifer, leading to saline water rising at the water table of unconfined coastal aquifers and they predicted more rapid seawater intrusion will lead to fast water table salinization, in accordance with a prediction of water table salinization during rapid water table decline. Werner and Lockington, (2006). Chang et al. (2011) tried to change in hydraulic head at the coast is followed by a rise of the water table throughout the domain, meaning that seaward flux of fresh groundwater is eventually reestablished. Research by Watson et al., (2010); Chang et al., (2011); Morgan et al., (2013) linked the rise in the water table and the time it takes to occur, with exceed being largest in systems where water table rise is slowest. Studies by Werner and Simmons, (2009); Werner et al., (2012) modeled sea level rise and seawater intrusion have been assessed using steady state sharp interface analytic modeling. They found the inland boundary condition to be important in determining sea level rise induced seawater intrusion, with greatest change occurring for head controlled conditions, compared to flux-controlled conditions.

Steady-state flow models were used to account for gravity-driven discharges of freshwater into the ocean. This type of simplified model assumes mass transfer by advection only, and predicts a sharp interface between seawater and freshwater. In coastal environments, both gravity and density-driven flows can occur due to pressure and density imbalances between seawater and freshwater. In addition, the saltwater-freshwater boundary is not a sharp interface; the size of the zone is controlled by the dispersive characteristics of the geological formation and heterogeneity of the layers. These finding will help guide the approach needed for the continued

development of these coastal aquifers because drinking water in coastal Bangladesh is mainly derived from groundwater aquifers where this water salinization poses the greatest threat to public health and sustainable economic development.

This research addresses for the first time the mixing mechanism of groundwater and seawater in coastal Bangladesh. This study of the coastal aquifers of the Ganges delta also examines flow regimes driven by topography and density variations; demonstrate the relation between topographic relief and groundwater flow; compares the hydrologic models with existing water table and salinity distribution data, and examines the physical and chemical effects of seawater intrusion on groundwater geochemistry.

STUDY AREA AND HYDROGEOLOGY

The study area for this research is situated within the Ganges-Brahmaputra Meghna delta, between 2409081.83 m to 2597420.85 m E, and 177525.65m to 332603.59 N, and the land area generally slopes from north to south (Fig. 1). The distribution of aquifer sediments in the subsurface is very complex as the aquifer and aquitard units can pinch out and swell within short distances. Clay or silty-clay aquitards are not continuous and their appearance may affect the hydraulic connectivity between the shallow and deeper aquifers. Commonly, 3 to 4 sandy aquifer layers separated by clay aquitards are encountered up to 350m of depth, and some degree of extraction of groundwater from any aquifer depth may not have any effect on the others. The flat tidal and deltaic lands in the coast are interwoven by an intricate river and tidal channel system, which carry flood water from the Ganges, Brahmaputra, Meghna and other rivers and also act as rainfall and tide drainage channels for the Bay of Bengal.

The Ganges-Brahmaputra-Meghna (GBM) delta and aquifer systems were built up during the Pleistocene and Holocene when large volumes of sediments were laid down in the delta

complex (Shamsudduha and Uddin 2007). The input of the sediments and their distribution was largely controlled by tectonic activities (rising Himalayas) and regional climatic changes (Uddin and Lundberg 1998). Subsurface lithologs reveal large lithologic variations down to depths of ~350 m of coastal sediments. Sediment types in the delta show localized stratigraphic variations, but consist primarily of coarse to medium sand, very fine to fine sands, silts, and clay. Two cross-sections were constructed using lithological logs from the BWDB borehole data for transects N-S (Fig. 2) and E-W (Fig. 3). Lithological logs included descriptions of sediment variations every 10 feet which consist mainly of very fine sand, fine sand, medium sand, coarse sand, silt, and clay.

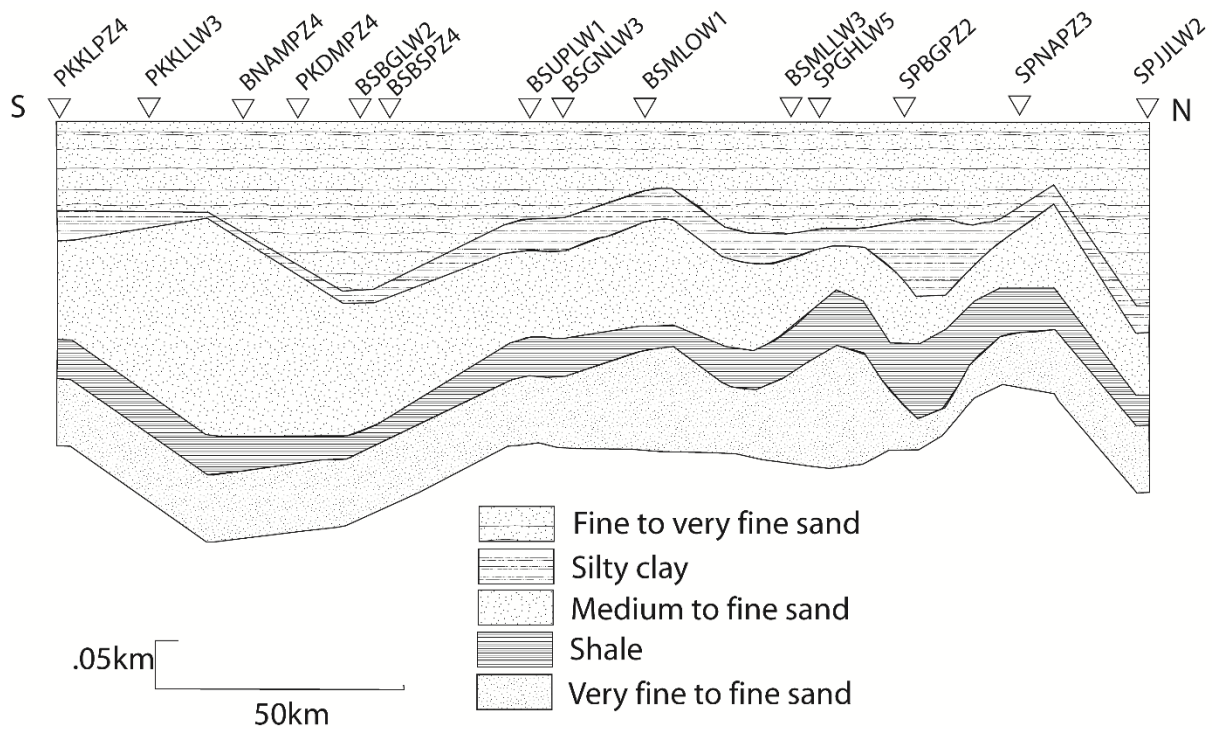


Fig.2. Diagrammatic general hydrostratigraphic units in the N-S transect used in the regional groundwater and solute transport modeling. Transect and well locations are shown in Fig 1.

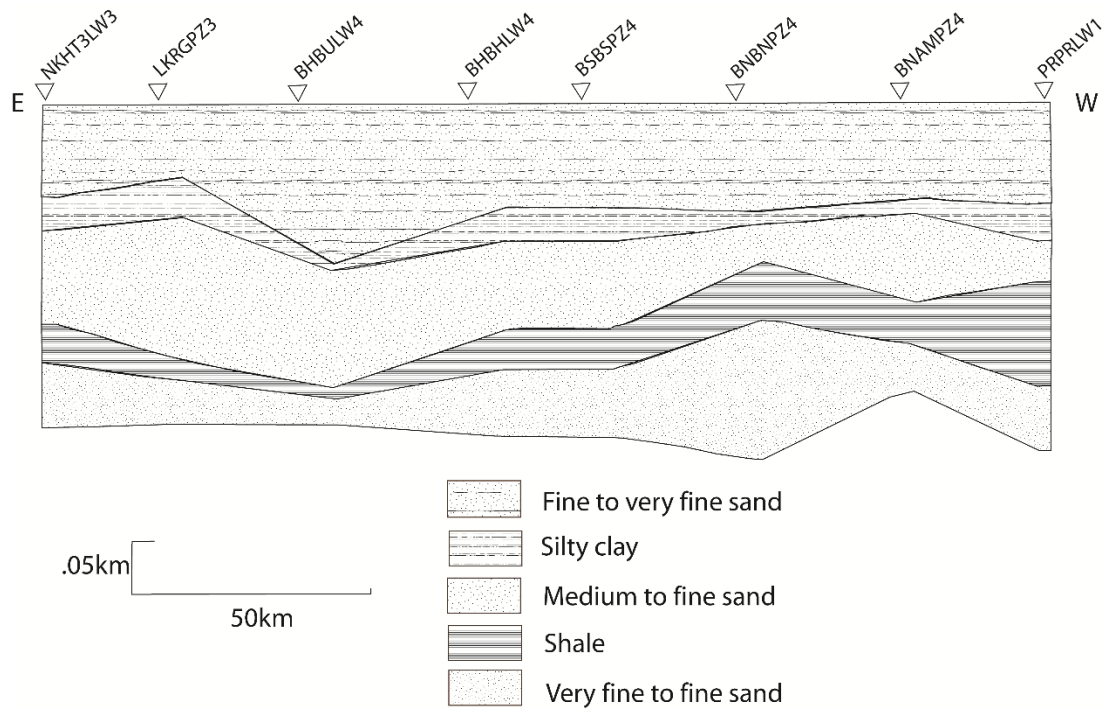


Fig.3. Diagrammatic general hydrostratigraphic units in the E-W transect used in the regional groundwater and solute transport modeling. Transect and well locations are shown in Fig 1.

Three sandy aquifers with clay lenses have been defined in coastal areas (UNDP, 1982), with the shallow, i.e. the 1st aquifer extends down to the depth of 50 to over 100 m, in many places overlain by a considerably thick upper clay and silt unit. The aquifer sediments are composed of fine to very fine sand with lenses of clay. The principal or the 2nd water bearing zone extends down to 250-350 m and is generally underlain and overlain by silty clay bed, and composed mainly of medium to fine sand, occasionally inter-bedded with clay lenses. It is either semi-confined/leaky or consists of stratified interconnected, unconfined water-bearing zones. The aquifers are mainly confined to leaky to unconfined in nature, varying in transmissivity from 1000 to 3000 m²/day at lower depth, but about 2000 m²/day at shallower depths within the study area (Davies and Herbert 1990). The deep, i.e., the 3rd aquifer has been encountered to depths of 300-350 m, generally below a silty clay aquitard. This aquifer is composed mainly of grey to

dark grey very fine sand that in places alternates with thin silty clay or clay lenses. In many places no significant clay or silty-clay layer has been encountered at any depth down to 350 m. This deep aquifer is separated from the overlying main aquifer by one or more clay layers of varying thickness. The confining clay layer ranges in thickness from 60 to 150 m in coastal areas.

In the coastal zone, the salinity of the composite and main aquifers is extremely variable and changes abruptly over short distances. In most areas, the water is too saline for domestic and irrigation use due to connate salts or estuarine flooding. Flushing out the saline water in some areas has resulted in freshwater pockets, thus the regional pattern of salinity distribution of the deep aquifer could be non-uniform. The change from potable water to very saline water could occur over a relatively short distance. Chloride and sodium are the dominant ions in the coastal area owing to seawater intrusion.

METHODS

Groundwater chemistry

Eleven monitoring wells were sampled in January 2015. The wells are located roughly along the flow paths from north to south and are maintained by the Bangladesh Water Development Board (Fig. 1). A peristaltic pump was used to purge the wells before collecting the representative groundwater samples in the aquifer. Well screen lengths and depths are shown in Table 1. At least three well volumes of water were removed and all water quality parameters readings were stabilized before sampling. After the well purging was completed, samples were analyzed for water quality parameters (temperature, pH, Eh, and electrical conductivity) in the field using mobile hand-held meters to avoid any parameter changes during sample

transportation and storage. After a water sample was collected in a clean beaker, it was then filtered with a 45 micron pore-diameter filter and acidified with 5% nitric acid for preservation before trace metal and cation analysis using the inductively coupled plasma mass spectrometry (ICP-MS) at Auburn University (Agilent 7900). A second sample was filtered for anion analysis using ion chromatography (IC) at Auburn University (Dionex DX-120). Additional twenty nine groundwater chemistry data in the coastal Bangladesh study area were acquired from a public database (DPHE and BGS 2001) for data interpretation and geochemical modeling.

The saturation indices ($\log Q/K$) (where Q is used to determine if a mineral is at saturated in a given groundwater sample and K is the known solubility products for a given mineral) of minerals and geochemical reactions of mixing of freshwater and seawater in coastal aquifers were calculated using Geochemist's Workbench (Lee and Bethke 1996; Bethke 2008). The Geochemist's Workbench (GWB) is one of a number of geochemical and reaction path models that calculate the species distribution in aqueous solutions and trace chemical evolution of groundwater systems involving fluids, minerals, and gases.

Numerical modeling

Groundwater flow and salinity distribution in the aquifers of the Ganges delta was modeled in two-dimensions using a basin-scale groundwater flow model Basin2 (Bethke et al. 2003).

Basin2 was used as the primary tool for constructing two-dimensional stratigraphic sections and for modeling groundwater flow and seawater intrusion processes. The program can model groundwater flow driven by topographic relief, compaction, density variation and solute (salt) transport by advection, diffusion, and mechanic dispersion using the following equation:

$$\frac{\partial(C)}{\partial t} = \frac{\partial}{\partial x} D_x \left(\frac{\partial c}{\partial x} \right) + \frac{\partial}{\partial z} D_z \left(\frac{\partial c}{\partial z} \right) - q_x \left(\frac{\partial c}{\partial x} \right) - q_z \left(\frac{\partial c}{\partial z} \right)$$

Where, C is concentration (mol cm^{-3}), q is specific discharge (cm sec^{-1}), t is time (sec), and D is hydrodynamic dispersion ($\text{cm}^2 \text{sec}^{-1}$), which accounts for molecular diffusion of solutes as well as mechanical dispersion. The model calculates the coefficients of hydrodynamic dispersion D_x and D_z from the following equations:

$$D_x = D^* + \alpha_L V_z' + \alpha_T V_x'$$

$$D_z = D^* + \alpha_L V_z' + \alpha_T V_x'$$

where D^* is the diffusion constant ($\text{cm}^2 \text{sec}^{-1}$), α_L and α_T are the dispersivities (cm) in the longitudinal and transverse directions, and V_x' and V_z' are lateral and vertical fluid flow velocities (cm sec^{-1}) in curvilinear coordinates.

RESULTS AND DISCUSSION

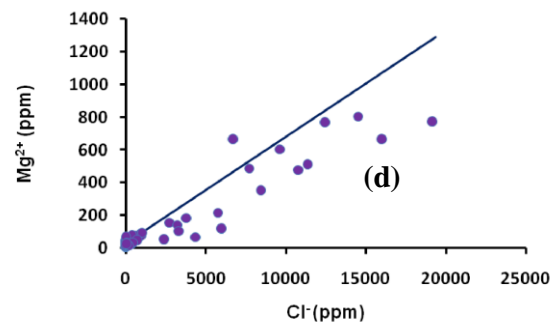
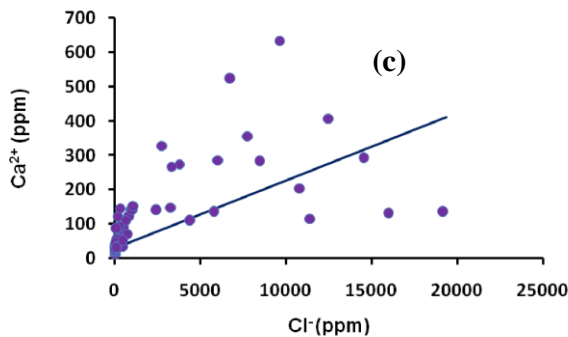
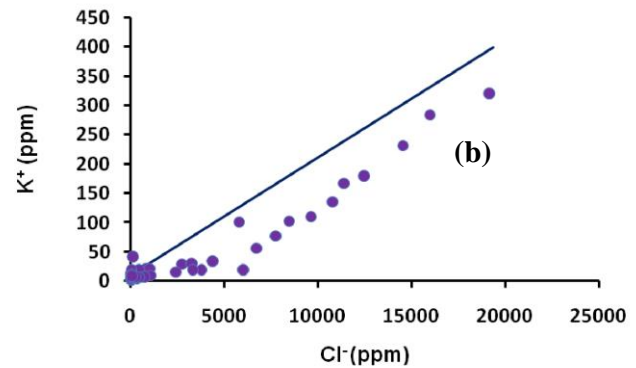
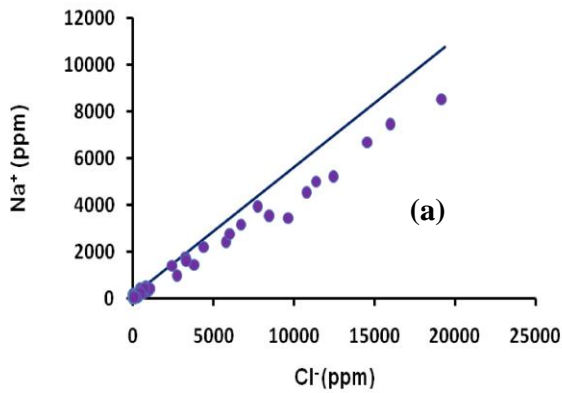
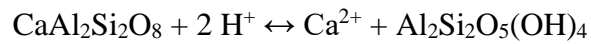
Geochemistry of saltwater intrusion

The behavior of Na⁺, Ca²⁺, Mg²⁺, K⁺ and H⁺ suggests that chemical processes are occurring in response to the physical fluid mixing of seawater and freshwater. Data points lying on or close to the conservative mixing line indicate that dissolved species exhibit conservative behavior. Non-conservative behavior is indicated if the data points deviate from the conservative mixing line by more than 10% (Liss 1976). Na⁺ exhibits relatively conservative behavior at low salinity whereas at higher salinity, non-conservative removal with the amount of removal generally increasing with seawater intrusion into coastal aquifers (Fig. 4a, Table. 1 and Appendix. 1).

Table 1. Groundwater chemistry in study area

| Sample ID | pH | Ca ²⁺ (ppm) | Mg ²⁺ (ppm) | Na ⁺ (ppm) | K ⁺ (ppm) | Cl(ppm) | HCO ₃ ⁻ (ppm) | SO ₄ ²⁻ (ppm) | NO ₃ ⁻ (ppm) | Well Screen(m) | Depth(m) |
|-------------|------|------------------------|------------------------|-----------------------|----------------------|---------|-------------------------------------|-------------------------------------|------------------------------------|----------------|----------|
| Freshwater | 5.9 | 33.4 | 45.2 | 244 | 13.4 | 196 | 678 | 4.3 | | | |
| Seawater | 8.3 | 411 | 1290 | 10760 | 399 | 19350 | 142 | 710 | | | |
| LK1K1PZ1 | 7.23 | 356 | 487 | 3944 | 77 | 7721 | 412 | 58 | 6 | 82-88 | 91 |
| LK1K1PZ2 | 6.42 | 525 | 666 | 3166 | 56 | 7101 | 359 | 94 | 2 | 142-148 | 152 |
| LK1K1PZ3 | 7.63 | 39 | 24 | 45 | 5 | 67 | 256 | 1 | 1 | 234-240 | 243 |
| LK1K1OW1 | 7.25 | 30 | 21 | 38 | 6 | 4 | 268 | 34 | 1 | 292-298 | 301 |
| LK1K1 Exist | 7.1 | 46 | 69 | 32 | 20 | 47 | 490 | 2 | 1 | 51-56 | 60 |
| LK1K2PZ1 | 8.56 | 35 | 23 | 50 | 5 | 122 | 164 | 1 | 1 | 82-88 | 91 |
| LK1K2 Exist | 8.06 | 32 | 33 | 14 | 13 | 94 | 179 | 1 | 1 | 61-67 | 70 |
| SPNAPZ1 | 7.3 | 70 | 51 | 439 | 7 | 736 | 318 | 3 | 3 | 97-103 | 106 |
| SPNAPZ2 | 7.29 | 54 | 36 | 230 | 6 | 450 | 217 | 1 | 1 | 289-295 | 329 |
| SPNAPZ3 | 7.1 | 94 | 16 | 50 | 7 | 236 | 129 | 1 | 1 | 295-301 | 304 |
| SPNA Exist | 7.2 | 88 | 27 | 74 | 8 | 58 | 472 | 1 | 1 | 71-77 | 80 |

K^+ displays non-conservative removal (Fig. 4b) from fluid with the amount of depletion generally increasing with chlorinity. Ca^{2+} demonstrates non-conservative enrichment or depletion to fluid and Mg^{2+} show depletion mostly, whereas H^+ displays non-conservative removal (Figs. 4c, 4d) from fluid with the amount of depletion generally decreasing with salinity. The conservative mixing line for pH vs. Cl^- is linear since pH is controlled by the equilibrium with carbonate species (Fig. 4e). The enrichment of Ca^{2+} and depletion of H^+ in coastal aquifers of the Ganges delta could be explained by the dissolution of calcite or calcium feldspar.



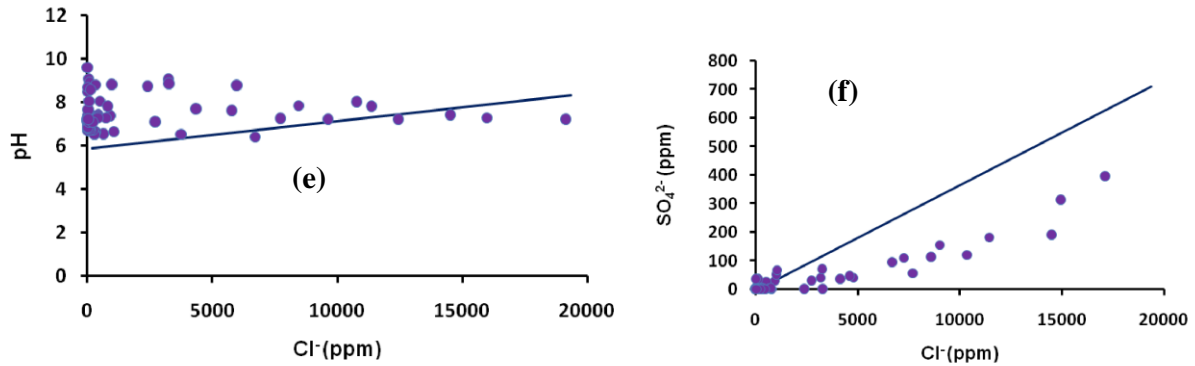


Fig.4. Plots of Na^+ , Ca^{2+} , Mg^{2+} , K^+ and H^+ vs Cl^- in the coastal aquifers of Ganges delta.

These reactions will consume H^+ and release Ca^{2+} . If the groundwater is undersaturated with respect to either of these minerals, then the reactions will proceed to the right. Moreover, cation exchange between groundwater and calcium rich clays could also be contributing to the enrichment in Ca^{2+} , as well as to the depletion in Na^+ . The net reaction between clays and seawater is primarily an exchange of seawater Na^+ for bound Ca^{2+} owing to the higher ratio of Na^+ to Ca^{2+} in seawater relative to freshwater (Sayles and Manglesdorf 1977). The cation exchange capacity of clays increases significantly with pH due to the increased abundance of negatively-charged exchangeable sites (Drever 1988).

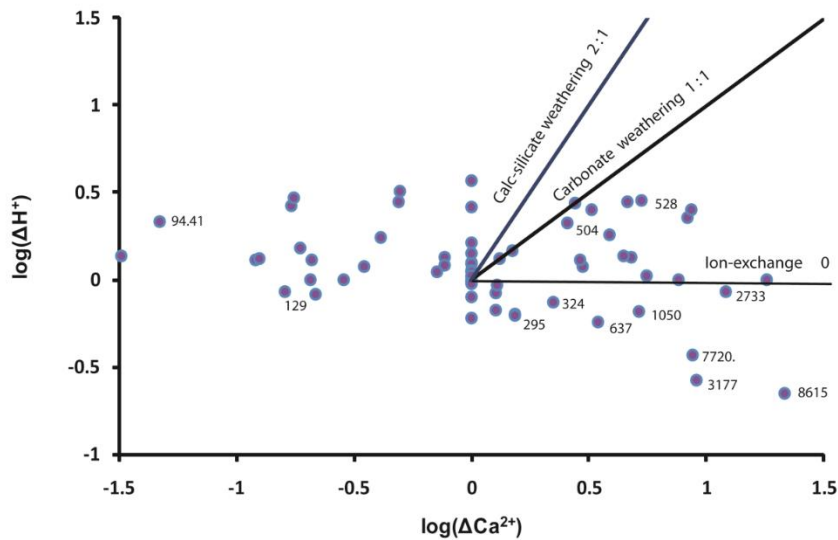
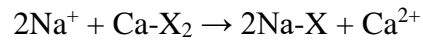


Fig.5. Plots of $\log(\Delta H^+)$ vs. $\log(\Delta Ca^{2+})$ of groundwater in the coastal aquifers of Ganges delta. Representative Cl^- concentrations of most groundwater are shown with numbers. The delta (Δ) sign represents the amount of enrichment (or depletion) of each species relative to the conservative mixing line.

Figure 5 shows how mineral dissolution and ion-exchange affect concentrations of Ca^{2+} and H^+ at different salinities. Mineral dissolution appears to be the dominant process responsible for the non-conservative trends in H^+ and Ca^{2+} at salinities near that of freshwater. This interpretation is supported by the relatively high depletion in H^+ probably as the result of calcium feldspar and calcite dissolution. Ion-exchanges may become more important at high salinities as indicated by the low depletion in H^+ to the ion-exchange line. In addition, the enrichment of Ca^{2+} reaches a maximum along the ion-exchange line at higher salinities, suggesting that ion-exchange may be more important than mineral dissolution in adding Ca^{2+} to groundwater. At the intermediate salinities, mineral dissolution and ion-exchange act together to control the groundwater composition.

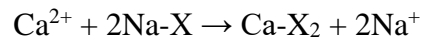
The fresh groundwater in Ganges delta is dominated by Ca^{2+} and HCO_3^- ions which results from the dissolution of calcite. When seawater intrudes into a coastal fresh water aquifer,

an exchange of cations takes place, where X denotes a fixed number of negative charges on the cation exchanger



This equation shows that ion-exchange can result in a 2:1 ratio of removal of Na^+ to enrichment of Ca^{2+} . This effect is demonstrated in Figure 6 for groundwater samples from Ganges delta coastal aquifers. At high salinities, samples of higher salinity groundwater plot close to a horizontal line corresponding to a 0.5 to 1 exchange of Ca^{2+} for Na^+ .

When freshwater displaces seawater, the cation affinity order is normally $\text{Ca}^{2+} > \text{Mg}^{2+} > \text{K}^+ > \text{Na}^+$ with Na^+ being displaced from the exchanger first and Ca^{2+} eventually dominating the exchanger on clay (Appelo 1994) via the following reaction:



Ion-exchange may be initiated when clays are exposed to an incursion of groundwater with different salinity. At low salinities, the amount of enrichment of Ca^{2+} relative to Na^+ is much greater (Figure 4). This result lends further evidence to mineral dissolution reactions as a possible control on the non-conservative behavior of Ca^{2+} in more dilute waters. Because these reactions do not affect the concentration of Na^+ , the ratio of Ca^{2+} to Na^+ should, therefore, increase as the reaction takes place.

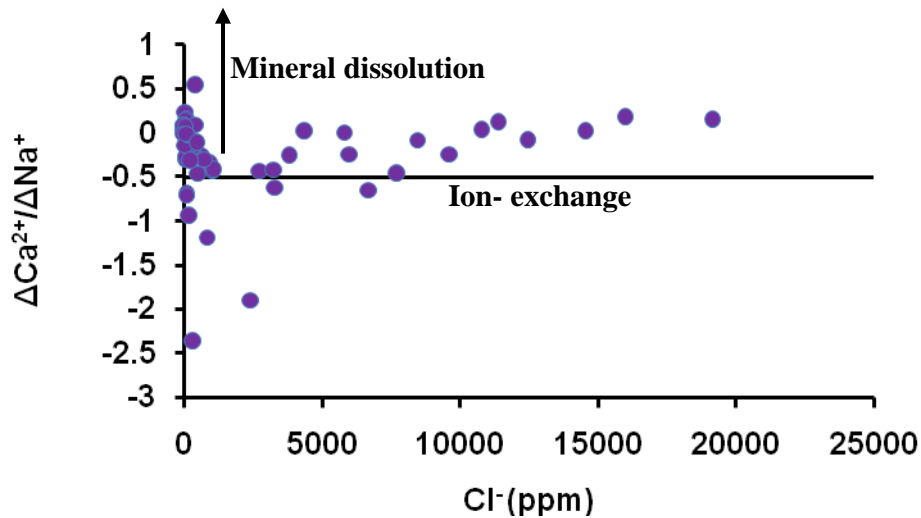


Fig.6. Plot of $\Delta\text{Ca}^{2+}/\Delta\text{Na}^{+}$ vs. Cl^{-} of groundwater. Ion-exchange between clay and groundwater is represented by a horizontal line intercepting the y axis at -0.5. The negative sign indicates that Na^{+} is depleted in the groundwater.

Stable isotopes

$\delta^{18}\text{O}$ and $\delta^2\text{H}$ values are used to identify the source of groundwater and its geochemical evolution in coastal aquifers. Figure 7 shows $\delta^2\text{H}$ and $\delta^{18}\text{O}$ ratios of groundwater relative to the seawater evaporation trajectory, local meteoric water line and the standard mean ocean water (SMOW) (Holser 1979). During evaporation, residual seawater becomes progressively enriched in $\delta^2\text{H}$ and $\delta^{18}\text{O}$ relative to SMOW, as the light isotopes ($\delta^2\text{H}$ and $\delta^{18}\text{O}$) are preferentially concentrated in the vapor phase. The local meteoric water line was constructed using rainfall data from Majumder et al. (2011).

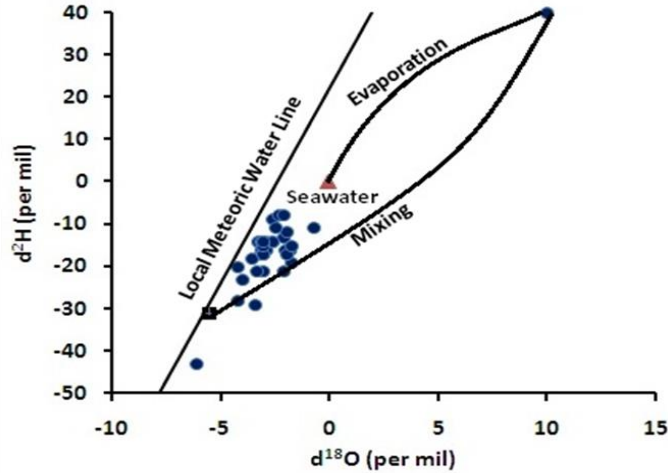
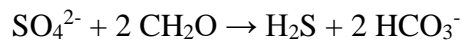


Fig.7. Relationship between $\delta^{18}\text{O}$ and $\delta^2\text{H}$ (Data Source: BGS and DPHE, 2001).

Analyses of the stable isotopes of the water molecule ($\delta^{18}\text{O}$, $\delta^2\text{H}$) show that the samples from the coastal aquifer plots along the mixing trends between the local meteoric water line (LMWL) and evaporated seawater (Fig. 7). Shallow groundwater samples fall close to the local meteoric water line, indicating their common association with a meteoric recharge source. This position under the LMWL can be attributed either to evaporation or to mixing with seawater.

All of the samples are depleted in SO_4^{2-} and enriched in HCO_3^- (Fig. 8). Sulfate depletion is commonly observed in aquifers affected by seawater intrusion because seawater provides sulfate as electron acceptors for bacterial sulfate reduction (Andersen et al. 2005; Yamanaka and Kumagai 2006). The depletion of sulfate indicated that bacterial sulfate reduction processes occur in the coastal aquifers of Ganges delta.



This reaction is caused by microbial activity which leads to the degradation of organic matter and to the production of H_2S and HCO_3^- . $\delta^{13}\text{C}$ values of the samples are isotopically light from -7.12 to -23.6 per mil when compared respectively to the seawater ($\delta^{13}\text{C}$ close to zero) (Fig. 9). These $\delta^{13}\text{C}$ values reflect the inputs of isotopically light organic source of carbon by

microbial respiration (Barker et al. 1998; Lee et al. 2007). Thus, sulfate reduction is a good marker for the head of the saline wedge.

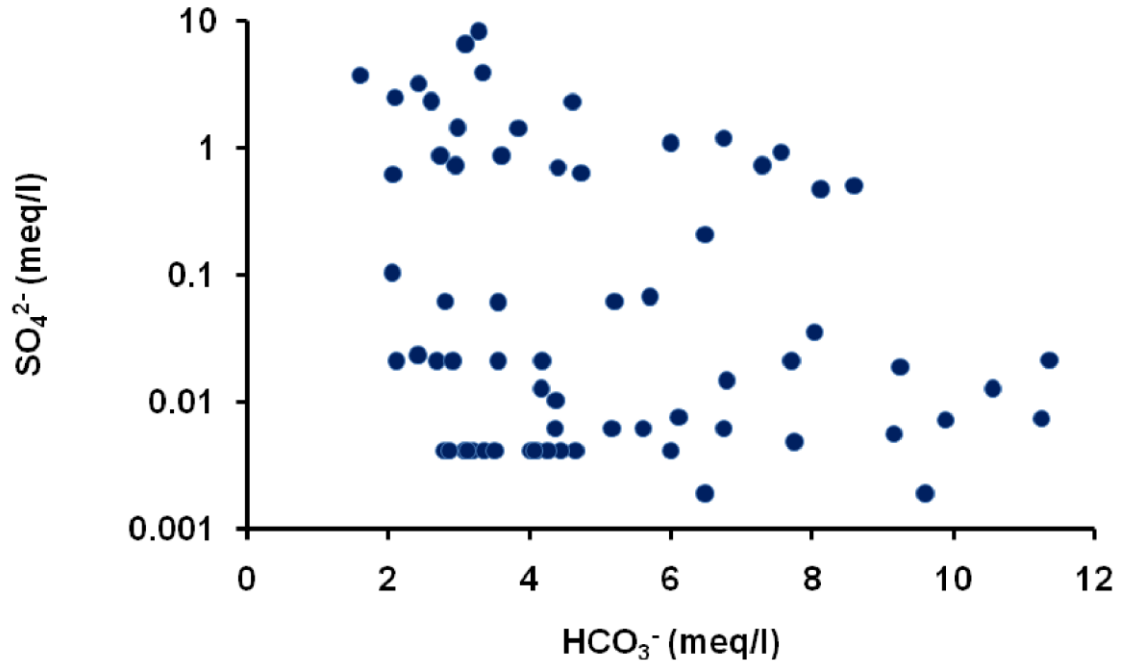


Fig.8. Plot showing the enrichment of HCO_3^- is plotted versus the depletion of SO_4^{2-} .

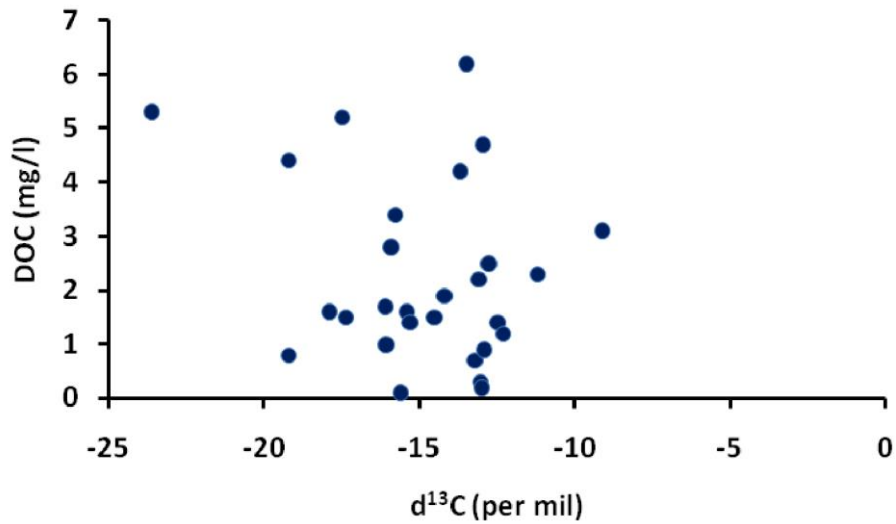


Fig.9. Plot of DOC and $\delta^{13}\text{C}$ (Data Source: BGS and DPHE, 2001).

Saturation indices

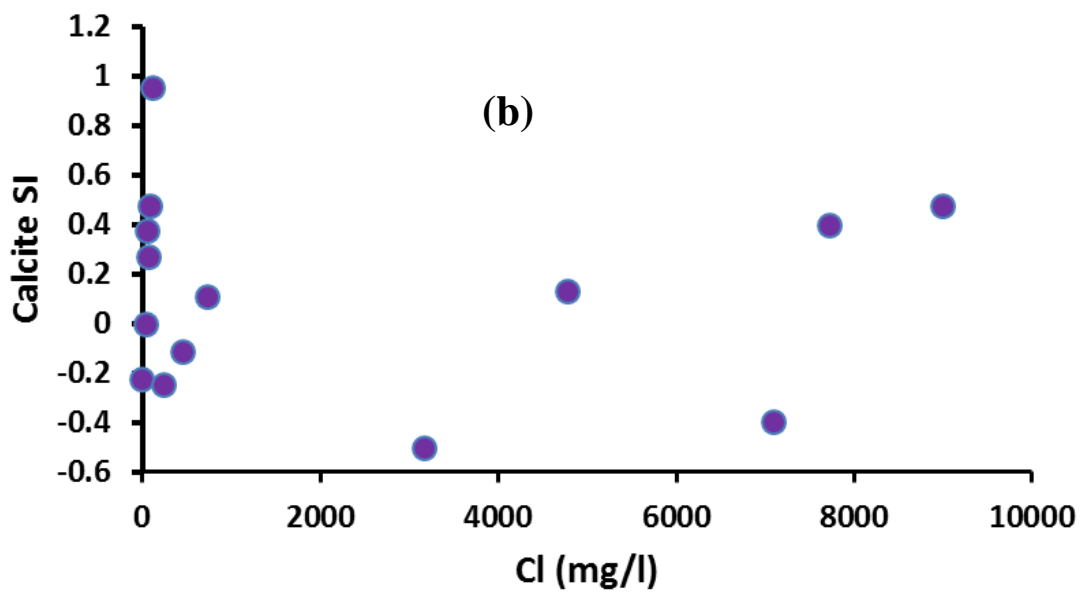
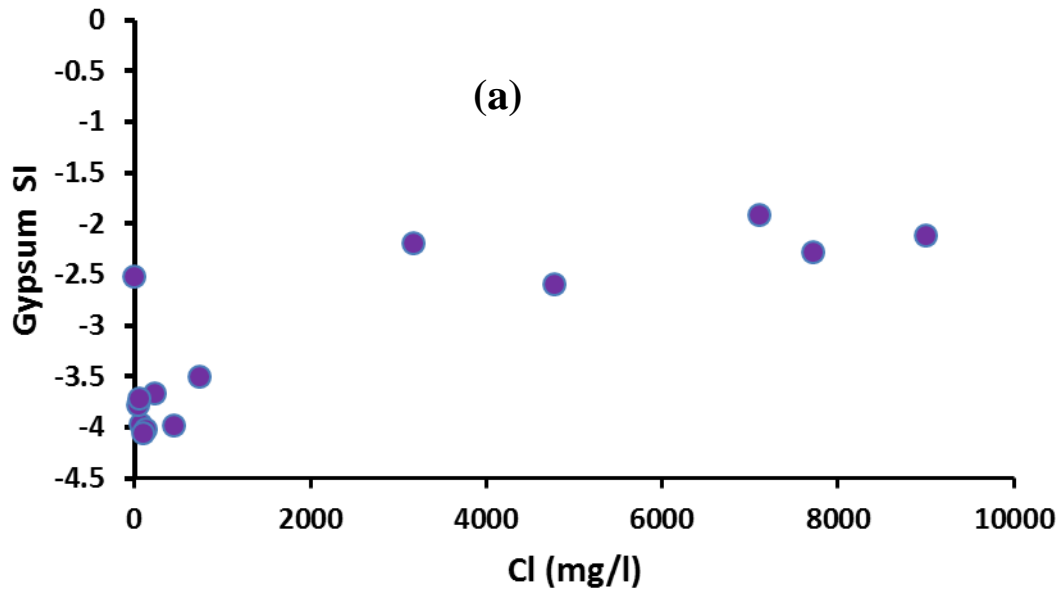
Geochemist's Workbench (GWB) was used to calculate the saturation indices (SI) of gypsum, calcite, and dolomite in groundwater samples obtained from coastal aquifers of Ganges delta. The increasing amount of bicarbonate produced by bacterial sulfate reduction, as well as the supplementary calcium contribution from the cationic exchange reaction, should displace calcite equilibriums and should cause supersaturation of calcite and dolomite according to



Calcite, dolomite and gypsum saturation indices (SI) were calculated to test the possibility that SO_4^- reduction and dolomitization processes are taking place. Gypsum saturation indices were also calculated for different mixing rates to assess the possibility of saltwater intrusion and SO_4^- reduction or gypsum dissolution (Fig. 10a).



The negative SI values of gypsum indicate widespread gypsum dissolution. The increasing Ca^{2+} concentration due to seawater intrusion or gypsum dissolution causes calcite to precipitate. The CO_3^{2-} concentration decreases as calcite precipitates, and provokes the dissolution of dolomite, increasing the Mg^{2+} concentration. A comparison with Boluda-Botella et al. (2008) however provides contrasting information on mineral saturation with dimensionless time.



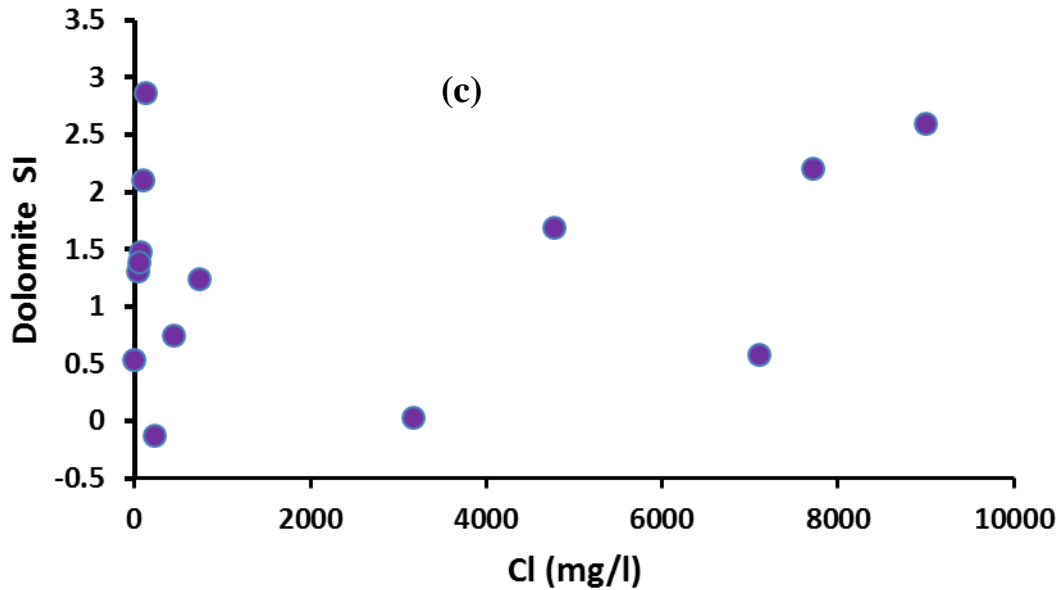


Fig.10. Plots of gypsum (a), calcite (b) and dolomite (c) saturation indices vs salinity.

In the landward part of the freshwater zone aquifer, groundwater samples are generally oversaturated with regard to calcite. Towards the coastline, the saturation index decreases to around saturation (SI= -0.5 to 0.95). The saturation state for calcite is a complex function of the distribution of Ca^{2+} , HCO_3^- in the groundwater, interaction with ion exchange processes, and mixing between freshwater and seawater (Fig. 10b). Calcite is oversaturate ion occurs locally in the freshwater zone aquifer, and likely is the result of slow (compared to the groundwater flow) dissolution of dispersed CaCO_3 fossil fragments. However, this ongoing calcite dissolution results in an increase in salinity although most of the released Ca^{2+} is taken up by the exchanger. In the fresh aquifer, sulfate reduction causes an increase in pH as H^+ ions are needed to make H_2S which makes supersaturation for calcite.

The behavior of dolomite is quite similar to calcite; samples containing low Cl^- concentrations are oversaturated of dolomite as most likely result of Mg^{2+} rich dissolution of dispersed CaCO_3 fossil fragments or cation exchange between Mg^{2+} rich clay minerals and

groundwater. The degree of saturation tends to increase with chlorinity in samples as shown in Fig. 10c. Ideal conditions for dolomitization are reached when $SI_{\text{calcite}} < 0$ and $SI_{\text{dolomite}} > 0$. However, conditions that causes the calcite SI to increase as a function of P_{CO_2} , and dolomitization is favoured as P_{CO_2} increases (Wigley and Plummer 1976). Margaritz et al. (1980) stated that a basic requirement for the deposition of dolomite is for the $\Delta\text{Mg}^{2+}/\Delta\text{Ca}^{2+}$ ratio to exceed 1. This condition is met in the samples that show a decrease over the same period. The fact that none of the samples have positive ΔMg^{2+} and negative ΔCa^{2+} suggests that de-dolomitization does not occurs in mixtures during intrusion (Fig. 11). Deficit in Mg^{2+} in the samples can be explained as being due to the cation exchange with Na^+ , but it is also true that the more saline of the samples yielded negative ΔNa^+ and ΔMg^{2+} in both cases. In contrast, the positive ΔCa^{2+} could point to dolomitization for these highly saline waters.

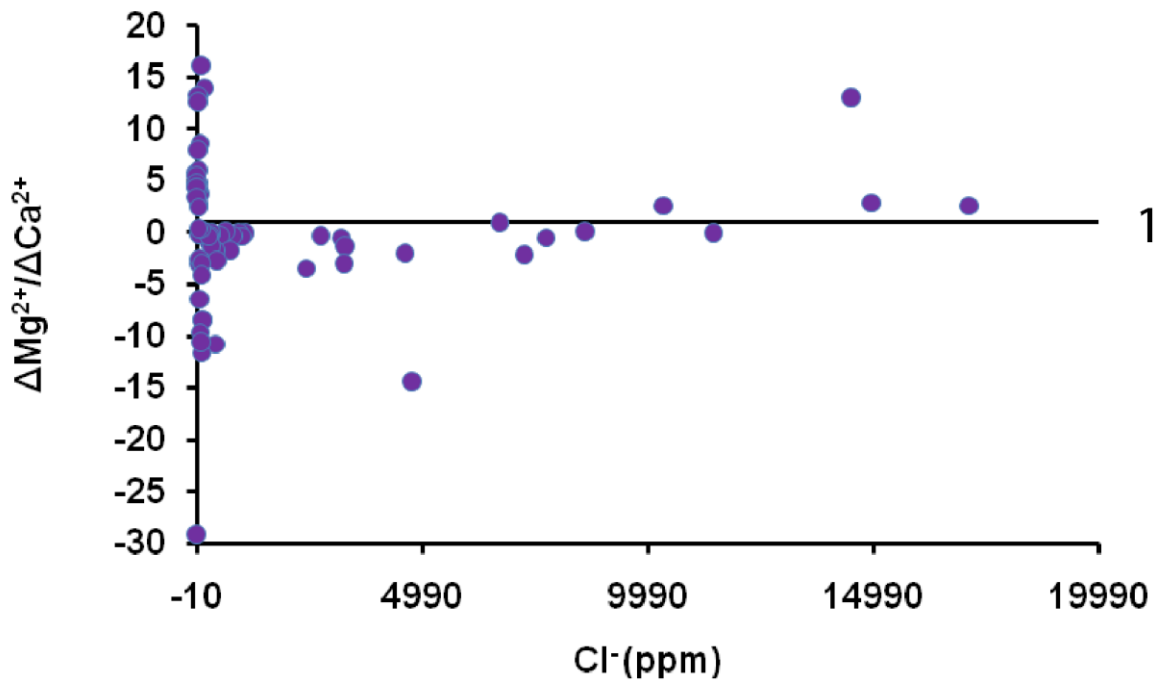


Fig.11. Plot of $\Delta\text{Mg}^{2+}/\Delta\text{Ca}^{2+}$ vs. Cl^- of groundwater

Hydrochemical facies analysis

Samples collected in coastal aquifers of the Ganges delta are presented in a hydrochemical facies evolution (HFE) diagram shown in Fig.12. The fresh water corresponds to the facies Na-HCO₃, whilst the seawater belongs to Na-Cl facies. The succession of facies along freshwater-seawater mixing indicates binary mixing with strong intervention of base exchanges reactions. During the phase of seawater intrusion, beneath the freshwater-seawater mixing line, there is an initial increase in salinity and a rapid, reverse exchange of Na by Ca, which is typical of Ca-Cl facies.

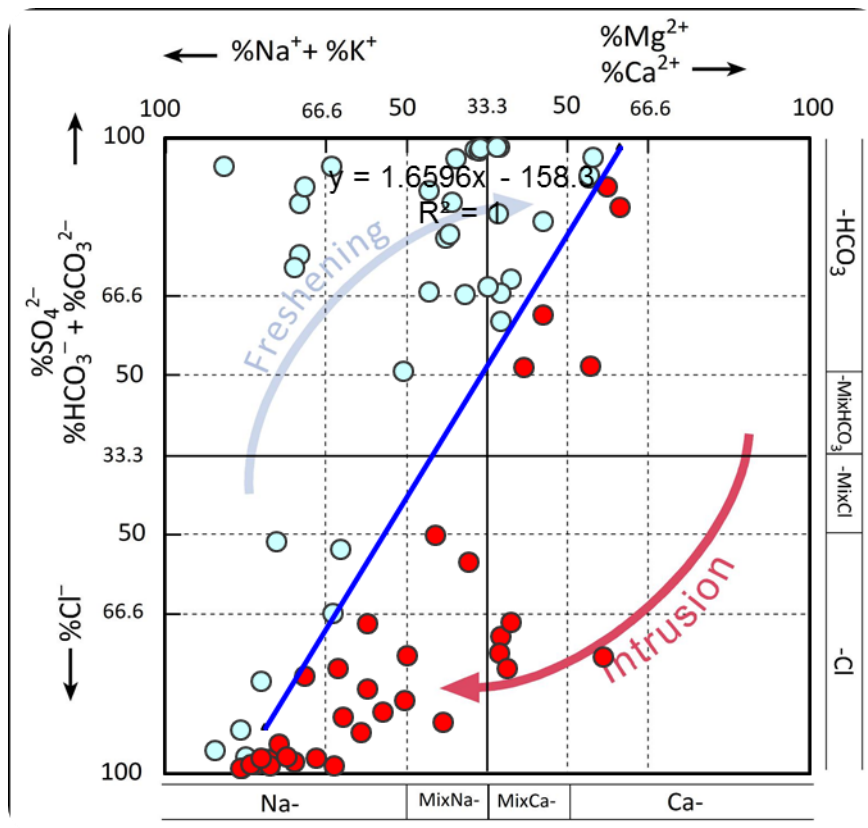


Fig.12. Hydrochemical facies evolution diagram (HFE-D) showing the main process interpreted to occur in intrusion and freshening stages.

Finally Ca-Cl type of groundwater evolves toward a Na-Cl facies that is closer seawater. In the freshening stage, above the freshwater and seawater mixing line, direct exchange processes occur more slowly; the waters gain Na^+ and release Ca^{2+} until Na- HCO_3 facies is achieved. The coastal aquifers of the Ganges delta only it is reached the facies Na-Mix HCO_3 . Then the groundwater evolves towards Na- HCO_3 types that are closer to recharge freshwater (Table 1 and Appendix 1). The effects of cation exchange are identical when analyses are plotted in a Piper diagram (Fig. 13). The groundwater chemistry is changing due to conservative mixing of two fluids both seawater and freshwater. Figure 13 shows that the samples fell in a wide range of hydrochemical facies. Sample SPNAPZ3 shows that plot near the far left portion of the graph represent groundwater enriched in Ca. The far right side of the piper diagram represents groundwaters that have similar compositions to seawater because study area is close to the coast, most of the aquifer samples plotted near seawater composition. A significant number of samples fall within the middle portion of the graph that represents meteoric mixing composition. The most dominant cations of the groundwater samples were Ca^{2+} and Na^+ and the predominant anions were HCO_3^- and Cl^- . The main hydrochemical facies in the aquifer can thus be characterized as a Ca- HCO_3 -Na-Cl type. As groundwater chemistry from coastal aquifers of the Ganges delta show a surplus of Ca^{2+} and Mg^{2+} , this can imply seawater intrusion in groundwater.

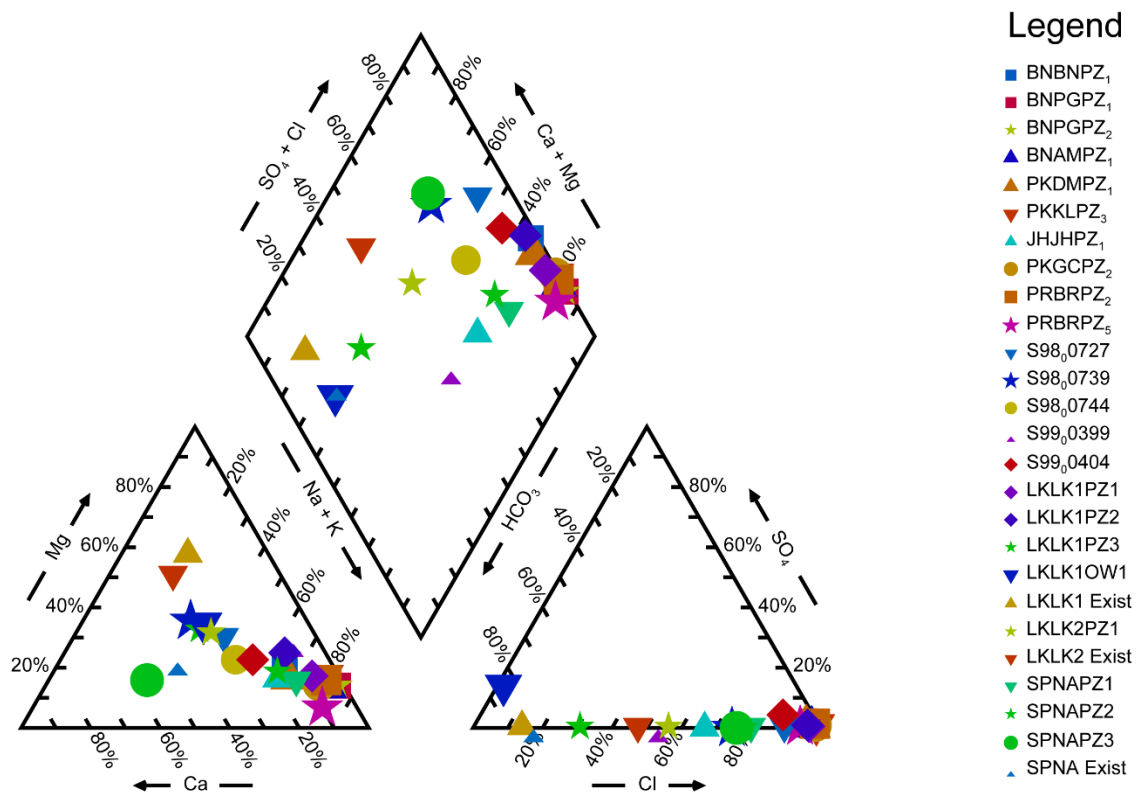


Fig.13. Piper diagram showing different hydrochemical facies from the coastal aquifers in the Ganges delta. Groundwater mixes with seawater exhibit higher proportions of Na⁺ and Cl⁻.

Geochemical model of fluid mixing

Saline groundwater is saturated with carbonate and oxide minerals. The saline water is rich in Ca²⁺ and Mg²⁺, whereas the fresh water contains abundant HCO₃⁻ (Fig. 14).

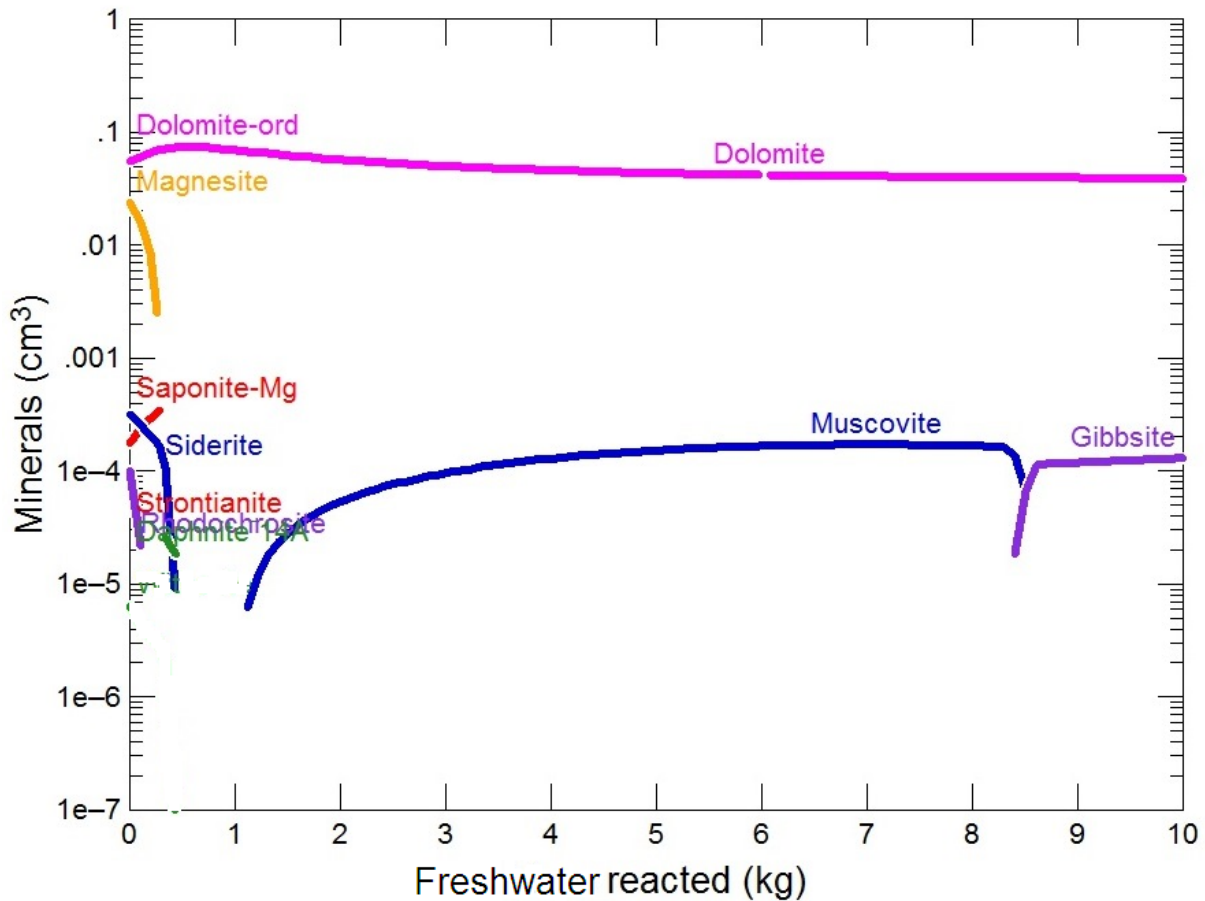
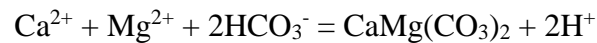
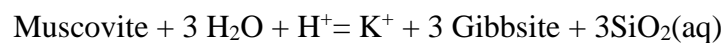
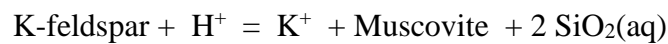


Fig.14. Predicted sequence of mineralogical reactions resulting from seawater is diluted by fresh groundwater in coastal aquifers of the Ganges delta. The plot shows changes in mineral volume as fresh groundwater is titrated into the saline groundwater. Mineral precipitation and dissolution is influenced by dilution effects. Model was created using GWB.

GWB subprogram React was used to model the titration of freshwater into an aquifer saturated with seawater. As the fluids mix, dolomite precipitates according to the reaction producing H^+ .



Many of the H^+ produced are consumed by driving the reaction of potassium feldspar to produce muscovite and gibbsite:



Gibbsite forms while microcline continues to dissolve in Figure 15. The net reaction release potassium and aluminum ions, H^+ , and silica to the solution, causing the fluid composition to move downward as both $a_{SiO_4(aq)}$ and a_{K^+}/a_{H^+} decrease. The fluid composition begins beyond the upper left corner of the diagram and gradually creeps downward and to the left. If pH is approximately ~8, the dominant reaction at this early stage is:

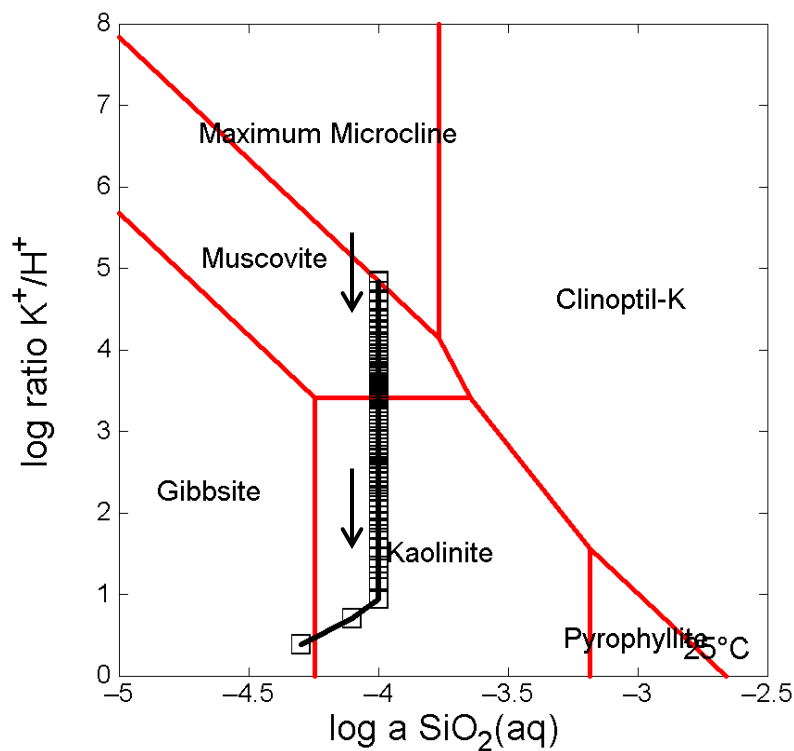
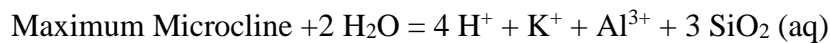
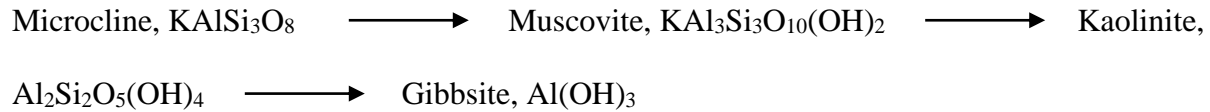


Fig. 15. Solubility diagram for dissolution of microcline in a closed system at 25°C. The reaction trace of geochemical mixing in Fig. 14 is projected as open squares onto the diagram. The reaction trace shows the sequence of mineral forms during freshwater and seawater mixing. Model was created using GWB.

Microcline in the initial system first becomes thermodynamically stable during freshwater-saltwater mixing and transforms over time to a sequence of progressively more stable minerals at more acidic state,



Thus basic-high K^+ concentration saline groundwater (Upper left) decrease in K^+ concentration and increase H^+ as they mix together ultimately terminating gibbsite mineral at more acidic state (Fig. 15).

SOLUTE TRANSPORT MODELING

Variable-density groundwater flow and solute transport simulations were conducted along north-south and west-east cross sections in coastal area (Fig. 1). For the purpose of basin-scale hydrologic modeling, coastal strata in the study area are divided into five hydrostratigraphic units (Fig. 2 and 3). Specifically, the simulations aim at evaluating effects of lateral seawater intrusion along the coast and vertical infiltration of surface seawater from intertidal channels. The hydrostratigraphic units of coastal aquifers in the calculations are composed of varying fractions of three types: sand, silt and clay. The cross section domain was divided into 40 columns vertically and 55 rows along stratigraphy in the finite difference grid. The columns have a uniform width (about 4 m) but the block height varies along the cross section with the thickness of the stratigraphic unit. Stratigraphic units were defined based on their sediment composition, which was calculated using mathematical weighted averages from the lithological logs from the BWDB data. Our basin-scale model assumes that the water table along the basin's top boundary lies at the land surface and the pressure along the water table is one atmosphere. The top surface of the basin is open to groundwater and subjected to freshwater recharge. The bottom of the cross section is set to be a no-flow boundary to reflect the low-permeability. The left and right sides of the cross section remain open to groundwater flow. The model calculates a steady state solution for coupled groundwater flow and salt transport by advection, dispersion,

and diffusion. The use of steady state model is based on the assumption that the subsurface flow has adjusted over time to regional water table configuration and distribution of sediment permeability and the regional flow regime experienced little fluctuations over reasonable geologic time. The initial conditions were a hydrostatic distribution for pressure and a vertical diffusive gradient for salinity. The topographic relief across the basin surface provides the head for the regional flow regime and downward recharge of freshwater. We calculate the evaluation of porosity and permeability of each sediment buried, using correlation (Table 2) compiled by Bethke et al. (1993).

Table 2. Correlations used in the hydrologic simulations to calculate porosity and permeability of Basin strata in the Ganges delta aquifers.

| | Porosity ^a | | | Permeability ^b | | |
|----------------|-----------------------|---------------------|----------|---------------------------|----|-----------|
| | ϕ_0 | b, km ⁻¹ | ϕ_1 | A | B | k_x/k_z |
| Coarse sand | 0.40 | 0.50 | 0.05 | 15 | 3 | 10 |
| Medium Sand | 0.40 | 0.50 | 0.05 | 15 | 1 | 10 |
| Fine Sand | 0.40 | 0.50 | 0.05 | 15 | -1 | 10 |
| Very fine sand | 0.40 | 0.50 | 0.05 | 15 | -2 | 10 |
| Silt | 0.45 | 0.60 | 0.05 | 12 | -2 | 10 |
| Clay | 0.55 | 0.85 | 0.05 | 8 | -5 | 10 |

^aHere $\phi = \phi_0 \exp(-bZ) + \phi_1$, expressed as a fraction; Z is burial depth (km).

^bHere $\log k_x (\mu\text{m}^2) = A\phi + B$.

The diffusion coefficient D^* is assumed to be $1.5 \times 10^{-5} \text{ cm}^2/\text{sec}$ in the simulations. The values of dispersivity and permeability tend to increase with the scale of observation due to geologic heterogeneity (Wheatcraft and Tyler 1988; Gelhar et al. 1992) thus the variations in dispersivity and permeability represent sources of uncertainty in modeling salinity distribution in aquifers.

These dispersivity values used in the simulations are in the same ranges as those used in the simulations large-scale migration of salt plumes or brines (Konikow and Bredehoeft 1974; Domenico and Robbins 1985; Person and Garven 1994). Rising sea level can cause lateral and vertical infiltration of seawater into freshwater-bearing aquifers near the coast and along the tidal

river channels, respectively. Lateral infiltration models were constructed along the north-south transect NS (Fig. 2) by setting a salinity concentration of 0.5 molal of surface seawater and 0 modal for land surface exposed to freshwater recharge. Each graphic output displays simulated groundwater flow, salinity distribution, a salinity contour at 1000 ppm, and a seawater-freshwater interface, with a salinity of 0.5 molal (of seawater) represented by red, 0 molal (of freshwater) denoted by white, and a zone of mixing and diffusion along the interface displayed in yellow. The size of the zone of diffusion is controlled by the dispersive characteristics (see equations) of the geologic layers (Freeze and Cherry 1979). In sensitivity analysis, the freshwater table heights (corresponding to surface topographic elevation), relative to sea level, were adjusted lower based on varying sea level rise scenarios of 0.5 meter, 1 meter, and 1.5 meter. Sensitivity analysis was also performed by increasing the slope of the “water depth” variable, which increase the hydraulic gradients that push the front of seawater back toward the ocean. Vertical infiltration models were constructed for east-west transect (Fig. 16 f, g) by setting a salinity concentration of 0.3 molal for surface water in tidal channels (assuming seawater invades and occupy water columns along channels) that intersect. Sensitivity analysis was performed by adding a low-permeability ($k = 10^{-8}$ darcy) confining clay layer below the uppermost aquifer impacted by surface seawater. This sensitivity analysis was conducted to investigate the presence of low-permeability clay confining layer may block or limit the downward vertical infiltration of seawater into deeper aquifers, which may explain higher water salinity in the shallow aquifer than in the deep aquifer. For the purpose of hydrologic modeling, coastal sediments in the study area are divided into 3 aquifers like shallow, main aquifers and deep with a depth less than 400 meters (Fig. 2 and 3). The modeling results (Fig. 16) show that the groundwater flow in study area is dominated by a local rather than a regional system, with undulations in the water table

controlled by local topographic highs and lows. Recharge areas occur mainly at local topographic highs, and discharge areas occur at nearby topographic lows. These recharge and discharge zones are represented in the Basin2 models by flow arrows; downward flow arrows denote recharge areas, and upward flow arrows denote discharge areas. The maximum flow velocity predicted by this model is on the order of 13.6 m/year near the recharge and discharge areas.

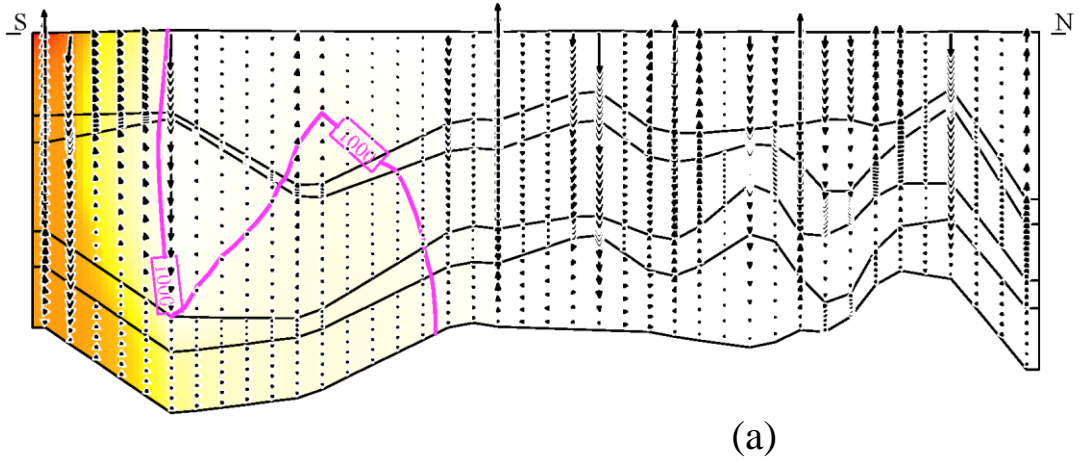
Density-driven groundwater flow occurs where there is a contrast in groundwater salinity in the aquifers, where saltwater migrates vertically or laterally in response to pressure gradients exerted by the density variation between saline water and freshwater (Bethke et al., 2003; Penny et al., 2003). Density-driven groundwater flow predicted in the study area is associated with lateral intrusion and vertical infiltration of high salinity seawater

Lateral seawater intrusion model

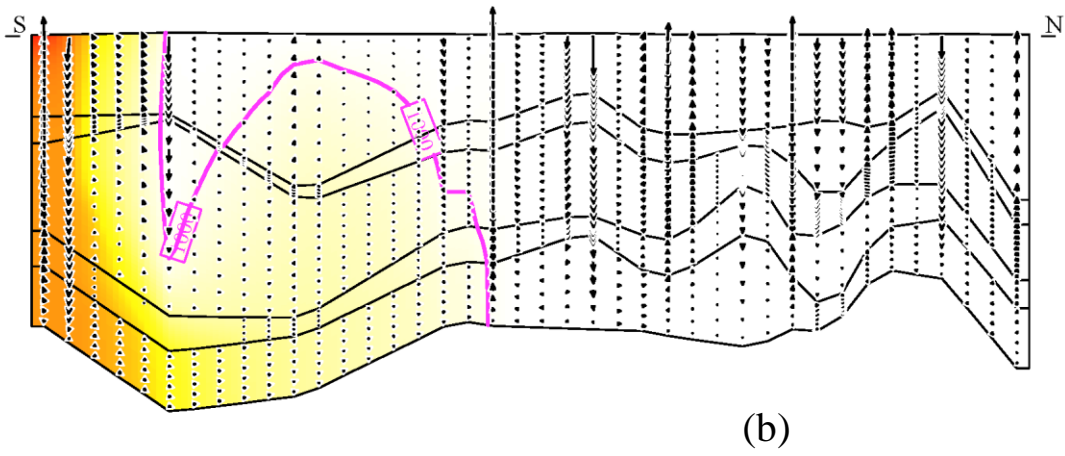
The first set of modeling simulates groundwater flow and solute (salt) transport influenced by lateral saltwater intrusion for three sea level rise scenarios at 0.5 meter (Fig 16 a), 1 meter (Fig. 16 b), and 1.5 meter (Fig. 16 c). The model calculates a steady state solution for coupled groundwater flow and salt transport by advection and dispersion. Both topographically and density-driven flow are included in the simulations. Figures 16a to 16e show various degrees of lateral saltwater intrusion with the seawater-freshwater interface dipping landward, which is consistent with the shape of the saltwater wedge predicted by the Ghyben-Herzberg relation (Ghyben 1888; Herzberg 1901):

$$Z_s = 40 Z_w$$

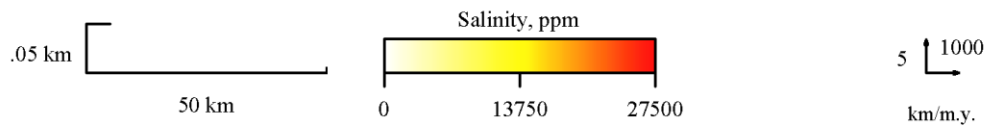
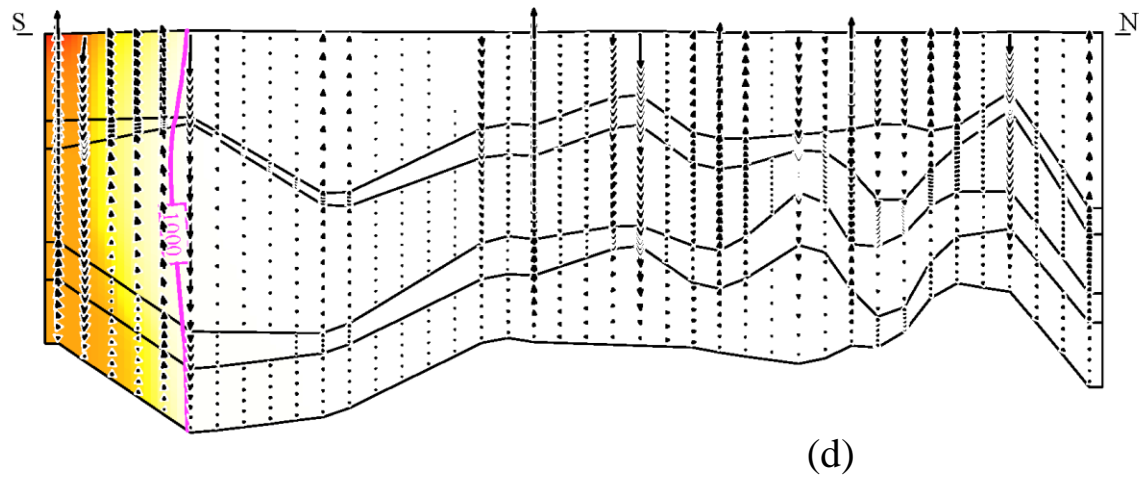
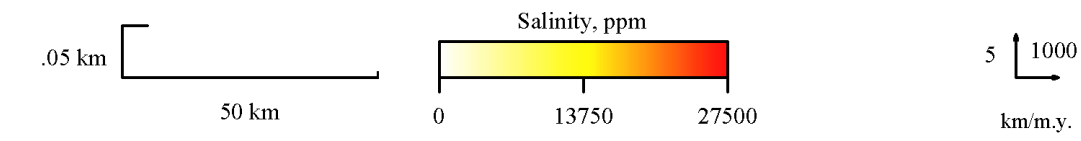
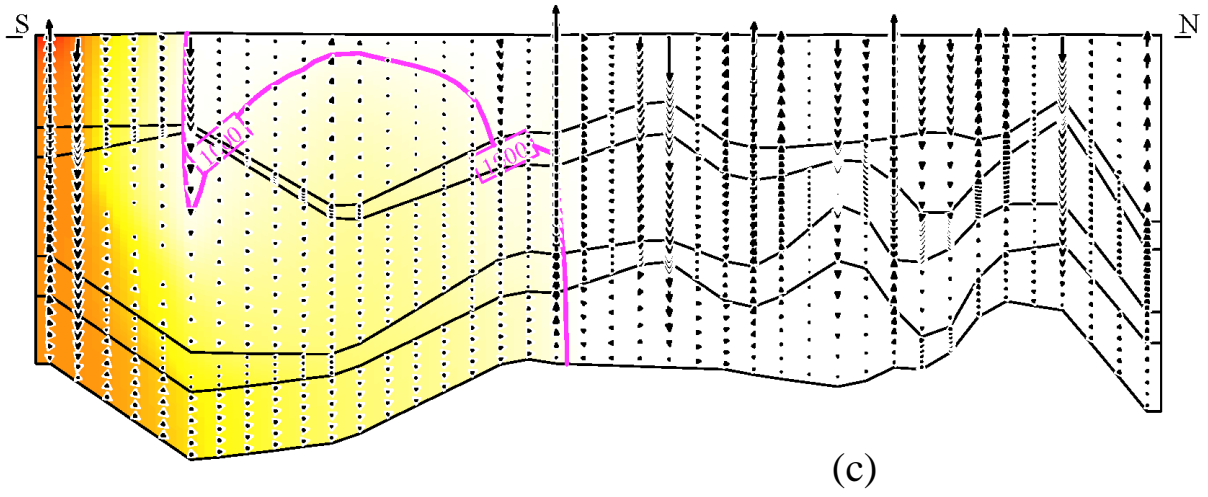
Where Z_s is the depth of the saltwater interface below sea level and Z_w is the height of freshwater above sea level. In the 0.5 m scenario, the predicted seawater-freshwater interface, defined as groundwater salinity of 1000 ppm, is located approximately 31, 87 kilometers inland at the bottom of the main and deep aquifers. The interface is located approximately 28 kilometers inland at the bottom of the shallow aquifer. At a 1 meter sea level rise (Fig. 16b), the seawater-freshwater interface is moving landward and upward, located approximately 96, 103 kilometers inland at the bottom of the main aquifer and deep aquifers whereas approximately 28 kilometers inland at the bottom of the shallow aquifer. Figure 16 c shows a 1.5 meter sea level rise, where the seawater-freshwater interface moves farther landward and extends approximately 87, 106 kilometers inland at the bottom of the main and deep aquifer and approximately 30 kilometers inland at the bottom of the shallow aquifer. According to actual field salinity data (Fig. 17), the interface of 500-1000 $\mu\text{s/cm}$ EC (or 320 - 641 ppm) are located farther inland (in many locations more than 100 km from coast line) as compared to those predicted by lateral intrusion models, indicating that water salinization processes may be influenced by other mechanisms (i.e., vertical infiltration via tidal channels or groundwater pumping). The predicted seawater-freshwater interfaces in Figures 16a-16c only consider lateral saltwater intrusion from oceans and reflect a steady state which has fully adjusted to specified boundary conditions of freshwater table and sea level. Figure 16d shows results of the sensitivity analysis for lateral intrusion models, which was performed to illustrate how a higher hydraulic gradient of freshwater may control the front of lateral intrusion. This was done by raising the elevation of the existing topographic high by 1 meters and creating steeper hydraulic gradients



(a)



(b)



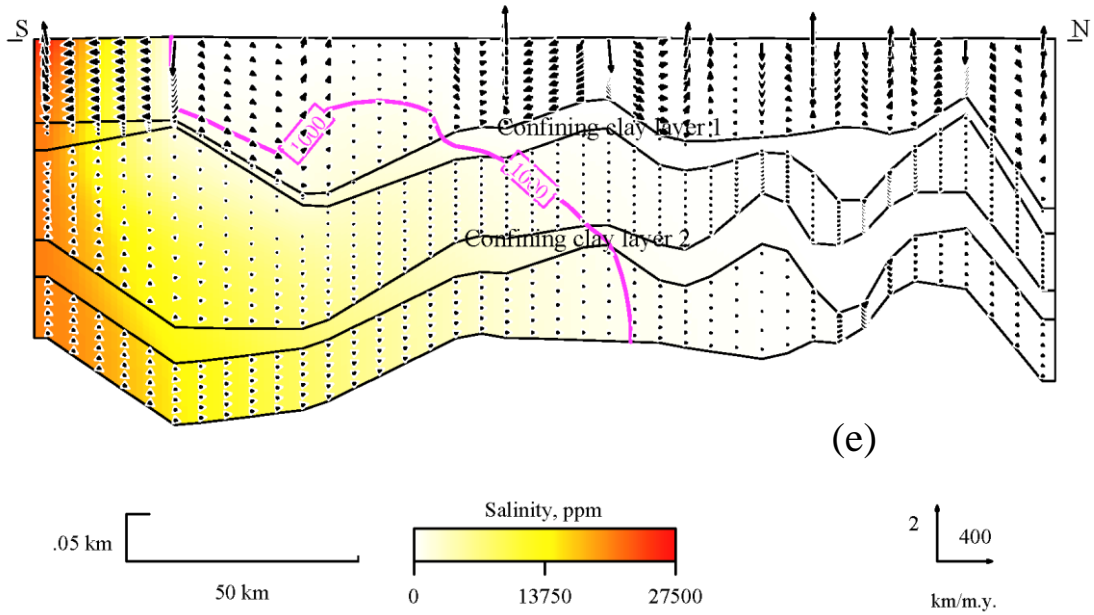


Fig.16 .Plot showing predicted groundwater flow and salinity distribution along N-S cross-section. Color map concentration of groundwater shows spatial distribution of Cl. Arrows show magnitude and flow direction; (a) Lateral intrusion model with 1000 ppm salinity contour, 0.5 meter sea level rise; (b) Lateral intrusion model with 1000 ppm salinity contour, 1 meter sea level rise; (c) Lateral intrusion model with 1000 ppm salinity contour, 1.5 meter sea level rise; (d) Sensitivity analysis for lateral intrusion model was performed during 1 meter sea level rise by increasing freshwater flux in upstream area ; (e) Lateral intrusion model at 1 meter sea level rise with confining clay.

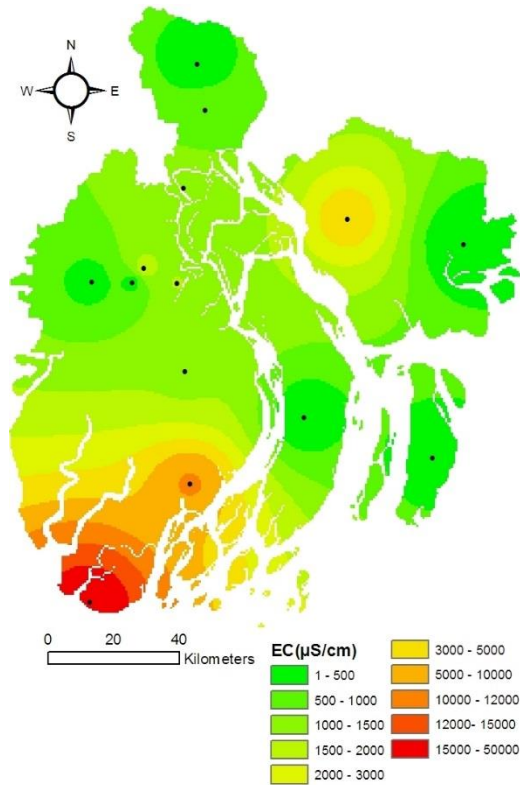


Fig.17. Spatial distribution of electrical conductivity (EC) in the deep aquifer (>250 m depth) of the study area showing lesser salt content in groundwater in the northern side. The southwestern areas show higher contents of salt which are migrating landward.

in the downgradient (southward) direction of fresh groundwater flow. The sensitivity analysis was performed on the 1 meter sea level rise scenario. Flow arrows in Figure 16d show that the higher hydraulic gradient allows fresh groundwater to move farther toward the south, which helps to push the front of seawater ocean-ward and results in a smaller seawater wedge, a steeper slope of the seawater-freshwater interface, and a smaller zone of diffusion. In the southern areas of coastal Bangladesh, the shallow aquifer does not meet drinking water quality standards, so the main aquifer that is currently used for potable water will begin to be contaminated with seawater. A deeper aquifer (>300 m) is being investigated as a potential drinking water source for Bangladesh (BWDB 2014), but lateral intrusion may have already impacted the deep aquifer in the southern areas. The actual stratigraphy is much more complexly interbedded than the models

are able to define, and stratigraphy complexity may not be captured by existing well logs. A sensitivity analysis shows that the presence of a confining clay layer in the coastal area could restrict the saltwater to the shallow layers and shows a large landward zone of diffusion in the deep layers (Fig. 16e). Nevertheless, the models presented in this study represent a first order effort to approximate the effects of sea level rise on the potential extent of lateral saltwater intrusion in coastal area of the Ganges delta.

Vertical seawater infiltration model

Vertical infiltration of surface seawater in the study area is a result of density-driven downward flow from brackish tidal channels into the layers below, and models of groundwater flow and salinity distribution were constructed along east-west transect (Fig. 18). There is evidence that vertical infiltration of seawater is already occurring in southern Bangladesh, which was shown by high EC concentrations in tidal channels (Fig. 19) and in the underlying shallow aquifer. Sensitivity analysis was also performed by adding a confining clay layer below the shallow aquifer and above the deep aquifer in the area of the tidal channels for the EW transect (Fig. 18 b). The salinity distribution maps and water quality data indicate that the salinity is much higher in the shallow aquifer (up to 17,200 mg/l) than in the deep aquifer (up to 7,861 mg/l), indicating that the downward infiltration of seawater may be locally blocked by the presence of a confining layer between shallow and deeper aquifers (Fig. 20).

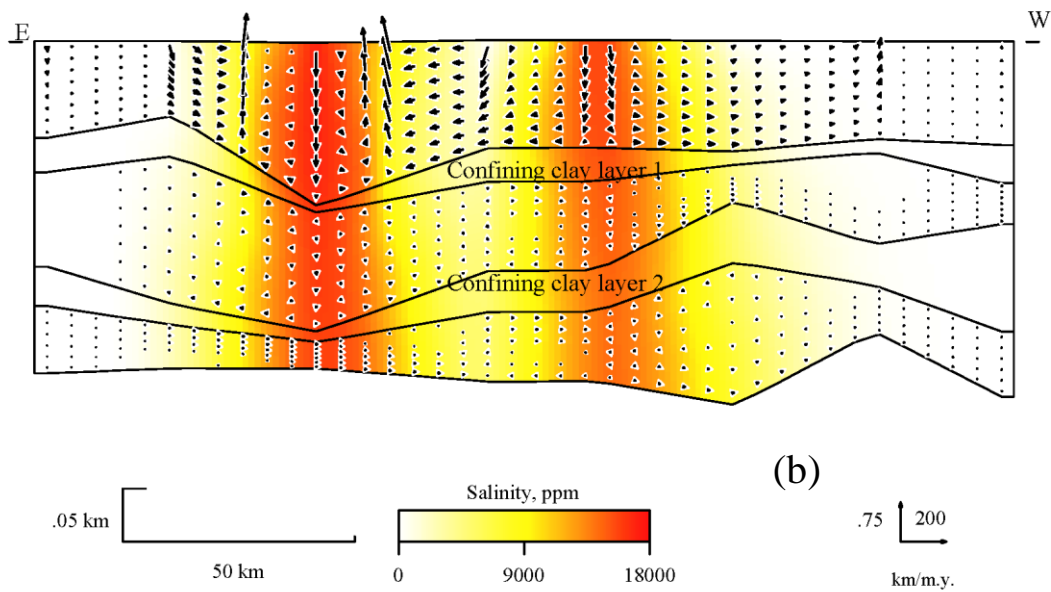
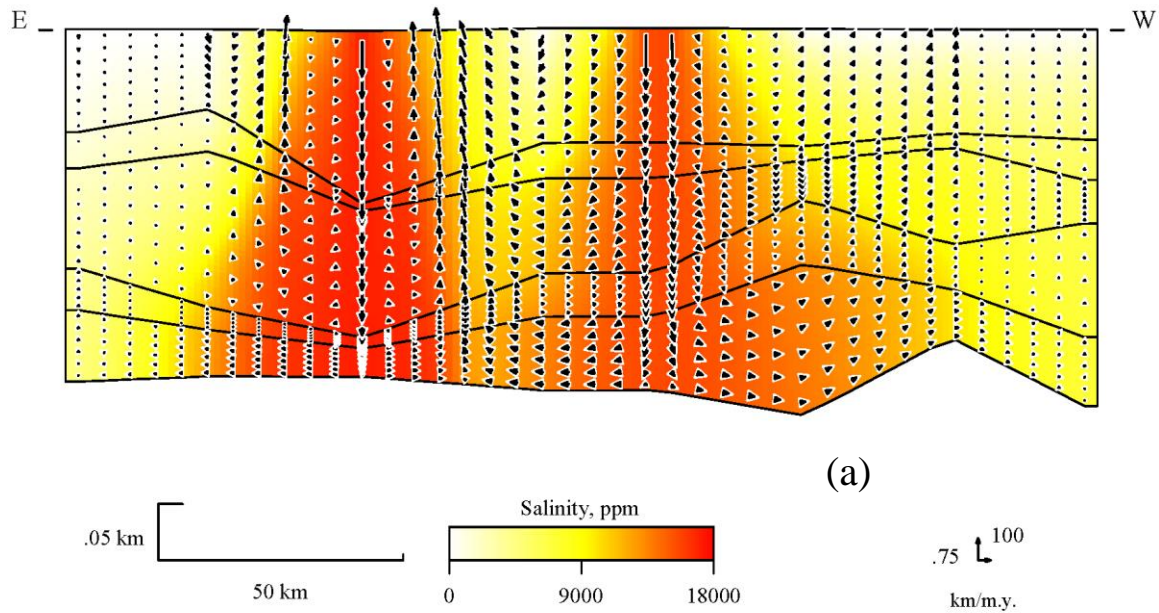


Fig.18. Plot showing predicted groundwater flow and salinity distribution along E-W cross-section. Color map concentration of groundwater shows spatial distribution of Cl. Arrows show magnitude and flow direction; (a) Vertical infiltration model in study area; (b) Sensitivity analysis for vertical infiltration model with confining clay.

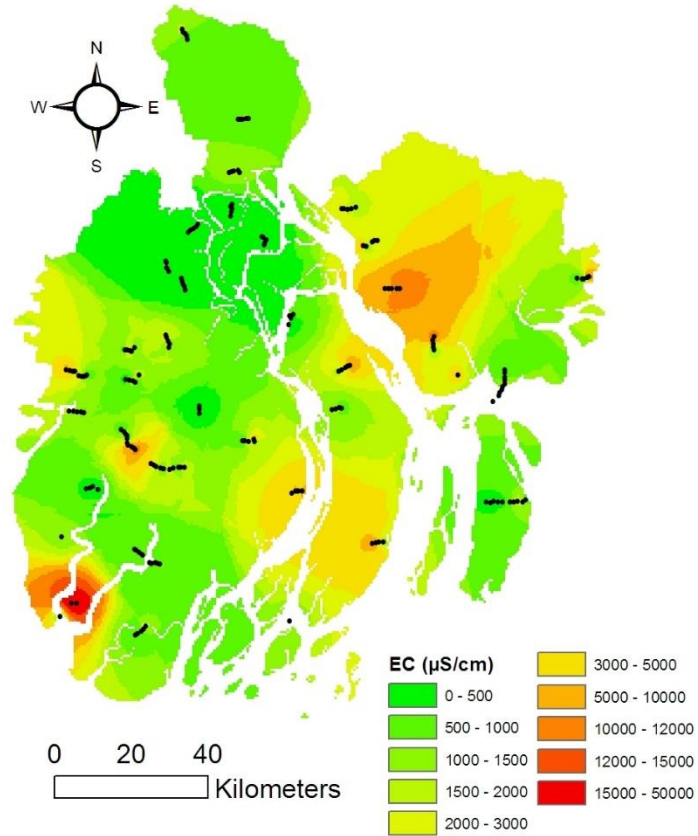
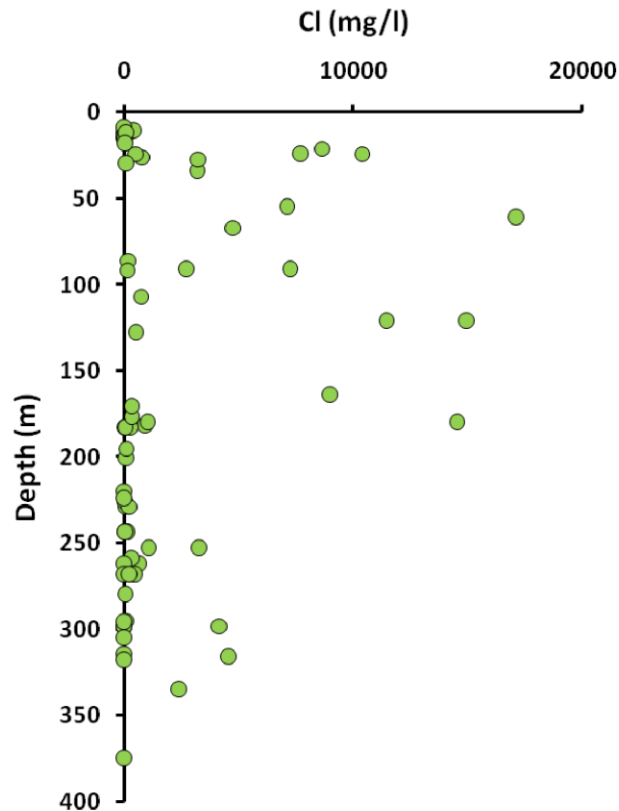


Fig.19 . Spatial distribution of electrical conductivity (EC) in the shallow aquifer or upper aquifer (20-150m depth) of the study area. This shows that most shallow aquifers are contaminated with surface seawater by vertical infiltration from intertidal channels.



result the high salinity plume originated from the smaller tidal channel extends only to the bottom of the shallow aquifer to the west (Fig. 19). The sensitivity analysis model for this transect (Fig. 18 b) shows the highest concentrations of salinity restricted to the shallow aquifer by the presence of a confining clay layer, which blocks the downward penetration of the saline plume to the deeper aquifer. The models of this transect shows seawater to the east along the Bay of Bengal, where small islands have isolated freshwater lenses surrounded by brackish water in the diffusion zone. To the east, Meghna channel shows intrusion of brackish water to the bottom of the main aquifer with a wide zone of diffusion. In the west, brackish water still reaches the bottom of the main aquifer, but the confining clay layer minimizes the size of the dispersion area.

CONCLUSIONS

This study combines hydrologic, geologic, geochemical data to develop an integrated reactive transport model for groundwater, solutes, isotopes and fluid mixing in the coastal aquifer systems. The results indicate that chemical composition of groundwater evolves by physical mixing, cation exchange, and geochemical processes as it moves downgradient into the subsurface.

Major ions exhibits non-conservative additional or removal relative to physical mixing, which may be influenced by a combination of ion exchange (i.e., clay-bound Ca^{2+} and Mg^{2+} are displaced by Na^+ and K^+) and carbonate diagenesis (carbonate precipitation or dolomitization). Groundwater of the Ganges delta is more saturated with respect to calcite and dolomite but undersaturated to gypsum. However, at high salinities ion-exchange predominates as suggested by 2:1 removal of Na^+ relative to addition of Ca^{2+} , the lower amount of depletion in H^+ and the higher saturation state with respect to calcite. The three groundwater types that were identified are carbonates groundwater, groundwater associated with seawater, and ground water of meteoric origin. An HFE Diagram showed that concentrations of Ca^{2+} and Na^+ identifies the direct and reverse ion exchange reactions as well as freshwater and seawater mixing. Dolomitization might take place in the coastal aquifer of the Ganges delta and would always appear in waters and would be indicated by a $\Delta\text{Mg}^{2+}/\Delta\text{Ca}^{2+}$ ratio of more than 1, negative ΔMg^{2+} and positive ΔCa^{2+} . Geochemical model of fluid mixing suggests precipitation of dolomite which produces H^+ and drives the reaction of potassium feldspar to produce muscovite and gibbsite.

Lateral saltwater intrusion models show a saltwater wedge consistent with the shape predicted by the Ghyben-Herzberg relation and intrusion can be limited by an increase in the freshwater hydraulic gradients in the southern direction or by the presence of a confining clay layer in the coastal region. Vertical saltwater infiltration models show small tidal channels have a local effect with a infiltration into the shallow layers, while larger tidal channels affect a larger area and can reach the deeper layers and main aquifer and the presence of a confining clay layer restricts intrusion of saline water into the deeper layers, but can cause a larger zone of diffusion in both shallow and deeper strata.

Both field data and numerical modeling results show that high salinity groundwaters are present in shallow aquifers, suggesting that shallow aquifers may be contaminated by downward infiltration of saline surface water from tidal channels. Presence of less saline groundwater in deeper aquifers may be derived from lateral saltwater intrusion from the ocean. Local groundwater flow system dominates in both shallow and main aquifers, where groundwater recharges in local topographically high areas and discharge toward near-by topographically low areas.

ACKNOWLEDGMENTS

I would like to thank Bangladesh Water Development Board, Bangladesh for allowing me to use groundwater dataset for the coastal area of Bangladesh. I also appreciate grants-in-aid from Auburn University, Geological Society of America, and Alabama Academy of Sciences.

REFERENCES

- Ahmed, K.M., Bhattacharya, P., Hasan, M.A., Akhter, S.H., Alam, S.M.M., Bhuyian, M.A.H., Imam, M.B., Khan, A.A., Sracek, O., 2004. Arsenic enrichment in groundwater of the alluvial aquifers in Bangladesh: An overview. *Applied Geochemistry* 19,181–200.
- Ali, A., 1996. Vulnerability of Bangladesh to climate change and sea level rise through tropical cyclones and storm surges. *Water, Air, and Soil Pollution* 92,171-191.
- Andersen, M.S., Nyvang, V., Jakobsen, R., Postma, D., 2005. Geochemical processes and solute transport at the seawater-freshwater interface of a sandy aquifer. *Geochimica et Cosmochimica Acta* 69, 3979-3994.
- Appelo, C.A.J., 1994. Cation and proton exchange, pH variations and carbonate reactions in a freshening aquifer. *Water Resource Research* 30,2793–2805.
- Appelo, C.A.J., 1996. Multicomponent ion exchange and chromatography in natural systems. In *Reactive Transport in Porous Media* (eds. Lichtner P. C., Steefel, and C. I. Oelkers E. H.). *Review in Mineralogy* 34, 193–222.
- Badaruddin, S., Werner, A.D., Morgan, L.K., 2015. Water table salinization due to seawater intrusion. *Water Resource Research* 51, doi:10.1002/ 2015WR017098.

BWDB, 2014. Hydro-geological Study and Mathematical Modelling to Identify Sites for Installation of Observation Well Nests, Selection on Model Boundary, Supervision of Pumping test, Slug test, Assessment of Different Hydro-geological Parameters, Collection and Conduct Chemical Analysis of Surface water and Groundwater, Tech. Report, 7 Volumes, BWDB, Dhaka

Barker, A.P., Newton, R.J., Bottrell, H.S., 1998. Processes affecting groundwater chemistry in a zone of saline intrusion into an urban sandstone aquifer. *Applied Geochemistry* 13,735-749.

Bear, J., 1972. *Dynamics of Fluids in Porous Media*. Elsevier, Amsterdam

Bear, J., Cheng, A.H.D., Sorek, S., Ouazar, D., Herrera, I., 1999. *Seawater Intrusion in Coastal Aquifers: Concepts, Methods and Practices. Theory and Application of Transport in Porous Media* 14, Kluwer Acad., Norwell, Mass

Beekman, H.E., 1991. Ion chromatography of fresh and salt water intrusions. Ph.D. thesis, Vrije University, Amsterdam

Bethke, C.M., 2008. *Geochemical and biogeochemical reaction modeling*, Cambridge University Press, 543 pp.

Bethke, C.M., Lee, M.-K., Quinodoz, H.A.M., Kreiling, W.N., 2003. *Basin modeling with Basin2: A guide to using Basin2, B2plot, B2video, and B2view*, Hydrogeology Program, University of Illinois, Urbana–Champaign

BGS and DPHE, 2001. Arsenic Contamination of Groundwater in Bangladesh, Vol. 2. Final Report, British Geological Survey Technical Report, WC/00/19, <<http://www.bgs.ac.uk/As>> accessed on January 7, 2016.

Boluda-Botella, N., Gomis-Yagu, V., Ruiz-Bevia, F., 2008. Influence of transport parameters and chemical properties of the sediment in experiments to measure reactive transport in seawater intrusion. *Journal of Hydrology* 357, 29–41.

Chang, S.W., Clement, T.P., Simpson, M. J., Lee, K.-K., 2011. Does sea-level rise have an impact on saltwater intrusion? *Advances in Water Resources* 34(10), 1283–1291, doi:10.1016/j.advwatres.2011.06.006.

Copper, H.H.Jr., Kohout, F.A., Henry, H.R., Glover, R.E., 1964. Seawater in coastal aquifers: U.S. Geologic Survey Water-Supply Paper 161C, 84pp.

Cuthbert, M.O., Burgess, W.G., Connell, L., 2002. Constraints on sustainable development of arsenic-bearing aquifers in southern Bangladesh. Part 2: preliminary models of arsenic variability in pumped groundwater. In: Hiscock, K.M., Rivett, M.O., Davison, R.M. (Eds.), *Sustainable Groundwater Development*. Geological Society of London 193, 165–179.

Domenico, P.A., Robbins, G.A., 1985. The displacement of connate water from aquifers. Geological Society of America Bulletin 96, 328-335, doi: 10.1130/0016-7606(1985)96

Drever, J.I., 1988. The Geochemistry of Natural Waters. 2nd Edition, Prentice Hall, Englewood Cliffs, 473pp.

Freeze, R.A., Cherry, J.A., 1969. Groundwater, 1st ed., Prentice Hall, Upper Saddle River, NJ, USA

Gelhar, L.W., Welty, C., Rehfeldt, K.R., 1992. A critical review of data of field-scale dispersion in aquifers. Water Resource Research 28, 1955-1974, doi: 10.1029/92WR00607

Ghosh, S., De, S., 1995. Source of the arsenious sediments at Kachua and Itina, Habra Block, North 24 Parganas, West Bengal – a case study. Indian Journal of Earth Sciences 22(4), 183-189.

Ghyben, W.B., 1888. Nota in verband met de voorgenomenputboring nabij Amsterdam (Notes on the probably results of proposed well drilling near Amsterdam, in Dutch), Tijdschrift van het Koninklijk Inst. van Ing

Giménez, E., Morell, I., 1997. Hydrogeochemical analysis of salinization processes in the coastal aquifer of Oropesa (Castellón, Spain). Environmental Geology 29, 118–131.

Harvey, C.F., Swartz, C.H., Badruzzaman, A.B.M., Keon-Blute, N., Yu, W., Ali, M.A., Jay, J., Beckie, R., Niedan, V., Brabander, D., Oates, P.M., Ashfaque, K.N., Islam, S., Hemond, H.F., Ahmed, M.F., 2002. Arsenic mobility and groundwater extraction in Bangladesh. *Science* 298, 1602–1606.

Herzberg, A., 1901. Die Wasser versorgung der Nordseebäder (The water supply of part of the North Sea coast in Germany, in German), *J. Gasbeleucht, Wasserversorg* 44, 815-819.

Horneman, A., van Geen, A., Kent, D., Mathe, P.E., Zheng, Y., Dhar, R.K., O'Connell, S., Hoque, M., Aziz, Z., Shamsudduha, M., Seddique, A., Ahmed, K.M., 2004. Decoupling of As and Fe release to Bangladesh groundwater under reducing conditions. Part I: Evidence from sediment profiles. *Geochimica Cosmochimica Acta* 68, 3459–3473.

Holser, W.T., 1979. Trace elements and isotopes in evaporates, *Short Course Notes Mineral Society of America* 6, 295-346.

Howard, K.W.F., Lloyd, J.W., 1983. Major ion characterization of coastal saline ground waters. *Ground Water* 21, 429–437.

Howard, K.W.F., Mullings, E., 1996. Hydrochemical analysis of ground-water flow and saline incursion in the Clarendon Basin, Jamaica. *Ground Water* 34, 801–810.

Islam, F., Gault, A., Boothman, C., Polya, D., Charnock, J., Chatterjee, D., Lloyd, J., 2004. Role of metal-reducing bacteria in arsenic release from Bengal delta sediments. *Nature* 430, 68-71.

Kim, Y., Lee, K.-S., Koh, D.-C., Lee, D.-H., Lee, S.-G., Park, W.-B., Koh, G.-W., Woo, N.-C. 2003. Hydrogeochemical and isotopic evidence of groundwater salinization in a coastal aquifer: A case study in Jeju volcanic island, Korea. *Hydrogeology Journal* 270, 282–294.

Konikow, L.F., Bredehoeft, J.D., 1974. Modeling flow and chemical quality changes in an irrigated aquifer system. *Water Resource Research* 10, 546-562, doi:10.1029/WR010i003p00546

Lacombe, P.J., Carleton, G.B., 1992. Saltwater intrusion into fresh groundwater supplies southern Cape May Country, New Jersey, 1890-1991: The Future Availability of Groundwater Resources, *American Water Resources Association* 287-297.

Lee, M.-K., Bethke, C.M., 1996. A model of isotopic fractionation in reacting geochemical systems. *American Journal of Science* 296, 965–988.

Lee, M.-K., Griffin, J., Saunders, J.A., Wang, Y., Jean, J., 2007. Reactive transport of trace elements and isotopes in Alabama coastal plain aquifers. *Journal of Geophysical Research* 112, G02026, doi:10.1029/2006JG000238.

Lee, M.-K., Natter, M., Keevan, J., Guerra, K., Saunders, J.A., Uddin, A., Humayun, M., Wang, Y., Keimowitz, A.R., 2013. Assessing effects of climate change on biogeochemical cycling of

trace metals in alluvial and coastal watersheds. *British Journal of Environmental and Climate Change* 3, 44-66.

LGED (Local Government Engineering Department) and BRGM (Bureau of Geological and Mining Research) , 2005. Municipal Services Project, Groundwater Resources and Hydrogeological Investigations in and around Khulna City.Final Report. Dhaka

Liss, P.S., 1976. Conservative and non-conservative behavior of dissolved constituents during estuarine mixing, in Burton JD, Liss PS eds *Estuarine chem*: New York, Academic Press, 93-130.

Majumder, R.K., Halim, M.A., Saha, B.B., Ikawa, R., Nakamura, T., Kagabu, M., Shimada, J., 2011.Groundwater flow system in Bengal Delta, Bangladesh revealed by environmental isotopes. *Environmental Earth Sciences* 64, 1343-1352, 10.1007/s12665-011-0959-2.

Margaritz, M., Goldenberg, L., Kafri, U., Asad, A., 1980.Dolomite formation in the seawater-freshwater interface. *Nature* 287, 622-624.

McArthur, J.M., Ravenscroft, P., Safiullah, S., Thirlwall, M.F. 2001. Arsenic in groundwater: testing pollution mechanisms for sedimentary aquifers in Bangladesh. *Water Resource Research* 37, 109-117.

Mercado, A., 1985. The use of hydrogeochemical patterns in carbonate sand and sandstone aquifers to identify intrusion and flushing of saline water. *Ground Water* 23, 635–645.

Michael, H.A., Voss, C.L., 2009. Controls on Groundwater Flow in the Bengal Basin of India and Bangladesh: Regional Modeling Analysis. *Hydrogeology Journal*, doi: 10.1007 /s10040-008-0429-4.

Michael, H.A., Voss, C.L., 2009. Estimation of Regional-Scale Groundwater Flow Properties in the Bengal Basin of India and Bangladesh. *Hydrogeology Journal*, doi: 1 0.1 007/s 1 0040-009-0443-1.

MOEF, 2006. Impact of Sea-Level Rise on Land Use Suitability and Adaptation Options: Coastal Land Zoning in the Southwest. Bangladesh, Dhaka, 160pp.

Morgan, L.K., Stoeckl, L., Werner, A.D., Post, V.E.A., 2013. An assessment of seawater intrusion overshoot using physical and numerical modeling, *Water Resource Research* 49, 6522–6526, doi:10.1002/wrcr.20526.

MPO, 1987. The Groundwater Resources and Its Availability for Development. Harza Engineering USA in Association with Sir MacDonald and Partners, UK, Met Consultant, USA and EPC Ltd., Dhaka. 180pp.

Person, M.E., Garven, G., 1994. A sensitivity study of the driving forces on fluid flow during continental-rift basin evolution, *Geological Society of America Bulletin* 106, 461-475, doi: 10.1130/0016-7606(1994)106.

Rahman, A.A., Ravenscroft, P., 2003. *Groundwater Resources and Development in Bangladesh*. 2nd ed. Bangladesh: Centre for Advanced Studies, University Press Ltd. Dhaka

Rashid, M., Islam, M.S., 1995. Adaptation to climate changes for sustainable development of Bangladesh agriculture. Presentation at third session of the technical committee of the Asian and Pacific Center for Agriculture Engineering and Machinery, November 20-21, Beijing

Reilly, T.E., Goodman, A.S., 1985. Quantitative analysis of saltwater–freshwater relationships in groundwater systems—a historical perspective. *Hydrogeology Journal* 80,125–160.

Rogers, K.G., Goodbred, S.L., Jr, Mondal, D.R., 2013. Monsoon sedimentation on the 'abandoned' tide-influenced Ganges-Brahmaputra delta plain. *Estuarine, Coastal and Shelf Science* 131, 297-309.

Saunders, J.A., Lee, M.-K., Uddin, A., Mohammad, S., Wilkin, R.T., Fayek, M., Korte, N.E., 2005. Natural arsenic contamination of Holocene alluvial aquifers by linked tectonic, weathering, and microbial processes. *Geochemistry, Geophysics, Geosystems* 6, doi:10.1029/2004GC000803.

Sayles, F.L., Mangelsdorf, P.C., 1977. The equilibrium of clay minerals with sea water: Exchange reactions. *Geochimica et Cosmochimica Acta* 41, 951-960.

Schmerge, D.L., 2001. Distribution and origin of salinity in the surficial and intermediate aquifer systems, Southwestern Florida. U.S. Geological Survey Water-Resources Investigations Report 01-4159. 46pp.

Shamsudduha, M., Uddin, A., 2007. Quaternary shoreline shifting and hydrogeologic influence on the distribution of groundwater arsenic in aquifers of the Bengal Basin. *Journal of Asian Earth Sciences* 31(2), 177-194.

Shamsudduha, M., Marzen, L.J., Uddin, A., Lee, M.-K., Saunders, J.A., 2009. Spatial relationship of groundwater arsenic distribution with regional topography and water-table fluctuations in the shallow aquifers in Bangladesh. *Environmental Geology* DOI: 10.1007/s00254-008-1429-3.

Smith, B.S., 1988. Groundwater flow and saltwater encroachment in the Upper Floridian aquifer Beaufort and Jasper Counties, South Carolina: U.S. Geological Survey Water-Resources Investigations Report 87-4285, 61pp.

Stuyfzand, P.J., 1993. Hydrochemistry and hydrology of the coastal dune area of the western Netherlands. Ph.D thesis, Nieuwegein, KIWA

Todd, D.K., 1980. *Groundwater Hydrology* 2nd edition Wiley, New York

Uddin, A., Lundberg, N., 1998. Unroofing history of the Eastern Himalaya and the Indo-Burman ranges: Heavy-mineral study of Cenozoic sediments from the Bengal basin, Bangladesh. *Journal of Sedimentary Research* 68, 465-472.

Uddin, A., Shamsudduha, M., Saunders, J.A., Lee, M.-K., Ahmed, K.M., Chowdhury, M.T., 2011. Mineralogical profiling of arsenic-enriched alluvial sediments in the Ganges-Brahmaputra floodplain in central Bangladesh. *Applied Geochemistry* 26, 470-483.

UNDP, 1982. Groundwater Survey, The hydrogeological Condition of Bangladesh. UNDP Technical Report DP/UN/BGD-74-009/1, 113pp.

Watson, T.A., Werner, A.D., Simmons, C.T., 2010. Transience of seawater intrusion in response to sea-level rise. *Water Resource Research* 46, W12533, doi:10.1029/2010WR009564.

Werner, A.D., Lockington, D.A., 2006. Tidal impacts on riparian salinities near estuaries. *Journal of Hydrology* 328, 511–522, doi:10.1016/j.jhydrol.2005.12.011.

Werner, A.D., Simmons, C.T., 2009. Impact of sea-level rise on sea water intrusion in coastal aquifers. *Ground Water* 47, 197–204.

Werner, A.D., Ward, J.D., Morgan, L.K., Simmons, C.T., Robinson, N.I., Teubner, M.D., 2012. Vulnerability indicators of seawater intrusion. *Ground Water* 50(1), 48–58, doi:10.1111/j.1745–6584.2011.00817.x.

Wheatcraft, S.W., Tyler, S.W., 1988. An explanation of scale-dependent dispersivity in heterogeneous aquifer using concepts of fractal geometry. *Water Resource Research* 24,566-578, doi: 10.1029/WR024i004p00566.

Wigley, T.M.L., Plummer, L.N., 1976. Mixing of carbonate waters. *Geochimica et Cosmochimica Acta* 42, 1117-1139.

Xue, Y., Wu, J., Ye, S., Zhang, Y., 2000. Hydrogeology and hydrogeochemical studies for salt water intrusion on the south coast of Laizhou Bay, China. *Ground Water* 38, 38–45.

Yamanaka, M., Kumagai, Y., 2006. Sulfur isotope constraint on the provenance of salinity in a confined aquifer system of the southwestern Nobi Plain, central Japan. *Journal of Hydrology* 325, 35-55.

Zheng, Y., Stute, M., Van Geen, A., Gavrieli, I., Dhar, R., Simpson, J., Ahmed, K.M., 2004. Redox control of arsenic mobilization in Bangladesh groundwater. *Applied Geochemistry* 19, 201–214.

CHAPTER 2

**TRACE ELEMENT REACTIONS IN THE GROUNDWATER FLOW SYSTEM OF
COASTAL AQUIFERS OF THE GANGES DELTA**

ABSTRACT

In this chapter, I combine groundwater geochemistry and numerical modeling techniques to study the reactive transport of metals and isotopes in the coastal aquifer of the Ganges delta. Geochemical data show that the elevated concentrations of Fe, Mn, Sr and As can be correlated with high pH and HCO₃. These geochemical correlations suggest that elevated metal concentrations may be derived from bacterial iron and manganese reduction. Higher $\delta^{13}\text{C}$ values are found to be correlated with elevated Fe, Mn and As concentrations and high pH values of groundwater. This result implies carbon isotopic fractionation processes associated with bacterial Fe(III) reduction and Mn(IV) reduction. Sediment and groundwater chemistry show strong correlation, which suggest that higher concentrations of trace elements in coastal aquifer (down to 350 m) were derived from same mineral sources and bacterial mediate geochemical processes. Petrographic and SEM studies of sediments show the formation of biogenic siderite and pyrite in sediments associated with Fe- rich groundwater. Filamentous and circular structures within layer suggest microbial involvement in lamina development through providing a growth medium for sulfate-reducing bacteria and potentially a template for mineral growth. Siderite and pyrite occur together as spheroids in which pyrite forms the center and siderite forms an outer rim, which is consistent with the redox sequence of mineral precipitation predicted by the geochemical

modeling. Geochemical modeling of bacterial Fe(III) and Mn(IV) reduction shows that chemical precipitation of iron and manganese minerals could control mobility and concentrations of Fe, Mn, and As in coastal aquifers. The continuous bands of siderite and pyrite observed in this study suggest that both Fe and SO₄ reduction in groundwater must have fluctuated over time. Variations of Fe and SO₄ reduction can be explained by Eh conditions consistent with Fe-Mn oxyhydroxide dissolution or SO₄ reduction.

INTRODUCTION

Qualitative and quantitative research on groundwater flow systems in coastal aquifers has advanced rapidly during the most recent decade. This development has happened in light of increasing water supply needs in coastal areas. Studies by Penny et al. (2003) and Lee et al. (2007) gave essential insight into geochemical development of groundwater on the basis of regional groundwater chemistry and mineral saturation states. Chapelle and Knobel (1983) and Appelo (1994) have explored the inorganic ion exchange between aquifer sediments and recharging fresh groundwater. Saunders et al. (2005) tried to link the elevated arsenic and occurrence of other trace elements in groundwater with the retreat of continental glaciation at the end of the Pleistocene, which led to the rise of sea level during the Early to Middle Holocene, and deposition of alluvium and extensive marsh and peat and finer sediments in Bengal lowlands. During the Pleistocene, mechanical weathering of rocks in source areas (e.g., Himalayas, Indian Shield, and Indo-Burman Mountains) was enhanced due to mountain building activities and glaciations. The aquifer sands in the Bengal Basin were largely derived from physical weathering and erosion at a time of extended glaciation in the Himalayas, but the intensity of chemical weathering was limited by the low temperatures during erosion (McArthur et al., 2004; Mukherjee and Fryar, 2008). Various geochemists have utilized $\delta^{13}\text{C}$ isotopes to

evaluate groundwater sources (Clark and Fritz, 1997) and biomineralization processes (Zhang et al., 2001; Romanek et al., 2003). Microbial activities have been investigated and reported in coastal plain aquifers of South Carolina and Alabama (Lovley et al., 1990; Murphy et al., 1992; Lovley and Chapelle, 1995; Chapelle, 2001; Penny et al., 2003; Park et al., 2006) where different microorganisms are responsible for iron, manganese, and sulfate reduction reactions that fundamentally change groundwater chemistry. Because biogeochemical reactions in regional aquifers are not well understood, hydrologists have utilized numerical modeling techniques to study hydrological transport processes and the nature of water-sediment-bacteria interaction (Bethke, 1989; Plummer et al., 1990; Lee and Saunders, 2003; Lee et al., 2005). Reactive transport processes have been investigated to measure the processes and to pinpoint the controlling parameters for As release to the groundwater (Postma et al., 2007; Charlet et al., 2007, Fendorf et al., 2010). To date, little has been done to evaluate or demonstrate reactive transport processes in coastal aquifers of the Ganges delta.

Since 1972, fresh groundwater aquifer has been an important resource and continues today supplying water for more than 40 million residents in 19 districts in Bangladesh (UNDP, 1982). Despite its importance as a major source of water supply, the origin of trace metals, the nature of water-sediment-bacteria interaction, freshwater recharge rates, and the influence of microbial processes on water chemistry remain poorly understood. Field data indicate that high metal concentrations correlate with elevated HCO_3 levels and pH values in groundwater (Penny et al., 2003). Fe(III)-reducing bacteria, found in the Fe- and Mn-rich groundwaters in western Alabama (Penny et al., 2003), could utilize organic matter deposited in sediments to grow and reduce Fe(III) and Mn(IV) oxides; this bacterial reduction process would release aqueous Fe^{2+} ,

Mn^{2+} , As^{3+} and other trace metals such as Sr^{2+} and Ba^{2+} that have been adsorbed or coprecipitated by oxides. The main objectives include (1) determining the sources of elevated trace

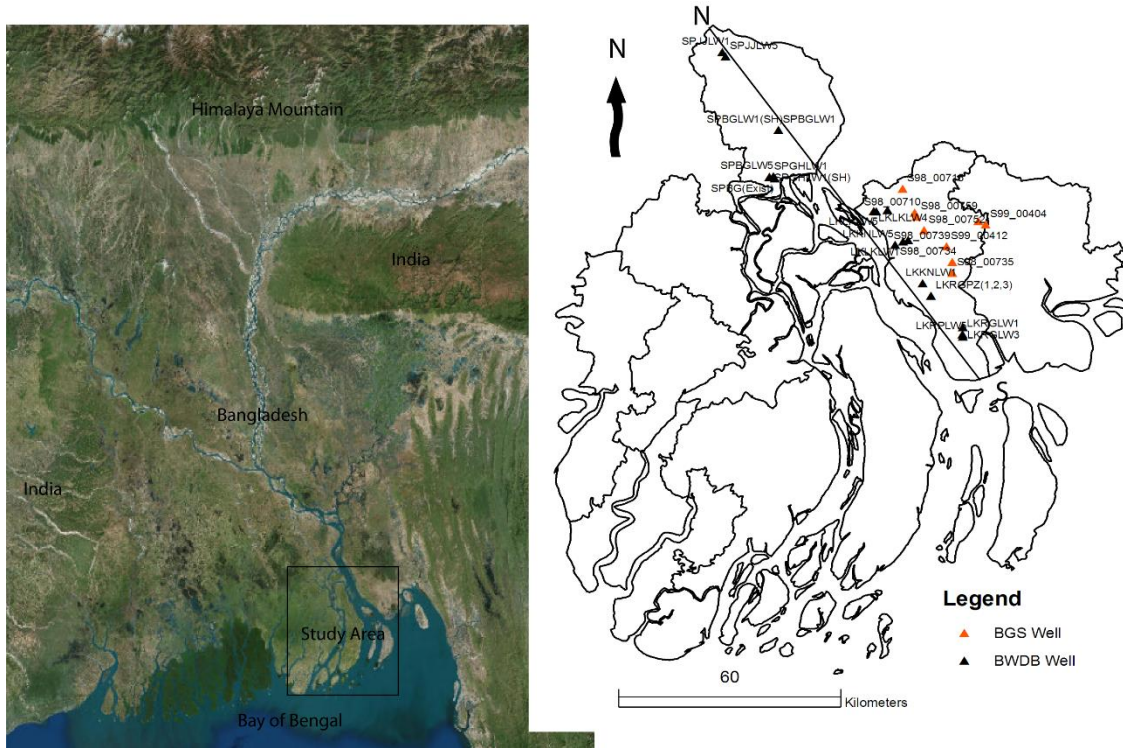


Fig. 1. Map showing well locations in the study area. Ganges, Brahmaputra, and Meghna are the major rivers in Bangal Basin, which formed one of the largest delta systems in the world called Ganges Delta. N-S transect line shown on this map corresponding to hydrostratigraphic cross-sections is shown in Figure 2.

metals concentration , alkalinity, and reactive carbon in the coastal aquifer; (2) characterizing the chemical alteration processes in Fe-rich groundwater and their effects on groundwater chemistry.

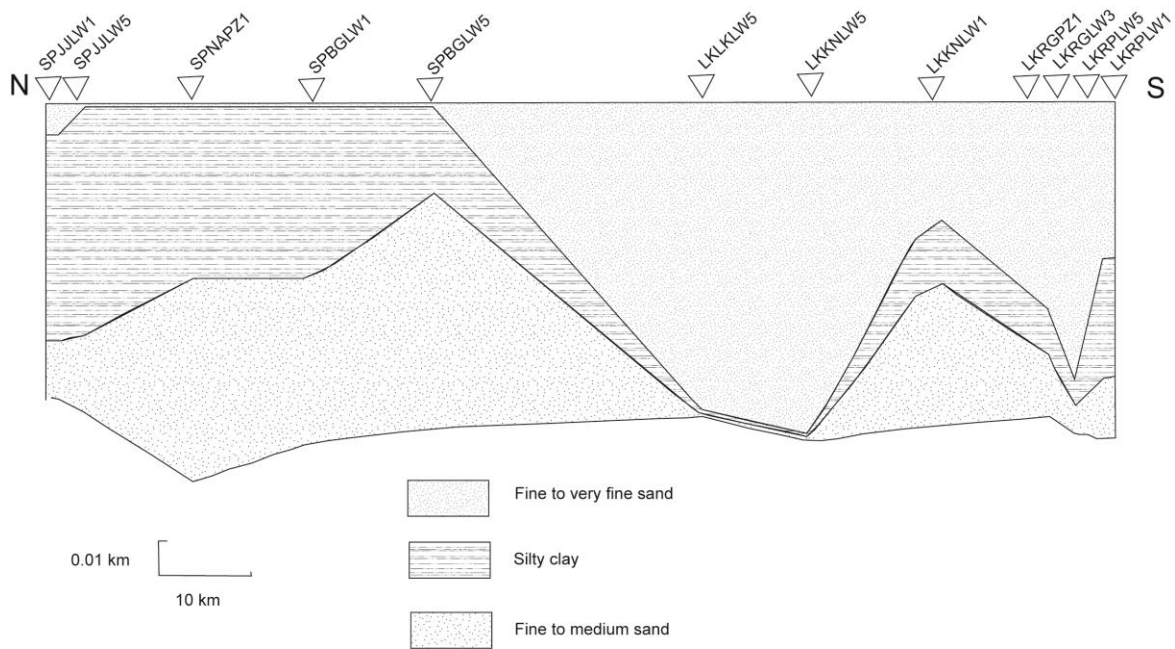


Fig. 2. Generalized N-S hydrostratigraphic cross section in study area is showing the Quaternary stratigraphic units. Transect line is shown in Figure 1. The cross section is constructed based on lithostratigraphic data from (BWDB, 2014).

GEOLOGY AND HYDROGEOLOGY

The Bengal Basin, located in South Asia has been the major depocenter of sediment flux from the Himalayas and Indo-Burman ranges drained by the Ganges–Brahmaputra–Meghna, the largest river system in the world. The basin (Fig. 1) is bounded by the Himalayas to the distant north, the Shillong Plateau, a Precambrian massif to the immediate north, the Indo-Burman ranges to the east, the Indian Craton to the west, and the Bay of Bengal to the south (Uddin and Lundberg, 1998). The basin includes one of the largest delta complexes (GBM delta) in the world, covering a vast portion of the basin filled with about $5 \times 10^5 \text{ km}^3$ of sediments (Johnson, 1994). Thick sedimentary deposits of the basin fill have been uplifted significantly along the north and eastern margins of the Sylhet trough in the northeast and along the Chittagong fold belts of eastern Bangladesh (Uddin and Lundberg, 1998). The western part of the Bengal Basin,

which covers the West Bengal of India, is mostly drained by the Bhagirathi Hooghly river, a major distributary channel of the Ganges river.

The study area in southern Bangladesh belongs to the Meghna river flood plain physiographic province of the Ganges delta. The area is of low relief with surface elevations ranging from 25–1000 m above sea level in the north to about <1–5 m in the south. The study area consists of unconsolidated Quaternary sediments overlies thick sequences of folded Pliocene sand, shale and siltstone (BGS and DPHE, 2001). The downdip portion of coastal plain is a thick (>100 m) wedge of sedimentary strata dipping south-southeast and trending approximately north-south (Fig. 2).

This study focuses on the hydrology and geochemistry of the shallow portion of the coastal aquifers situated in the eastern coastal plain. The study area stretches approximately 120 km from the updip area and trends southeast toward the Bay of Bengal. Groundwater migrates generally to the south in central-east direction of the potentiometric surface sub-parallel to the general topographic slope of the area.

Generally, this aquifer shows a leaky to confining behavior during short-term pumping tests, but the well response is more consistent with an unconfined aquifer over longer-term pumping tests (MPO, 1987). This portion of the coastal aquifers is subject to significant recharge and contains fresh water resources that are important for public water supplies and also used for agricultural needs such as shrimp production, livestock production, and irrigation. Groundwater in updip portion is mainly dilute (total dissolved solid <1000 mg/l) to the southern coastal plains where groundwater at shallow depths are saline due to geochemical reactions with soils during recharge and leaching of salts, and mixing with seawater (Aggarwal et al., 2000).

A previous study (UNDP, 1982) indicates that shallow aquifer is made up of “shoestring” lenses of sand at multiple levels inter-bedded with silt and clay. But over large areas there is sufficient overlapping and intersection of the sand lenses to consider this as one complex hydraulic unit. This aquifer unit is hydraulically connected with the rivers. Fining upward sequences are observed in the alluvial floodplain deposits throughout the basin demonstrating the shifting of the meandering channels. Silt and clay predominate in the updip area forming a surficial aquitard, generally 70 m thick. The upper aquitard is not present in the downdip parts of the study area. Below the silty clay aquitard, aquifers that occur along the Meghna river valleys are composed of fine to medium sand with occasional coarse sand and gravels. Hydraulic conductivity of this sand unit is typically 20-30 m/day with a transmissivity of 500-3000 m²/day (BGS and DPHE, 2001).

METHODS

Groundwater chemistry

Twenty-one monitoring wells were sampled in January 2016. The wells are located roughly along the flow paths from north to south and are maintained by the Bangladesh Water Development Board (Fig. 1). An in-situ portable suction pump (Honda GX) was used to purge the wells before collecting the representative groundwater samples in the aquifer. At least three well volumes of water were removed and all water quality parameter readings were stabilized before sampling. After the well purging was completed, samples were analyzed for water quality parameters (temperature, pH, Eh, and electrical conductivity) in the field using mobile hand-held meters to avoid any parameter changes during sample transportation and storage. After a water sample was collected in a clean beaker, it was then filtered with a 45 micron pore-diameter filter

and acidified with 5% nitric acid for preservation before trace metal and cation analysis using the inductively coupled plasma mass spectrometry (ICP-MS) at Auburn University (Agilent 7900). A second sample was filtered for anion analysis using ion chromatography (IC) at Auburn University (Dionex DX-120). Additional twelve groundwater chemistry data in the coastal Bangladesh study area were acquired from a public database (DPHE and BGS, 2001) for isotopic data interpretation.

Sediment chemistry

A total of 15 samples were selected from both LKLN2 (Lakshmiipur Sadar) and SPNA (Shariatpur Naria) sediment cores based on the information on groundwater trace element concentrations at different depths in the study area. Frequency of sediment sampling for geochemical analysis was primarily based on the occurrences of higher trace element concentration in groundwaters. Samples were dried in an oven at about 50°C for approximately 24 h. Approximately 20 g of dried sediment for each sample was crushed with a mortar and pestle. Powdered sediment samples were sent to the Bureau Veritas in Vancouver, Canada for analysis. In the lab, 0.50 g sample was leached with 3 mL 2–2–2 HCl–HNO₃–H₂O at 95 °C for 1 h and diluted to 10 mL, and analyzed with the inductively coupled plasma-mass spectrometry (ICPMS) method. A total of 36 major and trace elements were analyzed from the selected 15 sediment samples.

Sediment petrography

Well-cutting samples were taken from two monitoring wells in the study area, including LKLK2 and SPNA. Samples were obtained from wells core storage facility at Bangladesh Water Development Board in Dhaka, Bangladesh. Well cuttings consisted mainly of unconsolidated coastal plain sediments that were collected and boxed at the time of well installation. Twelve thin-sections were prepared from core sands at different depth intervals. Samples were analyzed using a petrographic microscope (Nikon model no. E600 POL) attached with a photomicrographic setup. Sediments grains exhibiting secondary mineral overgrowths in Fe- and Mn-rich zones were analyzed by a field emission scanning electron microscope (SEM).

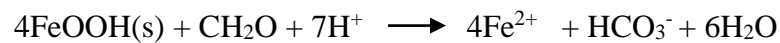
Reaction path modeling

Modeling bacterial Fe(III)- and Mn(IV)-reduction along the flow path of the coastal aquifer was accomplished by using a numerical program Geochemist's Workbench (GWB) (Bethke, 1996; Lee and Bethke, 1996). The initial conditions of the model were set according to the geochemical data of SPJLW-01 well upstream of the coastal aquifers. The model first equilibrates to SPJLW-01 well groundwater at 25 °C and assumes that initial concentrations of Fe and Mn reflect equilibrium with Fe (OH)₃ and pyrolusite (MnO₂) in aquifers under aerobic conditions. The simulation then linearly reduces redox potential (Eh) from 700 mV to -200 mV and simultaneously titrates 500 mmol of organic material (acetate) into 1 kg of fluid in the initial system. By lowering the Eh of the system and adding organic material, the model can simulate those mineralogical and geochemical reactions under which bacterial Fe(III)- and Mn(IV)-reduction occur. The model provides insights on groundwater geochemical evolution and the sequence of mineral reactions during the reductive dissolution of Fe- and Mn-oxides.

RESULTS AND DISCUSSION

Major ion and trace element geochemistry

For groundwater along the flow path in the coastal aquifers, significantly higher HCO_3^- and pH (Fig. 3b) can be related to parallel increases in Fe, Mn, Sr, and As concentrations (Fig. 3a). These connections suggest that increased Fe, Mn, Sr and As concentrations might be derived from bacterial iron and manganese reduction similar to that proposed by (Saunders et al., 1997, 2005; Zobrist et al., 2000)



Where CH_2O represents organic matter. Eh values of Fe-rich groundwaters range from -20 to -100 mV (Table 1). This iron reduction would discharge metals and raise HCO_3^- of groundwater at the expense of H^+ , natural organic carbon, and iron oxides.

Table 1. Groundwater chemistry in study area. Well ID locations are also shown in Figure 1.

11

| Well ID | Depth (m) | Na (ppm) | Mg (ppm) | K (ppm) | Ca (ppm) | Mn (ppb) | Fe (ppb) | As (ppb) | Sr (ppb) | Co (ppb) | Cu (ppb) | Zn (ppb) | HCO3 (ppm) | Cl (ppm) | NO3 (ppm) | SO4 (ppm) | pH | Eh (mv) | Screened Interval (m) |
|-------------|-----------|----------|----------|---------|----------|----------|----------|----------|----------|----------|----------|----------|------------|----------|-----------|-----------|------|---------|-----------------------|
| LK1LW1 | 85 | 1977.9 | 228.7 | 43.8 | 169.1 | 1358.5 | 6536.2 | 27.5 | 2177.0 | 1.7 | 2.1 | 195.5 | 283.5 | 3453.4 | 26.0 | 398.0 | 9.19 | -6 | 75-68 |
| LK1LW3 | 94 | 1019.7 | 164.0 | 29.9 | 159.4 | 552.0 | 19.2 | 20.4 | 1605.9 | 0.4 | 120.6 | 628.1 | 77.4 | 2296.9 | 15.3 | 125.0 | 6.56 | -21.5 | 84-90 |
| LK1LW4 | 88 | 1513.1 | 245.2 | 38.3 | 233.0 | 104.8 | 43.9 | 20.1 | 2412.6 | 0.3 | 10.6 | 45.6 | 270.3 | 2938.2 | 27.2 | 325.0 | 6.44 | -24.5 | 78-84 |
| LK1LW5 | 85 | 1242.3 | 236.0 | 26.3 | 270.1 | 330.0 | 123.5 | 22.7 | 2253.2 | 0.4 | 76.2 | 1244.8 | 222.0 | 2590.0 | 30.3 | 284.0 | 7.97 | -11.4 | 74-81 |
| LKRG1W1 | 82 | 1626.2 | 378.2 | 22.9 | 523.0 | 627.6 | 10272.0 | 17.9 | 3496.2 | 0.0 | 3.7 | 1.0 | 351.5 | 3892.8 | 35.7 | 410.0 | 6.98 | -5.2 | 72-78 |
| LKRG1W3 | 91 | 2355.8 | 416.8 | 17.8 | 762.1 | 3164.6 | 50304.2 | 18.2 | 3771.4 | 0.1 | 2.1 | 359.7 | 424.4 | 5294.8 | 37.4 | 634.5 | 8.28 | -110 | 81-87 |
| LKRG2Z | 268 | 6.4 | 21.7 | 14.3 | 88.7 | 139.8 | 2957.9 | 1.1 | 202.5 | 0.1 | 1.2 | 31.7 | 365.5 | 25.1 | 5.6 | 5.0 | 7.92 | -23 | 254-260 |
| LKKN1W5 | 94 | 2653.0 | 338.4 | 54.6 | 194.1 | 395.8 | 742.9 | 18.7 | 2553.4 | 0.8 | 1.7 | 106.9 | 348.8 | 4726.3 | 35.0 | 591.0 | 8.06 | 22.3 | 84-90 |
| LKKN1W1 | 91 | 3196.3 | 422.6 | 69.4 | 256.9 | 215.5 | 1884.8 | 13.6 | 3318.0 | 0.4 | 2.1 | 201.5 | 445.8 | 6221.9 | 40.6 | 654.0 | 8.11 | 3.5 | 81-87 |
| LKRN1W5 | 94 | 656.0 | 97.1 | 22.8 | 113.2 | 952.5 | 24.8 | 158.0 | 823.2 | 0.8 | 2.3 | 176.1 | 94.8 | 1448.1 | 39.0 | 92.0 | 7.07 | -27.6 | 84-90 |
| SPGHLW1 | 91 | 1593.6 | 195.0 | 25.8 | 146.7 | 274.7 | 327.1 | 16.3 | 1192.0 | 1.2 | 1.6 | 1.0 | 239.1 | 2997.2 | 30.2 | 380.0 | 7.32 | 8.8 | 81-87 |
| SPBGLW1(SH) | 30 | 105.5 | 24.7 | 7.3 | 55.5 | 53.0 | 5999.0 | 149.5 | 258.6 | 1.0 | 2.3 | 31.8 | 150.0 | 221.1 | 19.2 | 25.0 | 7.91 | -30 | 22-28 |
| SPBGLW5 | 91 | 942.7 | 79.1 | 16.2 | 90.4 | 194.6 | 8018.0 | 45.2 | 709.5 | 1.2 | 4.1 | 1233.1 | 213.5 | 1668.4 | 36.8 | 97.0 | 7.86 | -95.9 | 81-87 |
| LKRG2Z | 182 | 260.7 | 51.1 | 7.8 | 93.6 | 416.2 | 6739.7 | 3.4 | 608.7 | 0.1 | 3.8 | 114.2 | 283.5 | 510.4 | 35.2 | 42.9 | 7.21 | -17.7 | 172-178 |
| LKRN1W3(SH) | 31 | 43.3 | 36.5 | 7.6 | 116.4 | 1171.4 | 68.2 | 26.9 | 429.2 | 0.7 | 2.4 | 75.5 | 355.0 | 113.5 | 30.0 | 45.2 | 8.14 | -19.6 | 23-29 |
| SPGHLW1(SH) | 33 | 322.3 | 37.7 | 15.3 | 50.7 | 53.0 | 434.5 | 119.6 | 311.7 | 0.8 | 1.7 | 27.8 | 203.5 | 540.2 | 20.4 | 24.2 | 8.13 | -25.4 | 25-31 |
| SPBGLW1 | 94 | 234.4 | 16.3 | 9.0 | 20.1 | 322.6 | 1180.6 | 84.8 | 138.3 | 1.2 | 2.8 | 134.9 | 149.0 | 386.5 | 6.9 | 4.4 | 7.67 | -30 | 84-90 |
| SPBG(Exist) | 213 | 426.7 | 6.5 | 2.2 | 13.3 | 11.5 | 374.6 | 0.3 | 161.8 | 0.1 | 1.5 | 49.4 | 105.0 | 617.3 | 11.5 | 28.9 | 7.97 | -40 | 204-210 |
| SPJ1LW1 | 82 | 185.1 | 60.0 | 10.4 | 61.6 | 400.1 | 57.1 | 88.8 | 532.8 | 0.8 | 2.6 | 160.5 | 318.5 | 352.8 | 11.7 | 72.0 | 8.07 | -44.3 | 72-78 |
| SPJ1LW5 | 81 | 229.6 | 17.7 | 3.0 | 57.4 | 1207.4 | 27.8 | 65.1 | 373.3 | 0.7 | 1.0 | 74.2 | 237.9 | 337.9 | 21.8 | 31.0 | 7.77 | -23.6 | 73-79 |
| LKRG2Z | 60 | 5447.4 | 855.2 | 255.5 | 525.8 | 646.7 | 124.2 | 1.3 | 2964.8 | 0.3 | 4.8 | 53.2 | 523.5 | 11632.1 | 16.3 | 701.2 | 7.36 | 30 | 50-56 |

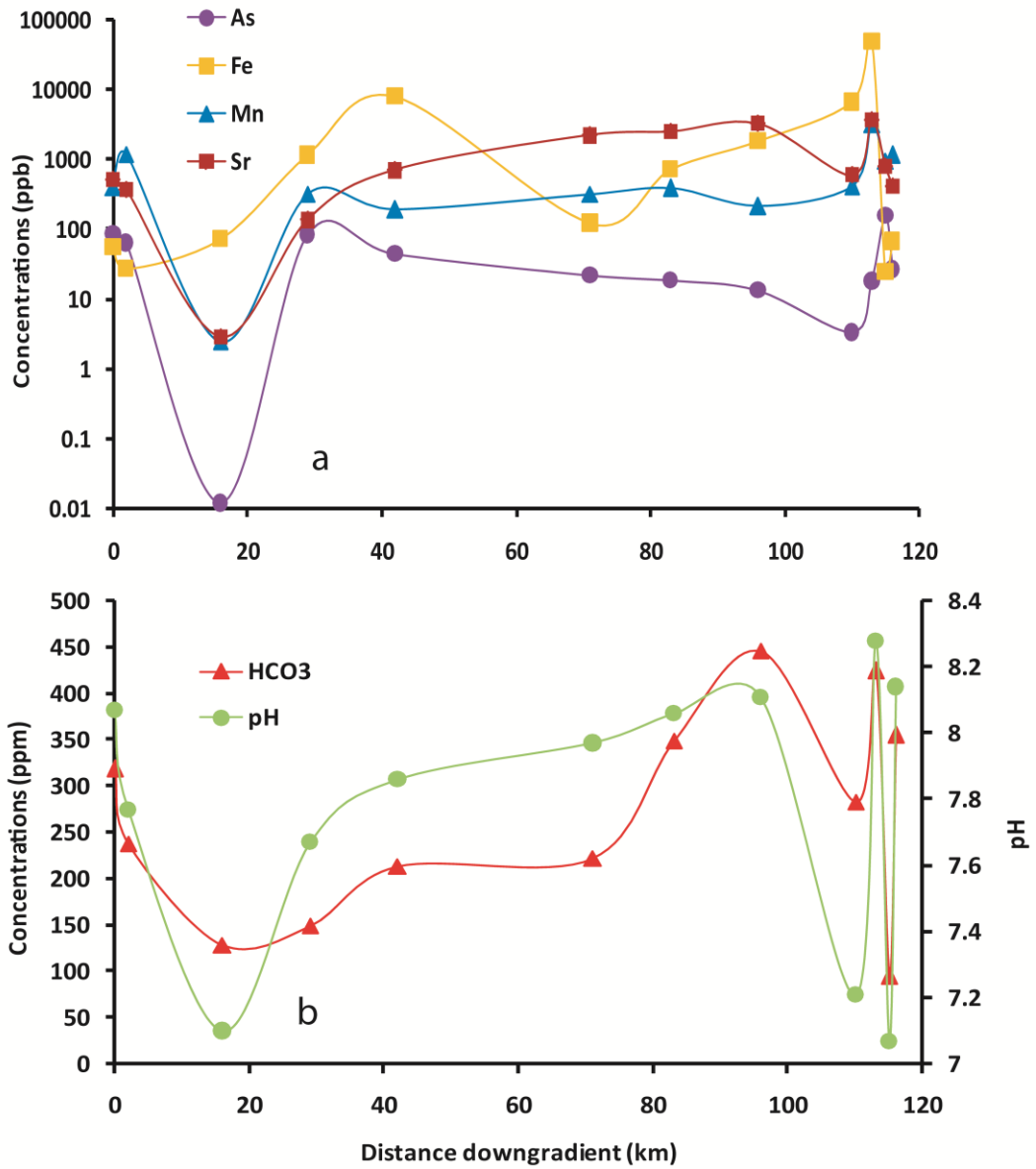


Fig. 3(a) Plot showing As, Fe, Mn, and Sr concentrations of groundwater samples at various distances from updip along the NS transect (Fig. 1) in central Ganges delta (b) HCO₃⁻ and pH along the same transect.

Concentrations of Sr also correlate well with dissolved Fe in the Ganges- Brahmaputra floodplain in the Bengal basin (Dowling et al., 2003; Turner, 2006). The sorbed Sr is subsequently desorbed when the redox conditions become favorable for bacterial iron reduction (Roden et al., 2002; Dowling et al., 2003). Similarly, other trace metals (Cu, Zn, Ba) generally show same trends found in Fe, Mn, and Sr with sequential rise and fall in concentrations.

Downgradient from the upstream area, a sequence of Ca^{2+} , Mg^{2+} , K^+ , and Na^+ dominated groundwater along the flow path (Fig. 4) indicates that ion exchange could control the subsurface water chemistry. Ion exchange and concurrent calcite dissolution may also lead to increase in pH and HCO_3^- of groundwater, much like bacterial Fe- and Mn-reduction, but they mainly release cations (Ca^{2+} , Mg^{2+} , K^+ , Na^+) into solution. Calcite is common in Ganges delta coastal sediments which is usually present as fossil shells and perhaps as cements between minerals (Dowling et al., 2003).

The dissolution of calcite in coastal aquifers results in the exchange of Na with Ca on the replacement substrate (Ex) as follows:



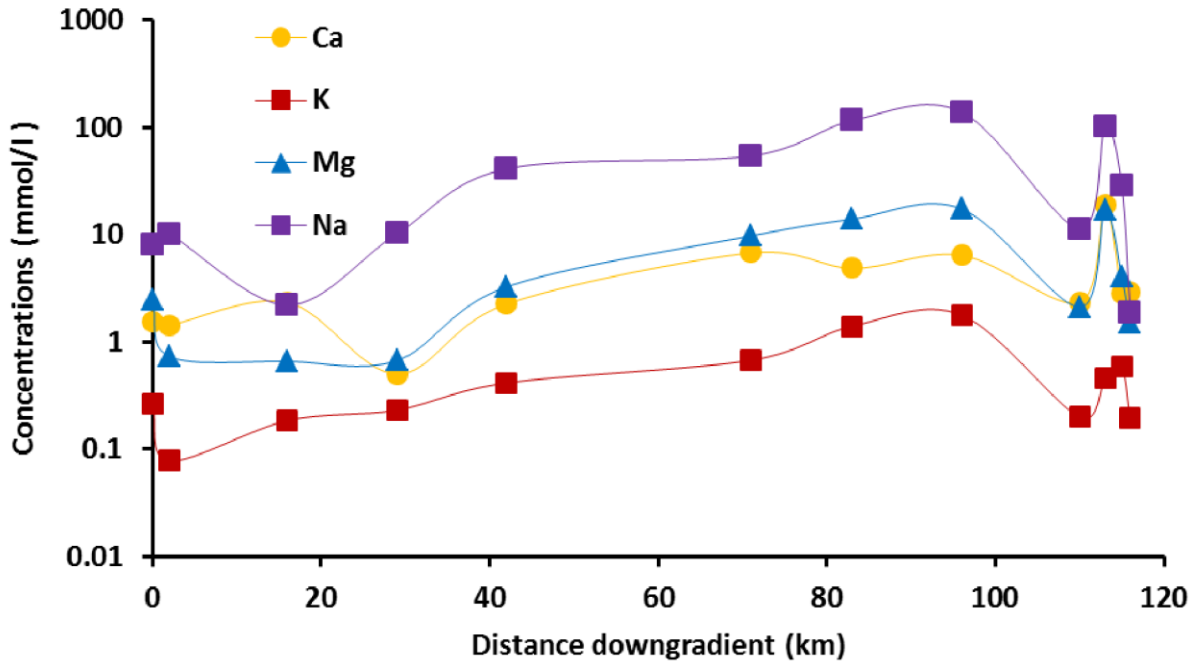


Fig. 4. Plot showing concentrations of dissolved Ca, Mg, K, and Na in the coastal aquifer as function of distance along a flow path in central Ganges delta.

This process would produce a Na-HCO₃ type groundwater with high Na/Cl molar ratios. Ion exchange between clay substrates and groundwater is a selective process. Chapelle and Knobel, (1983) proposed that cations with smaller hydrated radii are held more strongly to exchange sites than those with larger hydrated radii. Moreover, bonded divalent cations tend to be more stable than bonded monovalent cations. The observed sequential peaks of cations (Fig. 4) are generally consistent with the order of cations competing for exchange sites: Ca²⁺ > Mg²⁺ > K⁺ > Na⁺. The sequences of Ca²⁺ and Mg²⁺ are not so widely separated (Fig. 4) probably because both have two positive charges and are so similar in size. Our geochemical data suggest that the dominant water-sediment- bacteria interactions in the shallow coastal aquifers include a combination of microbially mediated Fe(III) and Mn(IV) reduction and ion exchange between groundwater and clay minerals.

Carbon isotope compositions of groundwater

Carbon isotopic signatures of groundwaters (Appendix 1) and coexisting authigenic minerals may be used to interpret relative influences of various geochemical reactions (e.g., bacterial Fe(III)-reduction, methanogenesis, and abiologic ion exchange) that control groundwater chemistry. Because both bacterial Fe(III)-reduction and ion exchange processes can raise the pH and alkalinity of groundwater, Carbon isotopic compositions can be used as a fingerprint that may indicate the relative dominance of biogeochemical process. The $\delta^{13}\text{C}$ compositions in coastal groundwater range from -16.63 ‰ to -12.48‰ (PDB) (Fig. 5). The relatively low $\delta^{13}\text{C}$ values indicate that the reactions controlling alkalinity predominantly involve biogenic sources, including the dissolution of biogenic soil CO_2 and oxidation of organic matter. It is interesting that isotopically heavier carbon (i.e., higher $\delta^{13}\text{C}$ values) generally correlates with elevated Fe and Mn concentrations (Appendix 1) and high pH values in groundwaters (Fig. 6). This remarkable result is unexpected because metabolism of Fe reducing bacteria would add isotopically lighter ^{12}C into groundwater. Figure 6 shows the speciation of various carbon species including dissolved CO_2 , H_2CO_3 , HCO_3^- and CO_3^{2-} of DIC is pH dependent. At low pH (<5), DIC is dominated by dissolved CO_2 , whereas at high pH (>8), DIC is comprised primarily of HCO_3^- and CO_3^{2-} . At 25°C, HCO_3^- and CO_3^{2-} are enriched in ^{13}C by about 9‰ relative to dissolved CO_2 (Clark and Fritz, 1997). Thus as bacterial iron reduction raises pH, the concentration of dissolved CO_2 decreases and that of HCO_3^- increases simultaneously; this perhaps would lead to higher $\delta^{13}\text{C}$ values. It is expected that bacteria may utilize lighter ^{12}C to form biogenic carbonate minerals, making the remaining groundwater relatively enriched in ^{13}C .

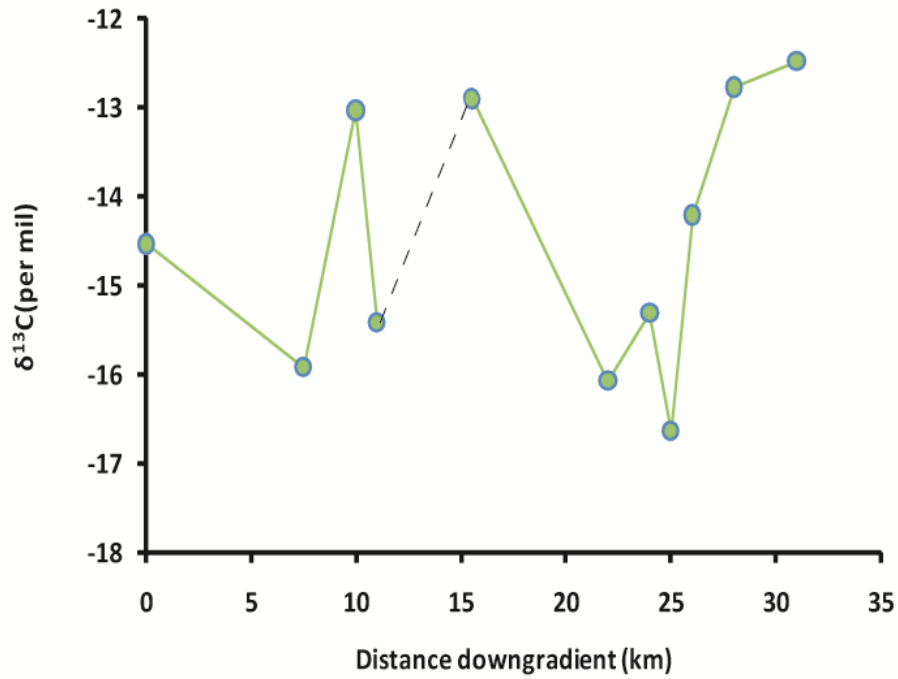


Fig. 5. Plot showing the $\delta^{13}\text{C}$ ratios of coastal groundwater as a function of distance along a flow path in the Ganges delta. Dash line indicates missing data.

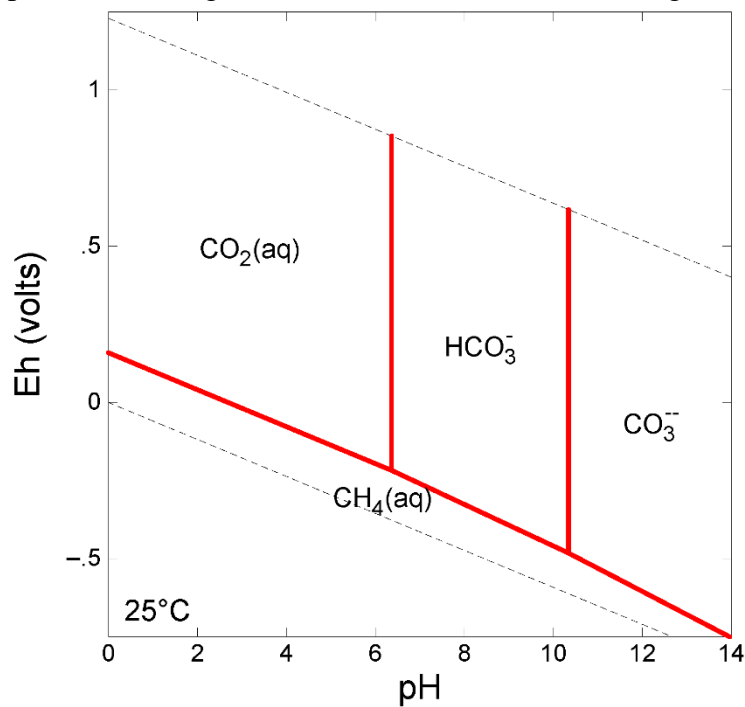


Fig. 6. Eh-pH diagram calculated for average geochemical conditions in C-H-O system and Activity of dissolved species: $\text{C} = 10^{-10}$ mol. This activity diagram was generated by the Geochemist' Workbench.

Sediment and groundwater chemistry

Geochemical results from total digestion geochemical analysis of the sediment samples show variations in concentrations of trace elements with depth (Table 2). The chemistry of groundwater in coastal aquifers is similar to other trace elements enriched areas in the Ganges delta. Fe is closely associated with Mn, As, Cu and Pb in groundwater and sediments in the Ganges delta study area. Enrichment of trace metals and sulfur in coastal aquifers sediments is revealed by high values aluminum-normalized enrichment factors (ANEF). Both wells LKLK2 and SPNA, concentrations of trace metals (e.g., Cu, Pb, Zn, Fe, Hg, As, etc.) are generally greater near the shallow aquifer but decline with depth (Fig. 7). The enrichment of trace metals in sediments is directly related to riverine inputs derived from terrigenous sediment sources. ANEF values for Fe in sediments range from 4.14 to 17.45, with an average ANEF values of approximately 5.34 and 7.12 in LKLK2 Well and SPNA well respectively. Mean ANEF values of Mn in sediments are 5.7 and 7.52 in wells LKLK2 and SPNA respectively. Maximum ANEF values of As are 23.01 in core LKLK2 and 29.04 in well SPNA. The mean ANEF values of S are approximately 18.08 and 7.71 in well LKLK2 and SPNA respectively. Concentrations of other trace elements in sediments (e.g., Ni, Cu, Pb, Zn, Sr, Co, La, Bi, V etc.) are also higher in the high Fe, Mn, As zones (Fig. 8 and 9). This enrichment pattern in sediments suggests that reductive dissolution Fe- and Mn-oxyhydroxides may lead to enrichment of Fe, Mn and As in groundwater as proposed by Gómez et al.(2006). However, presence of higher concentrations of Fe, Mn and As in sediments suggests that some desorption process may result in such pattern, which indicates that high Fe, Mn, As were released from samples (rich in detrital biotite) originally containing high Fe concentration.

Table 2: Concentrations of major, minor and trace element in sediment samples (total digestion) from the LKLIK2 and SPNA wells from the study area.

| | Depth | Cu | Pb | Zn | Ni | Co | Mn | Fe | As | Th | Sr | V | Ca | P | La | Cr | Mg | Ba | Al | Na | K | Hg | S |
|--------|---------|------|-----|-----|------|-----|-----|------|-----|------|-----|-----|------|-------|-----|-----|------|-----|------|-------|------|-------|-------|
| | m | ppm | ppm | ppm | ppm | ppm | ppm | % | ppm | ppm | ppm | ppm | % | % | ppm | ppm | % | ppm | % | % | % | ppm | % |
| SPNA | 15-18 | 42.7 | 7.3 | 65 | 17.7 | 7.2 | 369 | 1.76 | 1.5 | 5.0 | 15 | 19 | 0.38 | 0.039 | 10 | 17 | 0.39 | 82 | 0.77 | 0.025 | 0.20 | <0.01 | <0.05 |
| LKLIK2 | 18-21 | 9.5 | 5.2 | 24 | 13.7 | 4.9 | 281 | 1.14 | 2.3 | 6.1 | 10 | 11 | 0.25 | 0.040 | 8 | 12 | 0.19 | 21 | 0.44 | 0.010 | 0.10 | 0.02 | 0.22 |
| SPNA | 27-30 | 14.2 | 6.1 | 40 | 26.1 | 8.9 | 349 | 1.95 | 1.9 | 4.4 | 13 | 25 | 0.35 | 0.058 | 10 | 23 | 0.57 | 45 | 0.98 | 0.025 | 0.26 | <0.01 | <0.05 |
| LKLIK2 | 30-33 | 31.1 | 8.4 | 64 | 15.2 | 6.9 | 501 | 2.06 | 2.0 | 6.2 | 15 | 18 | 0.38 | 0.044 | 11 | 16 | 0.34 | 107 | 0.68 | 0.021 | 0.16 | 0.02 | <0.05 |
| LKLIK2 | 54-57 | 10.7 | 5.4 | 43 | 21.8 | 6.8 | 286 | 1.55 | 2.1 | 4.5 | 11 | 18 | 0.27 | 0.051 | 9 | 21 | 0.48 | 30 | 0.83 | 0.023 | 0.21 | 0.01 | <0.05 |
| SPNA | 76-79 | 15.7 | 6.9 | 41 | 21.5 | 8.5 | 302 | 1.83 | 2.7 | 6.4 | 19 | 26 | 0.72 | 0.055 | 11 | 21 | 0.54 | 47 | 0.88 | 0.025 | 0.23 | <0.01 | <0.05 |
| SPNA | 85-88 | 15.0 | 6.2 | 28 | 16.9 | 7.2 | 496 | 5.43 | 1.9 | 62.1 | 21 | 109 | 0.67 | 0.114 | 70 | 56 | 0.32 | 31 | 0.78 | 0.045 | 0.14 | <0.01 | <0.05 |
| SPNA | 94-97 | 9.6 | 4.7 | 28 | 14.2 | 6.2 | 228 | 1.23 | 1.6 | 5.6 | 11 | 16 | 0.38 | 0.030 | 10 | 14 | 0.31 | 31 | 0.62 | 0.021 | 0.16 | 0.02 | <0.05 |
| SPNA | 125-128 | 11.4 | 6.7 | 35 | 16.6 | 7.8 | 426 | 1.41 | 2.1 | 14.4 | 11 | 18 | 0.30 | 0.028 | 20 | 16 | 0.24 | 27 | 0.53 | 0.021 | 0.12 | <0.01 | <0.05 |
| SPNA | 128-131 | 6.8 | 3.3 | 15 | 9.4 | 3.4 | 227 | 1.04 | 2.7 | 7.9 | 10 | 13 | 0.31 | 0.042 | 13 | 17 | 0.16 | 51 | 0.36 | 0.016 | 0.07 | 0.02 | 0.10 |
| LKLIK2 | 237-240 | 11.6 | 6.8 | 43 | 21.4 | 7.7 | 255 | 1.47 | 4.1 | 4.4 | 10 | 16 | 0.15 | 0.031 | 9 | 18 | 0.32 | 31 | 0.69 | 0.010 | 0.16 | 0.02 | 0.19 |
| SPNA | 271-274 | 8.4 | 5.6 | 31 | 27.8 | 5.8 | 205 | 1.39 | 2.6 | 6.9 | 9 | 18 | 0.20 | 0.053 | 9 | 25 | 0.33 | 24 | 0.72 | 0.019 | 0.16 | 0.02 | <0.05 |
| LKLIK2 | 289-292 | 2.9 | 3.6 | 16 | 9.0 | 3.2 | 101 | 0.81 | 1.3 | 2.6 | 6 | 11 | 0.10 | 0.019 | 6 | 9 | 0.21 | 22 | 0.49 | 0.023 | 0.15 | <0.01 | <0.05 |
| LKLIK2 | 295-298 | 18.4 | 7.2 | 40 | 18.2 | 6.8 | 281 | 1.51 | 3.2 | 8.9 | 9 | 16 | 0.20 | 0.045 | 9 | 15 | 0.26 | 26 | 0.58 | 0.011 | 0.13 | 0.01 | 0.19 |
| SPNA | 301-304 | 8.1 | 3.4 | 19 | 10.4 | 4.0 | 140 | 0.93 | 0.6 | 4.1 | 10 | 15 | 0.26 | 0.050 | 8 | 11 | 0.26 | 21 | 0.55 | 0.030 | 0.14 | <0.01 | <0.05 |

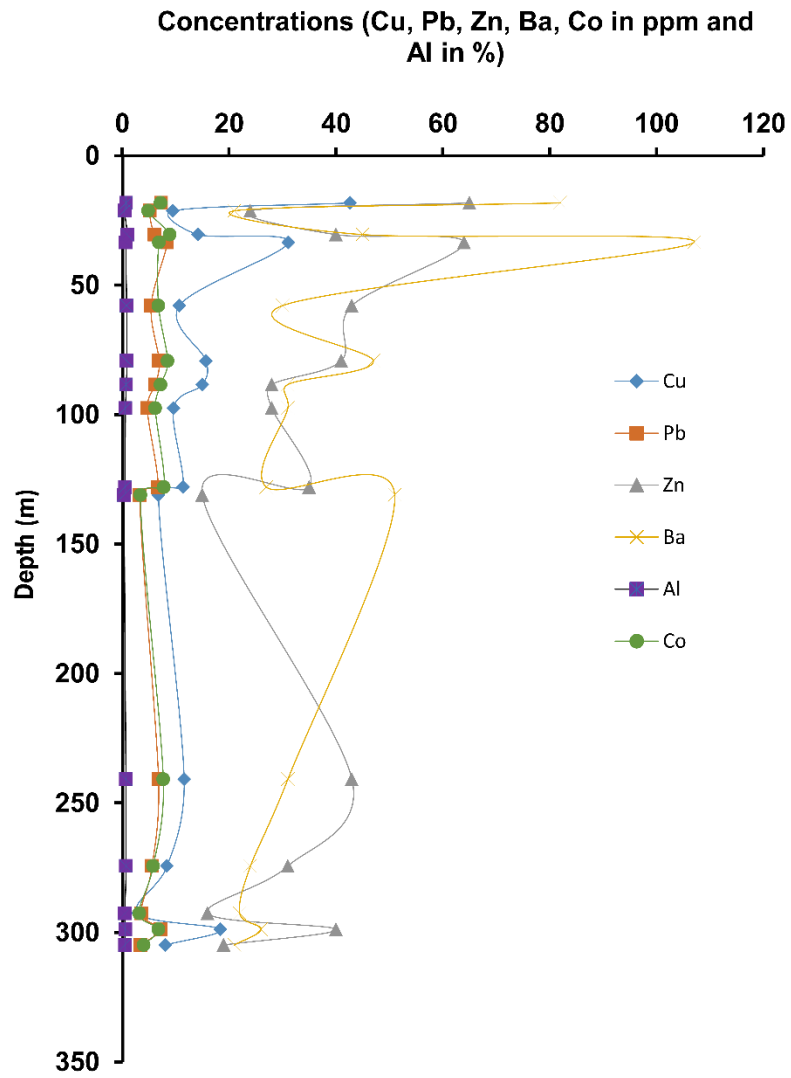


Fig.7. Plot showing concentrations of selected trace metals in sediments of study area in wells LKLN2 and SPNA as a function of depth.

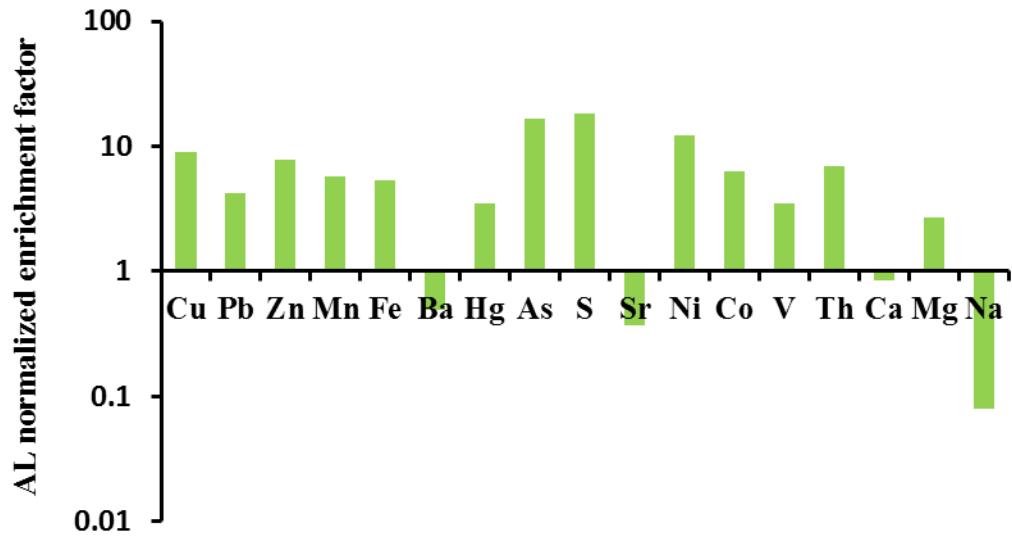


Fig. 8. Plot showing calculated average aluminum-normalized enrichment factors of various elements in LKLN2 well sediments.

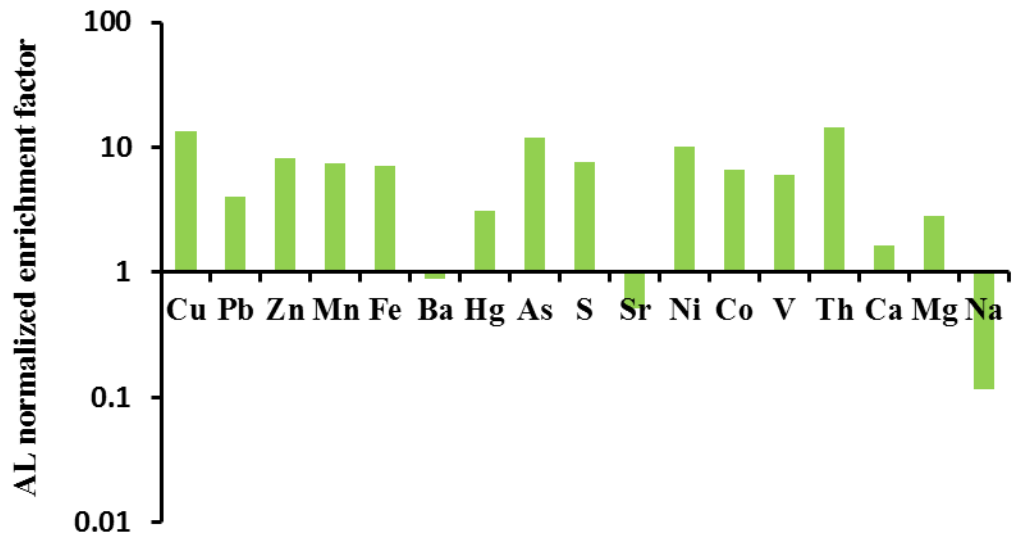


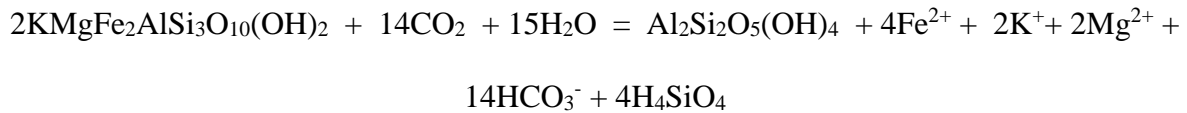
Fig. 9. Plot showing calculated average aluminum-normalized enrichment factors of various elements in SPNA well sediments.

These elements in groundwater typically shows a moderate to strong correlation in other parts of Bangladesh where groundwater Fe, Mn and As concentration is high (BGS and DPHE, 2001; Zheng et al., 2004). Bacteria breakdown of organic matter and influences the groundwater Fe concentration by carbon serving as an electron donor for the reductive dissolution of Fe- and Mn-oxyhydroxides in aquifer sediments. Correlation results suggest that Fe in sediments is strongly correlated with Mn, As, S and other trace metals (e.g., Zn, Ni, Co, Cr, Cu, La and Sr) in sediments (Table 2). Figure 10 shows general litho-stratigraphic logs of two wells in the study area. Sediment compositions both in shallow and deep aquifers are very similar. However, fine to coarse sediment ratio is smaller in the trace element-free deeper aquifers which are similar to other areas in the country and studies also have shown that high trace element concentrations are associated with gray to dark-gray sediments, whereas yellowish brown aquifer sediments host low groundwater trace element (BGS and DPHE, 2001; Horneman et al., 2004; Ahmed et al., 2004). These aquifer sediments vary from gray at the shallow (<100 m) depths (more reducing) to yellowish-brown at deeper depths (more oxidizing). Arsenic concentration in groundwater is higher at shallow depths than at depth. In the delta plain of the Ganges delta, the occurrence of groundwater trace element concentration (Fe, Mn, As) have been strongly influenced by glaciation and global changes in sea level during the Quaternary period (Goodbred and Kuehl, 2000; Saunders et al., 2005). During the Pliocene and Early Pleistocene, relatively steep hydraulic gradients and deeper water table in the delta plain extensively flushed the pre-existing sediments (e.g., Dupi Tila sands) as a result groundwater in deeper aquifer low trace elements concentration during low-stand of sea level. In contrast, Holocene sea level stand, gentle hydraulic gradients, sluggish hydrologic flushing, and reducing geochemical conditions lead to enrichment of trace element concentration in groundwater. Trace element is derived from

enhanced weathering of uplifted bedrocks in Himalayas and other highlands under warmer and humid climatic conditions (Fig. 10).

Higher concentrations of these three elements in aquifer sediments and groundwater suggest that these constituents were derived from similar geochemical processes and most likely from similar mineralogical sources. It has been widely accepted that Fe and Mn are dissolved into groundwater through the reductive dissolution process from Fe- and Mn oxyhydroxides and this dissolution process releases Fe^{2+} and Mn^{2+} into groundwater (Nickson et al., 2000; BGS and DPHE, 2001; Zheng et al., 2004; Saunders et al., 2005). Besides, high Si is often found with high Fe, Mg in groundwater that might be derived from chemical weathering (and dissolution) of phyllosilicates minerals (e.g., biotite) in aquifers and can release high concentration of As to groundwater (Sengupta et al., 2004).

As is adsorbed onto mineral particles including Fe and/or Mn oxyhydroxides/ oxides after release from the biotite; e.g., biotite is chemically weathered to release Fe as follows:



The released Fe^{2+} is then oxidized to form Fe and Mn oxyhydroxide/oxide and As fixed in secondary phases especially in Fe -and Mn-oxyhydroxide/oxide, which is more easily released into the groundwater than silicate-bound As with a change in redox conditions (Seddiq et al., 2008).

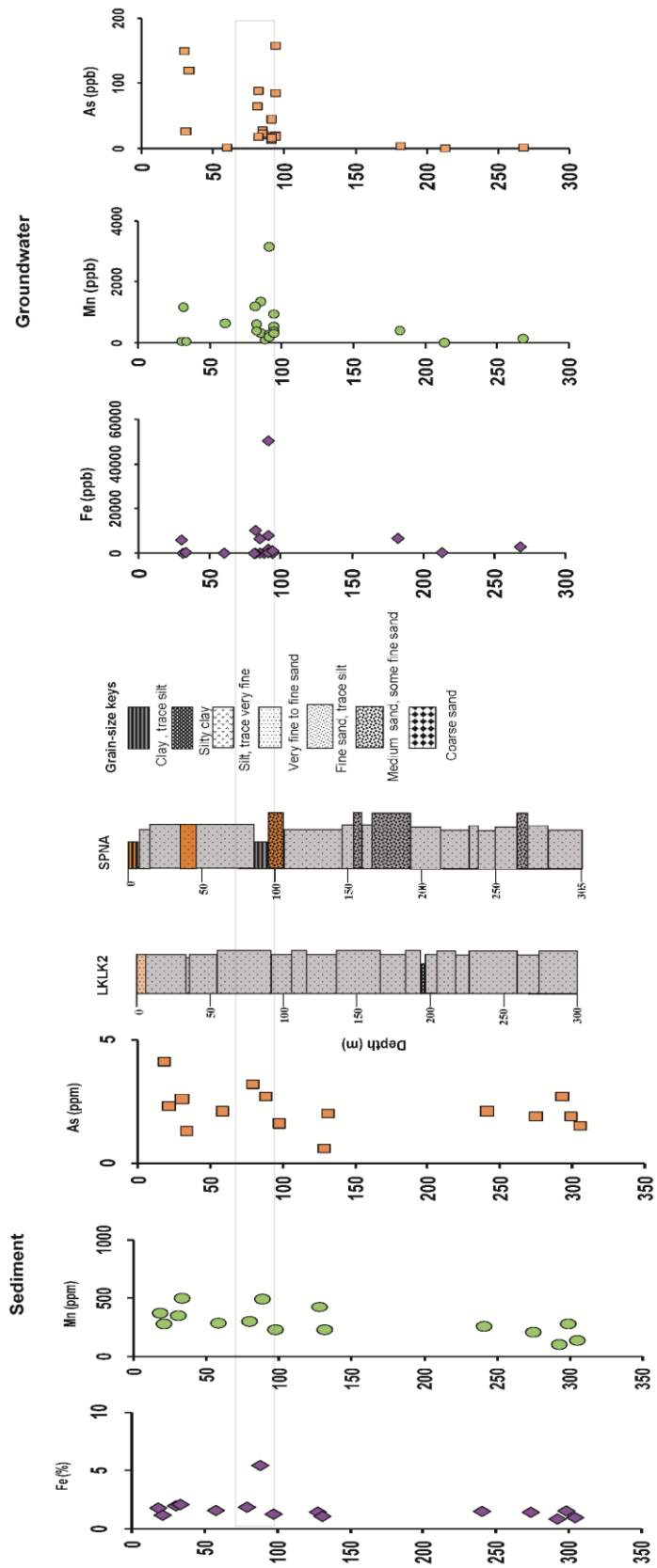


Fig.10. Diagram showing trace element concentrations of Fe, Mn and As both in groundwater and sediment as a function of depth in study area. Concentrations of elements in groundwater roughly match that of sediments with depth. Stratigraphic columns (LKLLK2 and SPNA wells) are also shown with depths (m) which show dominance of very fine to fine sand. Both wells record higher concentration of all three elements down to 100m depth.

If the primary reaction releasing As into the groundwater is initial chemical weathering of As-containing biotite, the redox condition of the groundwater will control the valence of the As species and thus the solubility of this element. However, the secondary behavior of As via desorption from Fe oxyhydroxides/ oxides must be an important mechanism for controlling trace element concentrations into groundwater.

Biom mineralization of sediments

Petrographic and SEM-based energy-dispersive analyses reveal the mineralogy, particle size, and authigenic nature of solids precipitated from Fe-rich groundwater. Heavy mineral thin section petrographic analysis shows the presence of a variety of primary and secondary minerals. Quartz is the most abundant mineral with minor amounts of plagioclase, potassium feldspar, biotite, chlorite and muscovite. Heavy minerals are mainly magnetite, garnet, amphibole, pyroxene, sillimanite, kyanite abundant in all well-cutting samples which are generally considered heavy (specific gravity > 2.8 g/cc). Similar heavy-mineral concentrations have been found in central Bengal basin (Shamusudduha et al., 2008; Uddin et al., 2011).

Biogenic minerals such as pyrite, which exhibits both cubic and framboidal morphologies are abundant in well-cutting samples (Fig. 11). Botryoidal forms of both siderite and pyrite are also present in well-cutting samples (Fig. 11b). Authigenic pyrite is found at depths where groundwater rich in Fe-concentration. Trace precipitates of pyrite and siderite occur together in Fe-rich zone as siderite forms in the center and pyrite forms an outer ring (Fig. 11b), which is consistent with the sequence of mineral precipitation predicted by the geochemical modeling (see

text geochemical modeling for more explanation). Thus the reduction of Fe(III) oxides and the formation of siderite occurs after Mn reduction is almost completed. These spheroids (Fig. 12c) are locally more abundant in Fe-rich zones from well LKLG2 and SPNA. The occurrence of spherical iron carbonates may be attributed to the merging growth of adjacent minerals from groundwater.

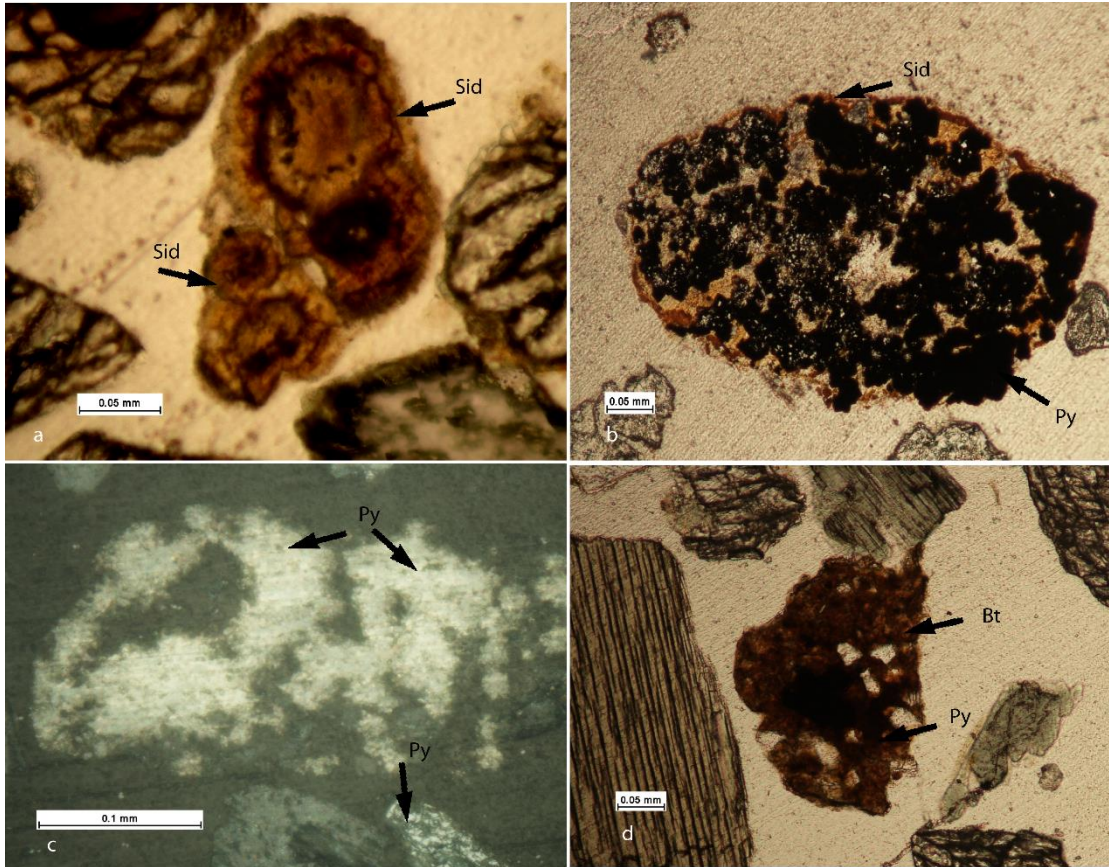


Fig. 11. Representative photomicrographs of minerals from Ganges delta sediments. Thin sections of (a) biogenic siderite (Sid) (cross polar) surrounded with rim (SPNA 301-304 m), (b) SPNA 198-201m and (c) LKLG2 54-57 m) framboidal pyrite (Py) (transmitted and reflected light) and pyrite formed by replacement of a biotite grain in (d) reflected light with varied polarization.

The mobility of Fe, Mn, and other metals (Sr, Ba) in groundwater may induce by precipitation and dissolution of various Fe carbonate and sulfide minerals. In strongly reducing

environment, anaerobic bacteria oxidize organic carbon which generates the energy required to the reduction of sulfate to produce sulfide. This sulfide subsequently reacts with solid phase

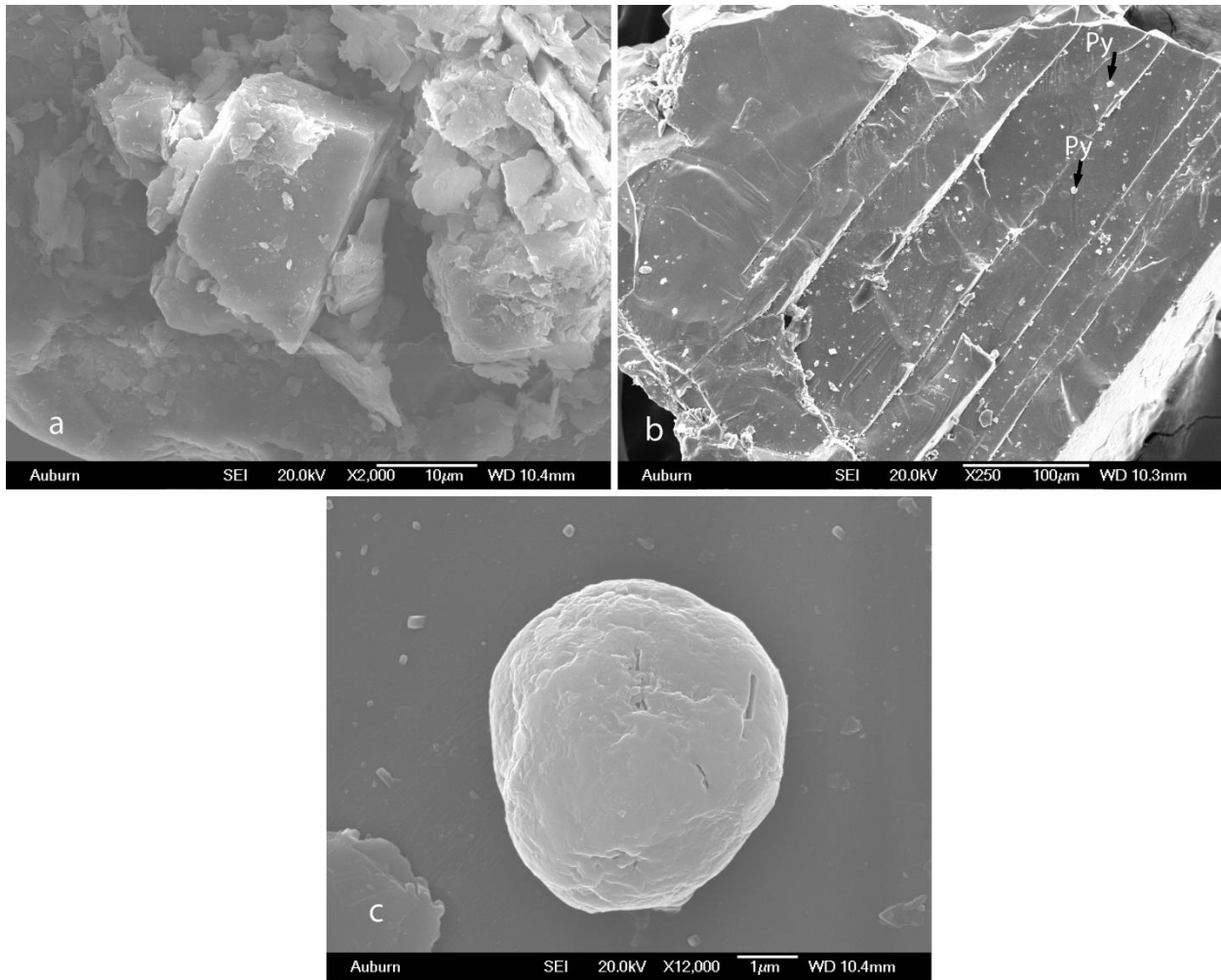
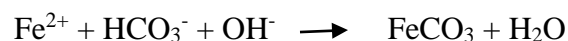


Fig. 12. SEM images of authigenic minerals form in sediment. (a) Biogenic pyrite(Py) texture (SPNA, 301-304 m); (b) Pyrite nucleating between biotite layers (LKLK2, 198-201m); (c) Siderite spheroid in well SPNA 301-304m.

iron oxides or hydroxides within the sediment to form pyrite (Ferris et al., 1987) showed that the formation of iron sulfides directly on the outer surfaces of bacterial cells and their membranous debris. The overall pathway is initiated by the reaction:



Similar authigenic (biogenic) siderite and rhodochrosite minerals were found in Mississippi coastal plain sediments (Saunders and Swann, 1992) and alluvial sediments in India and Bangladesh (Pal et al., 2002; Sengupta et al., 2004; Turner, 2006). The actual biogeochemical functions by which bacteria contribute to biomineralization in the Fe-rich sediments remain poorly understood. Prior studies (Lowenstam, 1981; Konhauser, 1998; Fredrickson et al., 1998) have showed that biogenic mineral can form in both direct and indirect link with bacteria. Direct contact, known as biologically restraint mineralization, is able to occur both intracellularly and extracellularly as bacteria electrostatically bind metal to their anionic cell wall surfaces providing nucleation sites for physiologically essential minerals (Mann, 1983; Konhauser, 1998). Biologically induced mineralization is the incidental mineral organization due to handout of byproduct into solvent by bacterial activity and is also the dominant process among bacteria. This process characteristically forms environmentally dependent biominerals based on available materials surrounding the bacteria. In this fashion, mineral size is expressed by association with the bacterial cell wall (nanometers to micrometers) as well as age of the rocks. This may be possible that Ganges delta Holocene sediments have low concentrations of organic carbon for bacteria metabolism as result authigenic minerals are small in size (Fig. 11). The sediment of the Cretaceous Eutaw formation of Alabama has larger crystal size (Lee et al., 2007) and is potentially able to reach greater sizes as those carbonates observed in this study (>1 mm). Overall growth and number of active cells in the subsurface environments indicate the level of microbial activity and its precipitation of pyrite crystal and its size. Because levels of Fe(II), Mn(II), and HCO_3^- are abundant in the coastal aquifer, biomineralization of FeCO_3 and trace MnCO_3 observed in Fe-rich zone, may be biologically induced as in the following equation:



In this reaction, the presence of Fe(II), bicarbonate, and hydroxyl ions released from bacterial Fe(III) reduction will directly precipitate siderite. Pyrite intergrowths with biotite and chlorite were common in deep sediment within Fe deficient micas. Figure 12 shows that geological formation of pyrite framboids within the sheets of iron-rich micas which eventually grow to replace the entire mica grain. Rickard et al. (2007) could nucleate pyrite framboids within the cell walls of celery via a two-step process whereby Fe(II) diffusion and subsequent S(-II) penetrate and react within the cell walls. Once formed, the pyrite seeds act as nucleation situation to expedite further pyrite growth (Rickard et al., 2007).

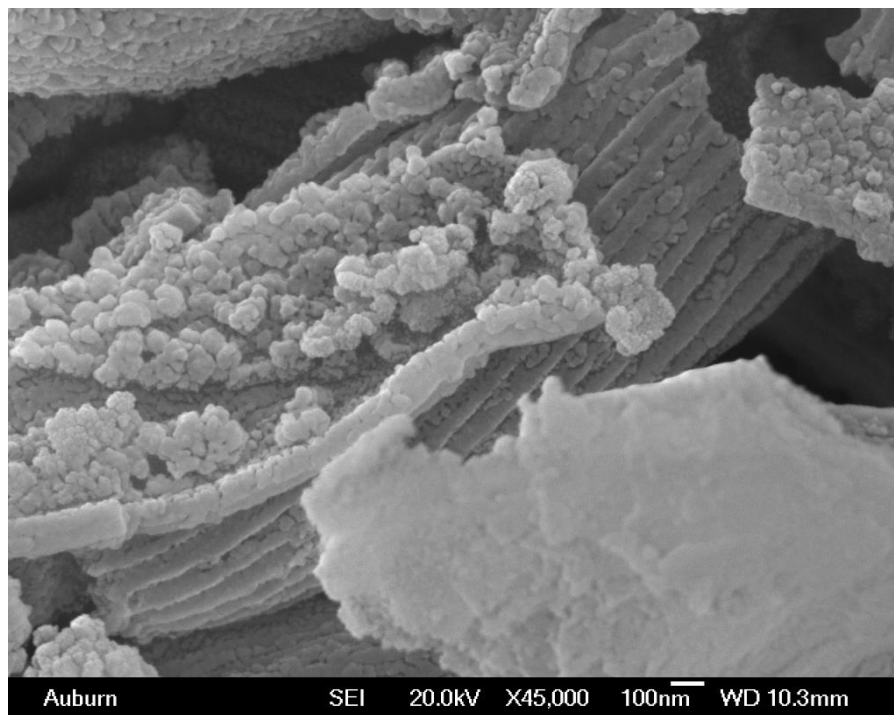


Fig.13.SEM images of microbial features in iron sulfide formation.

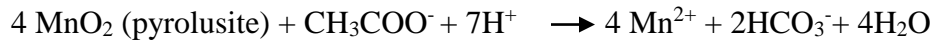
In subsurface environments oxidation and precipitation of sulfide minerals is greatly enhanced by microbial activity (Nordstrom and Southam, 1997). The ovoid bodies, tubes which are surrounded by filaments that have been observed by SEM in the iron sulfide grains (Fig. 13)

which resembles spherical bacteria and filaments that are usually observed in biofilms. Fig. 13 shows bundle of fused filaments that may at one time have been part of a sheet-like contiguous biofilm. The smooth oval bodies that form the cores of the iron sulfide encrusted ovoids and right size and shape for mineralized circular bacteria, and their perforations resemble features observed in cell walls of experimentally pyritized microbes (Bubela and Cloud, 1983). Thus, the mucus coatings suggested to above may actually have been biofilms that covered individual iron sulfide grains and promoted precipitation of sulfide minerals into new layer. Indirectly, these biofilms could have promoted outer layer formation by providing a substrate (culture medium) for sulfate-reducing bacteria that produced the H_2S necessary to precipitate iron sulfides on the surface. Further, the extracellular cellulose of such biofilms could also have acted as growth templates for sulfide minerals. Chan et al., (2004) pointed out that role of microbially produced cellulose as templates for mineral growth. Thus, microbial surface colonization and biofilm formation may have been an important factor to expedite chemical processes that led to the formation of coated iron sulfides grains.

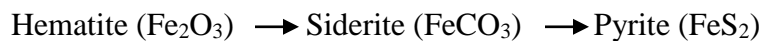
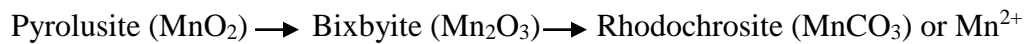
Bacterial reduction of Fe(III) and Mn(IV) oxides

I used GWB (Bethke, 1996) to trace the sequence of biogeochemical reactions that occur during the bacterial Fe(III) and Mn(IV) oxide reduction, which subsequently induces the precipitation of Fe carbonate and sulfide minerals. The purpose of the modeling is to provide insights on the sequence of mineral reactions during the reductive dissolution of Fe and Mn oxides and how mineral reactions affect metal mobility in groundwater. I begin by equilibrating a coastal groundwater upstream of an iron reduction zone under aerobic conditions at 25°C. The calculation uses the water chemical data collected from the coastal aquifer in SPJLW-01 well

and assumes the initial concentrations of Fe and Mn reflect equilibrium with (Fe (OH)₃, a proxy of Fe₂O₃) and pyrolusite (MnO₂, a proxy for Mn(IV) oxyhydroxides) in the sediments. I consider alteration of pyrolusite and Fe(OH)₃ by the following redox reaction:

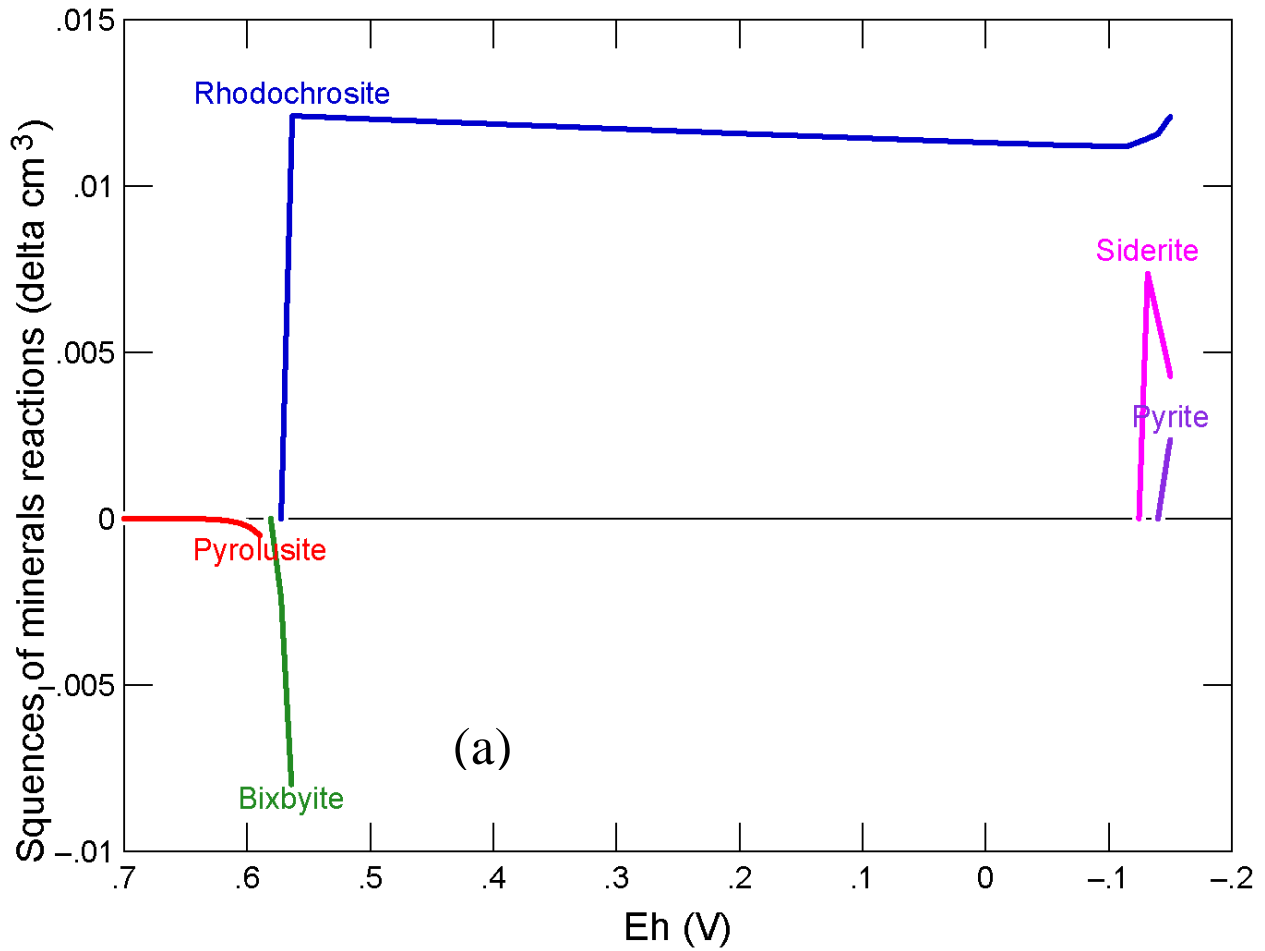


In the simulation, fluid reactants containing 500 mmol of acetate (CH₃COO⁻) displace existing fluid from the system and the values of Eh slide from +700 mV to -200 mV over the reaction path. The predicted mineral reactions of manganese and iron oxides (Fig. 14a) follow the well-known Ostwald's step rule (Morse and Casey, 1988). Pyrolusite in the initial system first becomes thermodynamically unstable during bacterial reduction and transforms over time to a sequence of progressively more stable manganese minerals and species (Fig. 14a) at lower oxidation states,



Once the reduction of Mn minerals has nearly been completed, the iron redox reactions start (Fig. 15a) and hematite (Fe₂O₃) begins to dissolve to form more stable siderite (FeCO₃) or pyrite at low oxidation states. The progression of calculated redox potential and pH values are projected in the activity diagrams showing various stability fields of Mn and Fe minerals and species (Fig. 14). The reduction of Fe(III) oxides occurs under more reducing conditions than Mn minerals. At the later stage of the reaction, reduced metal species also combine with HCO₃⁻ released from organic sources to form minerals such as rhodochrosite (MnCO₃) and siderite

(FeCO₃). Under highly reducing conditions, reduced aqueous Fe²⁺ reacts with H₂S to form pyrite, which can remove trace elements such as Co, Ni, and As from groundwater by



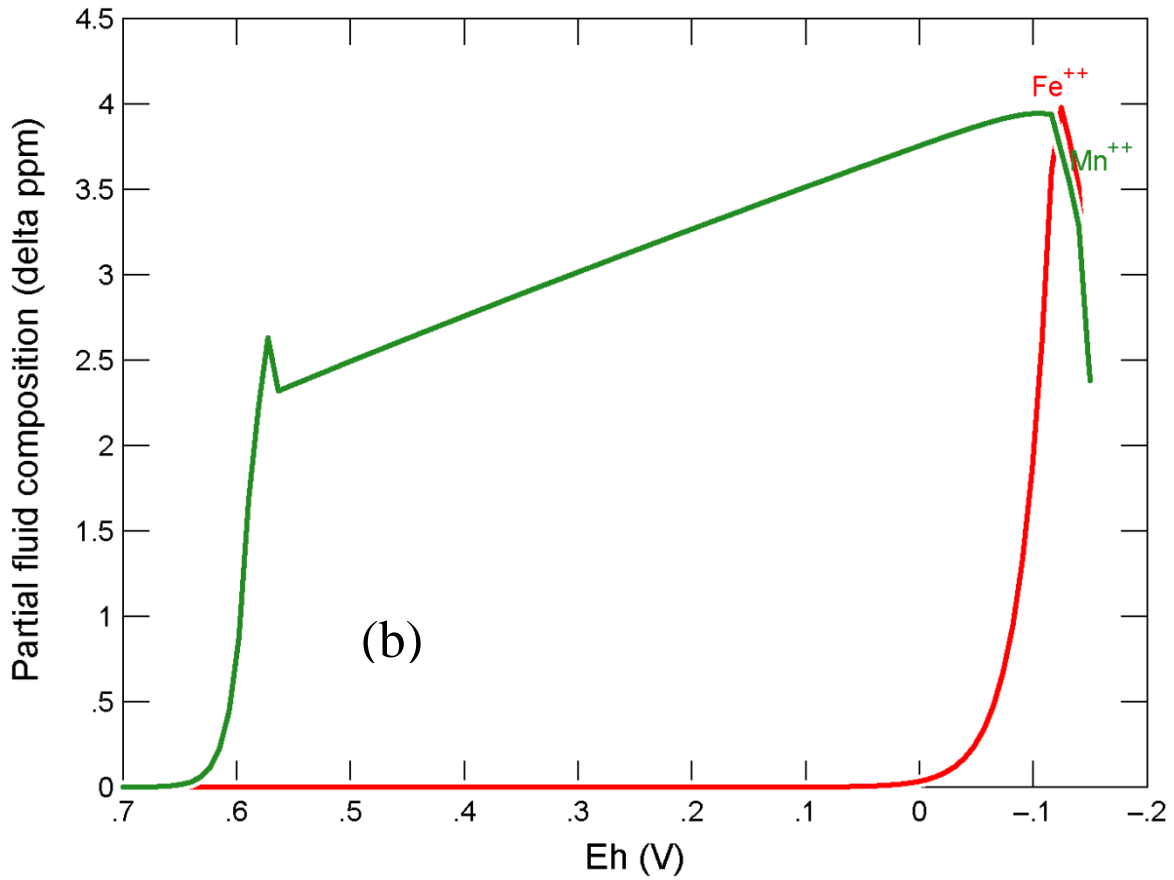


Fig. 14. (a) Plot showing predicted sequence of mineralogical reactions resulting from bacteria reduction of Fe and Mn oxides in equilibrium with coastal groundwater. The plot shows changes in mineral volume as organic carbon is titrated into the system and Eh decreases with time. Positive changes indicate precipitation, and negative changes show dissolution; (b) Calculated Fe and Mn species concentrations in fluid predicted by the same reaction path model.

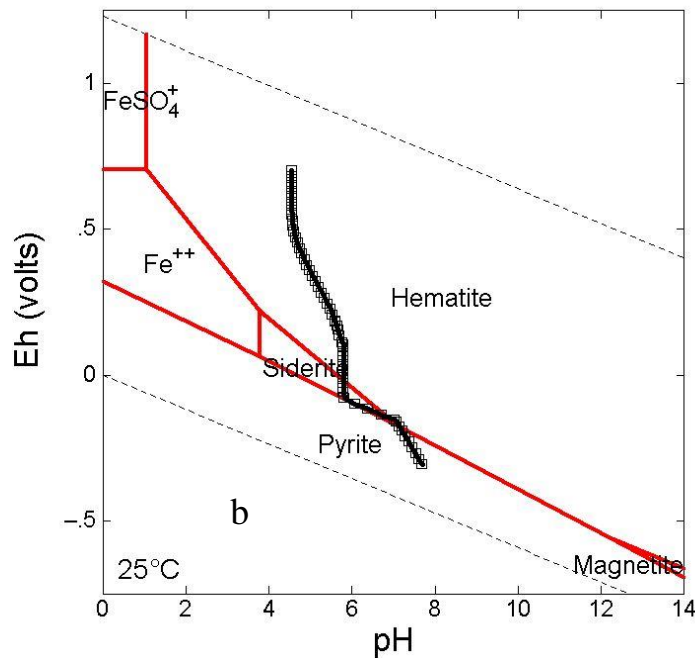
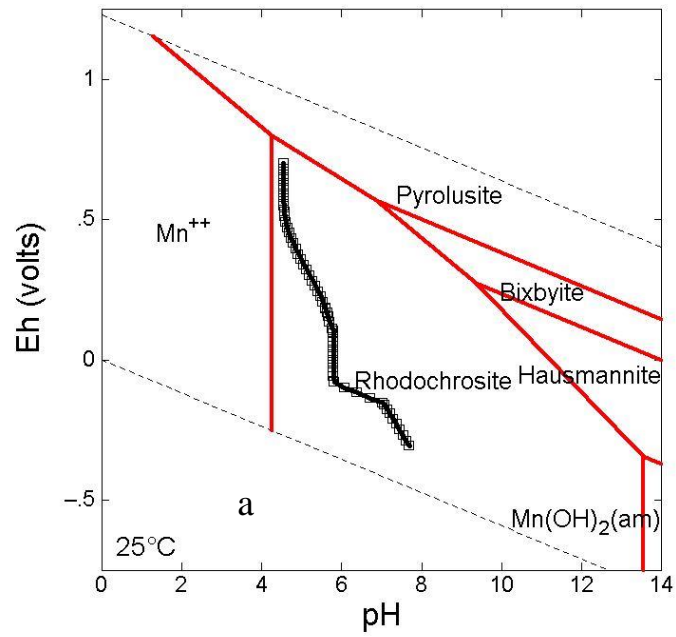


Fig. 15. Eh-pH diagram calculated for average geochemical conditions in (a) Mn-HCO₃-H₂O and (b) Fe-HCO₃-H₂O systems. Activity of dissolved species: Fe²⁺ = 10⁻², Mn²⁺ = 10^{-2.5}, SO₄²⁻ = 10⁻³, and HCO₃⁻ = 10⁻² mol. The reaction trace of bacterial Mn and Fe reduction in Figure 14 is projected as open squares onto the diagram. The reaction trace shows the sequence of mineral reactions during the reductive dissolution of Mn and Fe oxides as Eh decreases. This activity diagrams were generated by the Geochemist' Workbench.

coprecipitation (Saunders et al., 1997; Lehner et al., 2006). Figure 14b shows the calculated Mn and Fe concentrations in fluid over the same reaction path. It clearly demonstrates how the precipitation and dissolution of various Mn- and Fe minerals control the mobility of metals in groundwater.

Rapid rise and fall of metal concentrations observed a short distance along the flow path (Fig. 3) in the downgradient direction may be explained by the transformation of various iron and manganese minerals. Moreover, the modeling results imply that the transformation of iron and manganese minerals could control mobility of other metals such as arsenic in coastal aquifers.

It should be noted that the field data show no truly strong correlation among Fe, Mn, pH, HCO_3^- , and $\delta^{13}\text{C}$ values of groundwater because the chemical evolution of groundwater can be affected by various biogeochemical reactions (i.e. Bacterial iron reduction, sulfate reduction, methanogenesis) as well as mineral precipitation and dissolution. A perfect correlation among these parameters might be expected if a groundwater flow zone is dominated by a single biogeochemical or mineral reaction. Recent studies (Park et al., 2006; Turner, 2006), however, found no compelling evidence that the respiration of one type of microbes would exclude others from any of an aquifer's redox zones. This implies that a change of the groundwater from high-Fe into low-Fe facies over a short distance (Fig. 3) may result from a minor adjustment in the balance between the activities of iron and sulfate reducers or biotransformation of metals-bearing minerals. For instance, bacterial-induced precipitation of siderite will preferentially remove Fe relative to other ions in groundwater. Bacterial sulfate reduction and precipitation of iron sulfides could strip Fe^{2+} , SO_4^{2-} , H^+ , and perhaps other trace elements (by coprecipitation) from solution in different ratios.

The Eh-pH diagram (Fig. 15) suggests that siderite (FeCO_3) and pyrite (FeS_2) should occur minerals in coastal aquifers under reducing conditions. Thin-section petrographic study indicates that pyrite is commonly associated with siderite (Fig. 11), suggesting that the groundwater contained significant amounts of reduced S and HCO_3 during their precipitation. Therefore, the alternating siderite and pyrite bands may reflect fluctuations in the redox state of the groundwater at the site of authigenic mineral precipitation. The redox state of groundwaters is a primary control on the $a\text{Fe}^{2+}/a\text{Mn}^{2+}$ ratio (Barnaby and Rimstidt, 1989), which drives whether rhodochrosite or siderite will precipitate at a given pH and HCO_3 concentration. In addition, any change in equilibrium with both Fe- and Mn-oxyhydroxides, changes in pH can affect the $a\text{Fe}^{2+}/a\text{Mn}^{2+}$ ratio (Barnaby and Rimstidt, 1989). However, the pH in the coastal aquifer is relatively constant due to calcite buffering indicating that the redox condition is the primary control on the $a\text{Fe}^{2+}/a\text{Mn}^{2+}$ ratio.

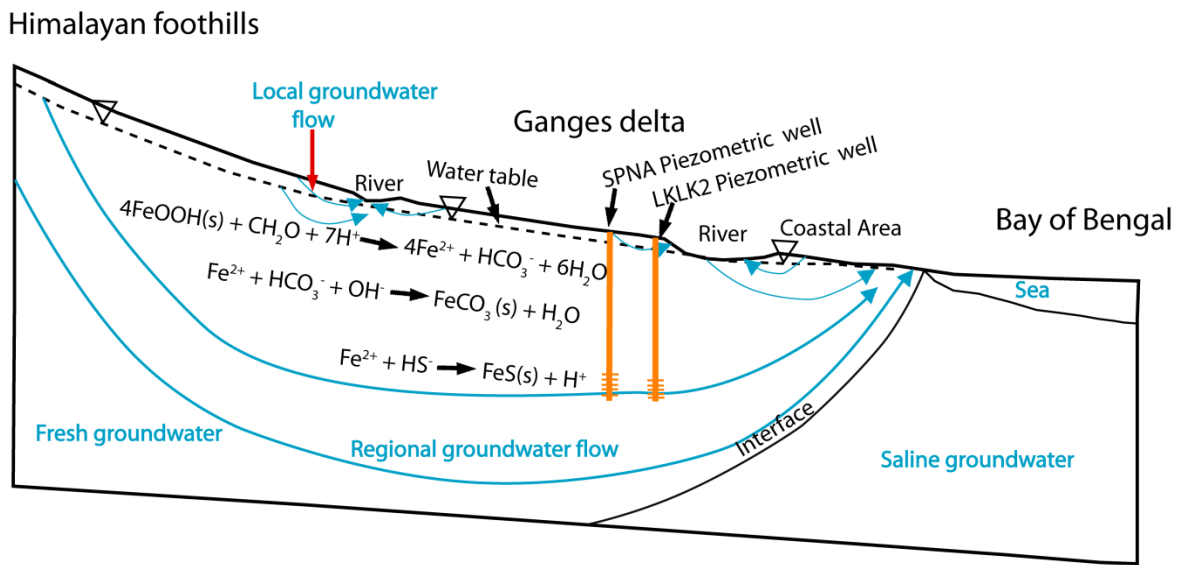


Fig. 16. Conceptual model of trace element and biominerals precipitation reactions in groundwater flow system in the Ganges delta (After BGS and DPHE, 2001; Fendorf et al., 2010)

The topographic relief at the Himalayan foothills provides the head of the regional flow regime and downward recharge of freshwater (Fig. 16). Trace element concentration in the groundwater of the Ganges delta suggests that freshwater in updip area is derived from the Himalayan drainage network system (Basu et al., 2001). The vertical hydraulic gradient in groundwater head reflects regional flow systems and flowpaths that link distant recharge and discharge areas at the Ganges delta beneath more dynamic shallow and local groundwater flow. Rivers within the delta, which carries colloidal size Fe and Mn-oxyhydroxides with their strongly adsorbed high concentration of trace elements (i.e., As) in fresh groundwater in shallow strata. As groundwater moves downgradient, Fe and Mn-oxyhydroxides go through bacterial reduction under moderately reducing condition which discharge metals and raise HCO_3^- concentration of groundwater at the expense of H^+ , natural organic carbon, and iron oxides. Bacterial iron

reduction followed by sulfate reduction aids in precipitating biominerals, like siderite and pyrite in aquifers and eventually groundwater is discharged into the Bay of Bengal (Fig. 16).

CONCLUSIONS

This research integrates geochemical data and numerical modeling techniques to analyze complex water sediment-bacteria interaction and hydrologic transport in coastal aquifers. Results indicate that both inorganic (ion exchange) and bacterially mediated (bacterial Fe(III)- and Mn(IV)-reduction) processes work together to produce groundwater with elevated levels of trace metals and cations that correlate with high pH and HCO_3^- . Geochemical correlations, reducing Eh values, and the presence of authigenic carbonate solids and light $\delta^{13}\text{C}$ signatures support the hypothesis that elevated Fe data indicate that the precipitation and dissolution of various Fe-minerals control the mobility of metals in groundwater; biotransformation of these minerals could be responsible for rapid rise and fall of metal concentrations observed over short distance along the flow path.

Iron was precipitated as the authigenic minerals pyrite and siderite as higher levels of reduced S and HCO_3^- . This change can be explained by Eh and pH variations that might reflect long-term climate changes such as may attend glacial-interglacial periods.

This study demonstrates that quantitative geochemical and hydrological transport models can be used in conjunction with field data to assess chemical evolution and complex water-sediment-bacteria interaction in regional groundwater systems. Results show that a wide variety of geochemical and microbial processes, including such diverse phenomena as bacterial metal

reduction, biomineralization, diagenesis, ion exchange, and transport and fractionation of isotopes, are the results of reactive transport in the subsurface.

REFERENCES

- Aggarwal, P.K., Basu, A.R., Poreda, R.J., 2000. Isotope hydrology of groundwater in Bangladesh: implications for characterization and mitigation of arsenic in groundwater. International Atomic Energy Agency, Vienna, TC Project BGD/8/016, 23 pp.
- Ahmed, K.M., Bhattacharya, P., Hasan, M.A., Akhter, S.H., Alam, S.M.M., Bhuyian, M.A.H., Imam, M.B., Khan, A.A., Sracek, O., 2004. Arsenic enrichment in groundwater of the alluvial aquifers in Bangladesh: An overview. *Applied Geochemistry* 19,181–200.
- Appelo, C.A.J., 1994. Cation and proton exchange, pH variations, and carbonate reactions in a freshening aquifer. *Water Resource Research* 30, 2793–2805.
- Basu A.R., Jacobsen S.B., Poreda R.J., Dowling C.B., Aggarwal P.K., 2001. Large groundwater strontium flux to the oceans from the Bengal Basin and the marine strontium isotope record. *Science* 293, 1470–1473.
- Bethke, C.M., 1989. Modeling subsurface flow in sedimentary basins. *Geologische Rundschau* 78, 129–154.
- Bethke, C.M., 1996. *Geochemical Reaction Modeling*. Oxford University Press, New York.
- Barnaby, R.J., Rimstidt, J.D., 1989. Redox conditions of calcite cementation interpreted from Mn and Fe contents of authigenic calcites. *Geological Society of America Bulletin* 101, 795-804.
- BGS and DPHE, 2001. Arsenic contamination of groundwater in Bangladesh, Vol. 2. Final Report, BGS Technical Report WC/00/19.
- Bubela, B., and Cloud, P., 1983. Sulfide mineralization of microbial cells: Bureau of Mineral Resources. *Journal of Australian Geology and Geophysics* 8, 355–357.
- BWDB, 2014. Hydro-geological Study and Mathematical Modelling to Identify Sites for Installation of Observation Well Nests, Selection on Model Boundary, Supervision of Pumping test, Slug test, Assessment of Different Hydro-geological Parameters, Collection and Conduct Chemical Analysis of Surface water and Groundwater, Tech. Report, 7 Volumes, BWDB, Dhaka
- Charlet, L., Chakraborty, S., Appelo, C.A.J., Roman-Ross, G., Nath, B., Ansari, A.A., Lanson, M., Chatterjee, D., Mallik, S. B., 2007. Chemodynamics of an arsenic “hotspot” in a West Bengal aquifer: A field and reactive transport modeling study. *Applied Geochemistry* 22, 1273-1292.

- Chan, C.S., Stasio, G.De., Welch, S.A., Girasole, M., Frazer, B.H., Nesterova, M.V., Fakra, S., Banfield, J.F., 2004. Microbial polysaccharides template assemble nanocrystal fibers. *Science* 303, 1656–1658.
- Chapelle, F.H., and Knobel, L.L., 1983. Aqueous geochemistry and the exchangeable cation composition of glauconite in the Aquia Aquifer, Maryland. *Ground Water*, 21, 343–352.
- Chapelle, F.H., 2001. *Ground-Water Microbiology and Geochemistry*, John Wiley, Hoboken, N. J.
- Clark, I., and Fritz, P., 1997. *Environmental Isotopes in Hydrogeology*, CRC Press, Boca Raton, Fla.
- Dowling, C.B., Poreda, R.J., Basu, A.R., 2003. The groundwater geochemistry of the Bengal basin: Weathering, chemisorption, and trace metal flux to the oceans. *Geochimica et Cosmochimica Acta* 67, 2117–2136.
- Fendorf, S., Michael, H. A., A. van Geen., 2010. Spatial and temporal variations of groundwater arsenic in South and Southeast Asia. *Science*, 328 (5982), 1123–1127.
- Ferris, F.G., Fyfe, W.S., Beveridge, T.J., 1987. Bacteria as nucleation sites for authigenic minerals in a metal-contaminated lake sediment. *Chemical Geology* 63, 225–232.
- Fredrickson, J.K., Zachara, J.M., Kennedy, D.W., Dong, H., Onstott, T.C., Hinman, N.W., Li, S.-M., 1998. Biogenic iron mineralization accompanying the dissimilatory reduction of hydrous ferric oxide by a groundwater bacterium. *Geochimica et Cosmochimica Acta* 62, 3239–3257.
- Goodbred, S.L., and Kuehl, S.A., 2000. The significance of large sediment supply, active tectonism, and eustasy on margin sequence development: late Quaternary stratigraphy and evolution of the Ganges–Brahmaputra delta. *Sedimentary Geology* 133, 227–248.
- Gómez, J.J., Lillo, J., Sahún, B., 2006. Naturally occurring arsenic in groundwater and identification of the geochemical sources in the Duero Cenozoic Basin, Spain. *Environmental Geology* 50, 1151–1170.
- Hem, J.D., 1985. Study and interpretation of the chemical characteristics of natural water. U.S. Geological Survey Water-Supply Paper 2254.
- Hem, J.D., and Lind, C.J., 1983. Nonequilibrium models for predicting forms of precipitated manganese oxides. *Geochimica et Cosmochimica Acta* 47, 2037–2046.
- Horneman, A., van Geen, A., Kent, D., Mathe, P.E., Zheng, Y., Dhar, R.K., O'Connell, S., Hoque, M., Aziz, Z., Shamsudduha, M., Seddique, A., Ahmed, K.M., 2004. Decoupling of As and Fe release to Bangladesh groundwater under reducing conditions. Part I: Evidence from sediment profiles. *Geochimica et Cosmochimica Acta* 68, 3459–3473.

- Johnson, M.R.W., 1994. Volume balance of erosional loss and sediment deposition related to Himalayan uplifts. *Journal of the Geological Society of London* 151, 217–220.
- Konhauser, K.O., 1998. Diversity of bacterial iron mineralization. *Earth-Science Reviews* 43,91-121.
- Lee, M.-K., and Bethke, C.M., 1996. A model of isotopic fractionation in reacting geochemical systems. *American Journal of Sciences* 296, 965–988.
- Lee, M.-K., and Saunders, J.A., 2003. Effects of pH on metals precipitation and sorption: Field bioremediation and geochemical modeling approaches. *Vadose Zone Journal* 2, 177–185.
- Lee, M.-K., Saunders, J. A., Wilkin, R. T., Mohammad, S., 2005. Geochemical modeling of arsenic speciation and mobilization, in *Advances in Arsenic Research: Integration of Experimental and Observational Studies and Implications for Mitigation*, Symp. Ser., vol. 915, edited by P. O'Day et al., American Chemical Society Washington, D. C.398–413
- Lee., M.-K., Griffin, J., Saunders, J.A., Wang, Y., Jean, J., 2007. Reactive transport of trace elements and isotopes in Alabama coastal plain aquifers. *Journal of Geophysical Research* 112, G02026, doi:10.1029/2006JG000238.
- Lehner, S.W., Savage, K.S., Ayers, J.C., 2006. Vapor growth and characterization of pyrite (FeS₂) doped with Co, Ni, and As: Variations in semiconducting properties. *Journal of Crystal Growth* 286, 306–317.
- Lovley, D.R., and Chapelle, F.H., 1995. Deep subsurface microbial processes. *Review Geophysics* 33, 365–381.
- Lovley, D.R., Chapelle, F.H., Phillips, E.J.P., 1990. Fe (III)-reducing bacteria in deeply buried sediments of the Atlantic coastal plain. *Geology* 18, 954–957.
- Lowenstam, H.A., 1981. Minerals formed by organisms, *Science* 211, 1126–1131.
- McArthur, J.M., Banerjee, D.M., Hudson-Edwards, K.A., Mishra, R., Purohit, R., Ravenscroft, P., Cronin, A., Howarth, R.J., Chatter- jee, A., Talukder, T., Lowry, D., Houghton, S., Chadha, D.K., 2004. Natural organic matter in sedimentary basins and its relation to arsenic in anoxic ground water: the example of West Bengal and its worldwide implications. *Applied Geochemistry* 19, 1255–1293.
- Mann, S., 1983. Mineralization in biological systems. *Structural Bonding* 54, 125–174.
- MPO, 1987. Groundwater Resources of Bangladesh. Technical Report No. 5. Master Plan Organisation, Dhaka. Harza Engineering, USA, Sir M. MacDonald and Partners, UK, Meta Consultants, USA, and EPC Ltd., Bangladesh.

- Morse, J.W., and Casey, W.H., 1988. Ostwald processes and mineral paragenesis in sediments. *American Journal of Sciences* 288, 537–560.
- Mukherjee, A., Fryar, A.E., 2008. Deeper groundwater chemistry and geochemical modeling of the arsenic affected western Bengal basin, West Bengal, India. *Applied Geochemistry* 23, 863–892.
- Murphy, E.M., Schramke, J.A., Frederickson, J.K., Bledsoe, H.W., Francis, A.J., Sklarew, D.S., Linehan, J.C., 1992. The influence of microbial activity and sedimentary organic carbon on the isotope geochemistry of the Middendorf Aquifer. *Water Resource Research* 28, 723–740.
- Nickson, R.T., McArthur, J.M., Ravenscroft, P., Burgess, W.G., Ahmed, K.M., 2000. Mechanism of arsenic release to groundwater, Bangladesh and West Bengal. *Applied Geochemistry* 15, 403–413.
- Nordstrom, D.K., Plummer, L.N., Langmuir, D., Busenberg, E., May, H.M., Jones, B.F., Parr-Hurst, D.L., 1990. Revised chemical equilibrium data for major water-mineral reactions and their limitations. In *Chemical Modeling of Aqueous Systems II* (Eds D. C. Melchior And R. L. Basserr), American Chemical Society Symposium Series 416, 398-413.
- Nordstrom, D.K., and Southam, G., 1997. Geomicrobiology of sulfide mineral oxidation, in Banfield, J.F., and Nealson, K.H., eds., *Geomicrobiology; Interactions between Microbes and Minerals: Reviews in Mineralogy* 35, 361–390.
- Pal, T., Mukherjee, P.K., Sengupta, S., 2002. Nature of arsenic pollutants in groundwater of Bengal Basin-a case study from Baruipur area, West Bengal, India. *Current Science* 82, 554–561.
- Park, J., Sanford, R.A., Bethke, C.M., 2006. Geochemical and microbiological zonation of the Middendorf Aquifer, South Carolina. *Chemical Geology* 230, 88–104.
- Penny, E., Lee, M.-K., Morton, C., 2003. Groundwater and microbial processes of Alabama coastal plain aquifers. *Water Resource Research* 39(11), 1320, doi: 10.1029/2003WR001963.
- Plummer, L.N., Busby, J.F., Lee, R.W., Hanshaw, B.B., 1990. Geochemical modeling of the Madison Aquifer in parts of Montana, Wyoming, and South Dakota. *Water Resource Research* 26, 1981–2014.
- Postma, D., Larsen, F., Hue, N.T.M., Duc, M.T., Viet, P.H., Nhan, P.Q., Jessen, S., 2007. Arsenic in groundwater of the Red River floodplain, Vietnam: controlling geochemical processes and reactive transport modelling. *Geochimica et Cosmochimica Acta* 71, 5054–5071.
- Rickard, D., Grimes, S., Butler, I., Oldroyd, A., Davies, K.L., 2007. Botanical constraints on pyrite formation. *Chemical Geology* 236, 228–246.

- Roden, E.E., Leonardo, M.R., Ferris, F.G., 2002. Immobilization of strontium during iron biomineralization coupled to dissimilatory hydrous ferric oxide reduction. *Geochimica et Cosmochimica Acta* 66, 2823–2839.
- Romanek, C.S., Zhang, C.L., Li, Y., Horita, J., Vali, H., Cole, D.R., Phelps, T.J., 2003. Carbon and hydrogen isotope fractionations associated with dissimilatory iron-reducing bacteria. *Chemical Geology* 195, 5–16.
- Saunders, J.A., and Swann, C.T., 1992. Nature and origin of authigenic rhodochrosite and siderite from the Paleozoic aquifer, northeast Mississippi, U.S.A. *Applied Geochemistry* 7, 375–387.
- Saunders, J.A., Prichett, M.A., Cook, R.B., 1997. Geochemistry of biogenic pyrite and ferromanganese stream coatings: A bacteria connection? *Geomicrobiology Journal* 14, 203–217.
- Saunders, J.A., Mohammad, S., Korte, N.E., Lee, M.-K., Castle, D., Barnett, M.O., Fayek, M., Riciputi, L., 2005. Groundwater geochemistry, microbiology and mineralogy in two arsenic-bearing Holocene alluvial aquifers from the USA, in *Advances in Arsenic Research Integration of Experimental and Observational Studies and Implication for Mitigation*, Symposium Series vol. 915, edited by P.
- Seddique, A.A., Masuda, H., Mitamura, M., Shinoda, K., Yamanaka, T., Itai, T., Maruoka, T., Uesugi, K., Ahmed, K.M., Biswas, D.K., 2008. Arsenic release from biotite into a Holocene groundwater aquifer in Bangladesh. *Applied Geochemistry* 23, 2236–2248.
- Sengupta, S., Mukherjee, P.K., Pal, T., and Shone, S., 2004. Nature and origin of arsenic carriers in shallow aquifer sediments of Bengal delta, India. *Environmental Geology* 45, 1071–1081.
- Shamsudduha, M., Uddin, A., Saunders, J.A., Lee, M.-K., 2008. Quaternary stratigraphy, sediment characteristics and geochemistry of arsenic-contaminated alluvial aquifers in the Ganges-Brahmaputra floodplain in central Bangladesh: *Journal of Contaminant Hydrology* 99, 112–136.
- Turner, J., 2006. Groundwater geochemistry, geology, and microbiology of arsenic-contaminated Holocene alluvial aquifers, Manikganj, Bangladesh, (MS thesis), Auburn University, Alabama, 76 pp.
- UNDP, 1982. Groundwater survey: the hydrogeological conditions of Bangladesh. UNDP Technical Report, DP/UN/BGD-74-009/1.
- Uddin, A., and Lundberg, N., 1998. Cenozoic history of the Himalayan–Bengal system: sand composition in the Bengal Basin, Bangladesh. *Geological Society of America Bulletin* 110, 497–511.

Uddin, A., Shamsudduha, M., Saunders, J.A., Lee, M-K., Ahmed, K.M., Chowdhury, M.T., 2011, Mineralogical profiling of arsenic-enriched alluvial sediments in the Ganges-Brahmaputra floodplain in central Bangladesh. *Applied Geochemistry* 26, 470-483.

Zhang, C.L., Horita, J., Cole, D.R., Zhou, J., Lovley, D.R., Phelps, T.J., 2001. Temperature-dependent oxygen and carbon isotope fractionations of biogenic siderite. *Geochimica et Cosmochimica Acta* 65, 2257–2271.

Zheng, Y., Stute, M., van Geen, A., Gavrieli, I., Dhar, R., Simpson, J., Ahmed, K.M., 2004. Redox control of arsenic mobilization in Bangladesh groundwater. *Applied Geochemistry* 19, 201–214.

Zobrist, J., Dowdell, P.R., Davis, J.A., Oremland, R.S., 2000. Mobilization of arsenite by dissimilatory reduction of adsorbed arsenate. *Environmental Sciences and Technology* 31, 4646-4753.

CONCLUSIONS

The aim of this study has been to examine in detail the hydrogeology of a low-lying coastal aquifers formed of layered unconsolidated sediments. Groundwater is the main source for drinking water in Bangladesh, but trace element contamination from natural sources and groundwater salinization from saltwater intrusion have severely deteriorated the groundwater quality in the southern region. Sea level rise complicated this problem by causing vertical infiltration of brackish water from tidal channels and lateral intrusion of seawater from the ocean into the aquifers. It is also likely that sea level rise will cause an increase in pH and salinity of the groundwater, which may result in the mobilization of more trace elements into the groundwater as a result of ionic competition for sorbing sites or desorption of elements in anion form.

Hydrochemical facies of major ions were analyzed using piper diagrams which showed groundwater type is highly variable, with Na-Ca-Mg-HCO₃ as the dominant water type and Na-Cl type in some areas affected by saltwater intrusion. Wells from both shallow and deep layers show that there is a trend toward Na-Cl type water in wells close to the Bay of Bengal and the tidal channels.

Lateral saltwater intrusion models constructed for the sea level rise scenarios of 0.5 meter, 1 meters, and 1.5 meters for transect NS show a saltwater wedge consistent with the shape predicted by the Ghyben-Herzberg relation. Sensitivity analysis for these models shows

that saltwater intrusion can be limited by an increase in the freshwater hydraulic gradients in the southern direction or by the presence of a confining clay layer in the coastal region.

Vertical saltwater infiltration models show larger tidal channels affect a larger area and can reach the deeper aquifers. Sensitivity analysis for these models shows that the presence of a confining clay layer restricts intrusion of saline water into the deeper layers, but can cause a larger zone of diffusion in both shallow and deeper strata. One sensitivity analysis model combining lateral and vertical infiltration shows that saline water is restricted to the areas adjacent to tidal channels and the Bay of Bengal, while a mixing zone is extensive throughout the area in both shallow and deep layers.

Trace element concentrations were compared to Cl^- concentrations for all wells and showed none to moderate positive correlation. While the pH and salinity effect from saltwater intrusion can cause the mobilization of trace elements in this area, the pH of wells included in this study have a mean of 7.75. It is likely that other mechanisms (e.g., bacterial reduction of iron oxides, chemical weathering, and bacterial sulfate reduction) are responsible for trace elements release, but the pH effect could become problematic in the future should seawater intrusion continue to drive up the pH in the aquifers.

Continuation of monitoring the wells in the BWDB network is necessary for fully understanding how groundwater geochemical dynamics respond to the effects of climate change and sea level rise. Future data from additional wells should be useful in generating a complete picture of spatial and temporal variations in groundwater chemistry in coastal subsurface geology in the Ganges delta.

Chapter 1

Appendix 1. Groundwater chemistry in study area.

| Bangladesh Water Development Board(BWDB) Data , 2014 | | | | | | | | | | | | | | |
|--|-------------------------|-------------------------|-----|------------------------|-----------------------|---|------------------------|---|--|--------|------|-----|------|-----------|
| Sample ID | Ca ²⁺ (mg/l) | Mg ²⁺ (mg/l) | PH | Na ⁺ (mg/l) | K ⁺ (mg/l) | HCO ₃ ⁻ (mg/l) | Cl ⁻ (mg/l) | SO ₄ ²⁻ (mg/l) | NO ₃ ⁻ (mg/l) | d13C | d18O | d2H | DOC | Depth (m) |
| BNBNPZ_1 | 633.0 | 603.7 | 7.2 | 3449.7 | 110.0 | 282.1 | 8614.8 | 111.8 | 12.2 | | | | | 21 |
| BNBNPZ_2 | 122.2 | 39.5 | 7.3 | 128.2 | 8.1 | 496.5 | 183.1 | 22.4 | 0.1 | | | | | 86 |
| BNBNPZ_3 | 143.4 | 87.5 | 7.4 | 335.0 | 17.8 | 289.8 | 935.9 | 30.7 | 1.4 | | | | | 182 |
| BNBNPZ_4 | 40.4 | 18.3 | 9.1 | 207.9 | 6.2 | 587.1 | 43.7 | 0.1 | 48.9 | | | | | 280 |
| BNPGPZ_1 | 137.3 | 774.4 | 7.2 | 8531.5 | 320.6 | 200.1 | 17132.9 | 394.5 | 46.3 | | | | | 61 |
| BNPGPZ_2 | 132.7 | 667.0 | 7.3 | 7487.5 | 283.8 | 189.8 | 14971.0 | 312.1 | 40.8 | | | | | 121 |
| BNPGPZ_3 | 111.5 | 68.4 | 7.7 | 2204.9 | 34.0 | 181.3 | 4167.3 | 34.6 | 5.3 | | | | | 298 |
| BNAMPZ_1 | 137.9 | 217.7 | 7.6 | 2437.8 | 100.8 | 167.8 | 4773.4 | 41.5 | 19.1 | | | | | 67 |
| BNAMPZ_2 | 90.6 | 53.6 | 8.1 | 284.4 | 15.1 | 396.5 | 503.9 | 0.1 | 1.7 | | | | | 128 |
| BNAMPZ_4 | 13.0 | 7.8 | 8.5 | 210.9 | 3.8 | 603.3 | 18.3 | 0.4 | 0.7 | | | | | 299 |
| PKDMPZ_1 | 274.2 | 184.9 | 6.6 | 1456.5 | 19.0 | 221.1 | 3176.7 | 41.1 | 2.5 | | | | | 34 |
| PKDMPZ_2 | 327.1 | 156.3 | 7.1 | 978.1 | 28.6 | 127.0 | 2733.2 | 30.0 | 15.5 | | | | | 91 |
| PKDMPZ_3 | 29.0 | 15.4 | 7.5 | 161.2 | 5.9 | 396.5 | 94.6 | 10.1 | 1.8 | | | | | 201 |
| PKDMPZ_4 | 27.0 | 11.3 | 9.6 | 127.4 | 2.9 | 473.6 | 24.5 | 0.2 | 0.3 | | | | | 314 |
| PKKLPZ_1 | 114.6 | 513.6 | 7.8 | 5018.9 | 166.5 | 127.9 | 10362.5 | 120.9 | 32.6 | | | | | 24 |
| PKKLPZ_2 | 407.1 | 768.8 | 7.2 | 5243.2 | 179.5 | 97.4 | 11436.2 | 182.6 | 7.4 | | | | | 121 |
| PKKLPZ_3 | 293.8 | 803.2 | 7.4 | 6687.9 | 230.9 | 203.3 | 14516.6 | 189.7 | 11.8 | | | | | 180 |
| PKKLPZ_4 | 67.9 | 27.4 | 7.4 | 433.0 | 12.2 | 686.3 | 423.9 | 0.4 | 3.8 | | | | | 268 |
| JHJHPZ_1 | 123.2 | 67.5 | 7.8 | 504.2 | 20.6 | 693.9 | 807.6 | 1.0 | 9.7 | | | | | 26 |
| JHJHPZ_4 | 34.6 | 13.0 | 8.9 | 173.6 | 3.8 | 558.4 | 78.3 | 0.3 | 0.4 | | | | | 295 |
| PKGCPZ-1 | 145.6 | 47.1 | 8.8 | 263.5 | 12.9 | 525.3 | 528.5 | 24.6 | 2.7 | | | | | 24 |
| PKGCPZ_2 | 283.9 | 353.8 | 7.9 | 3546.7 | 101.9 | 159.3 | 7238.9 | 110.9 | 1.6 | | | | | 91 |
| PKGCPZ_3 | 141.9 | 80.0 | 8.8 | 435.6 | 21.0 | 366.0 | 998.5 | 51.6 | 4.4 | | | | | 180 |
| PKGCPZ_4 | 39.7 | 15.7 | 8.7 | 142.8 | 9.6 | 565.1 | 15.1 | 0.9 | 2.6 | | | | | 298 |
| PRBRPZ_1 | 148.4 | 141.4 | 9.0 | 1762.2 | 30.3 | 235.3 | 3241.1 | 69.0 | 14.3 | | | | | 27 |
| PRBRPZ_2 | 203.7 | 477.4 | 8.0 | 4549.4 | 135.2 | 148.1 | 9004.3 | 156.2 | 6.2 | | | | | 164 |
| PRBRPZ_3 | 267.4 | 105.0 | 8.8 | 1626.3 | 18.9 | 373.6 | 3297.2 | 0.4 | 3.7 | | | | | 253 |
| PRBRPZ_4 | 142.3 | 54.5 | 8.7 | 1417.9 | 15.3 | 411.8 | 2406.3 | 0.3 | 2.3 | | | | | 335 |
| PRBRPZ_5 | 285.5 | 121.8 | 8.8 | 2773.5 | 18.8 | 461.0 | 4591.9 | 45.0 | 5.6 | | | | | 316 |
| BGS and DPHE, 2001 dataset | | | | | | | | | | | | | | |
| S98_00702 | 32.9 | 20.8 | 7.2 | 55.7 | 5.6 | 285.0 | 44.1 | 0.2 | 0.3 | -13.47 | -3.2 | -14 | 6.2 | 183 |
| S98_00704 | 26.9 | 18.7 | 6.9 | 46.1 | 4.1 | 251.0 | 37.1 | 0.2 | 0.3 | -17.48 | -3.2 | -14 | 5.2 | 229 |
| S98_00710 | 25.3 | 17.3 | 6.9 | 40.9 | 4.6 | 266.0 | 6.7 | 0.3 | 0.3 | -15.92 | -2.6 | -14 | 2.8 | 220 |
| S98_00715 | 23.8 | 16.9 | 7.0 | 33.2 | 4.4 | 254.0 | 3.5 | 0.6 | 0.3 | -14.53 | -2.6 | -9 | 1.5 | 375 |
| S98_00720 | 27.4 | 19.4 | 6.7 | 28.1 | 3.7 | 195.0 | 47.3 | 0.2 | 0.3 | -14.19 | -3.1 | -14 | 1.9 | 226 |
| S98_00723 | 66.0 | 47.7 | 6.5 | 84.6 | 6.8 | 205.0 | 295.0 | 0.2 | 0.3 | -12.95 | -3.1 | -16 | 4.7 | 183 |
| S98_00727 | 111.0 | 75.8 | 6.5 | 201.0 | 6.9 | 125.0 | 637.0 | 4.9 | 0.3 | -13.69 | -4 | -23 | 4.2 | 262 |
| S98_00730 | 35.2 | 20.1 | 6.7 | 33.2 | 3.8 | 188.0 | 68.0 | 0.2 | 0.3 | -15.76 | -3.1 | -17 | 3.4 | 244 |
| S98_00734 | 27.9 | 16.9 | 7.1 | 43.8 | 6.0 | 271.0 | 24.7 | 0.2 | 0.3 | -12.77 | -1.8 | -16 | 2.5 | 183 |
| S98_00735 | 38.0 | 24.4 | 7.1 | 55.2 | 8.3 | 261.0 | 74.6 | 0.2 | 0.3 | -12.48 | -2 | -16 | 1.4 | 244 |
| S98_00739 | 80.4 | 51.6 | 6.7 | 81.6 | 7.6 | 188.0 | 324.0 | 0.2 | 0.3 | -16.07 | -3 | -17 | 1 | 259 |
| S98_00744 | 61.2 | 31.0 | 6.6 | 128.0 | 3.8 | 171.0 | 310.0 | 3.0 | 0.3 | -15.41 | -4.2 | -20 | 1.6 | 177 |
| S98_00745 | 66.3 | 50.5 | 6.6 | 83.9 | 7.2 | 149.0 | 310.0 | 1.1 | 0.3 | -17.37 | -3.5 | -18 | 1.5 | 171 |
| S98_00752 | 24.0 | 16.9 | 7.0 | 32.3 | 3.7 | 246.0 | 3.7 | 0.2 | 0.3 | -2.3 | -2.3 | -8 | 1.8 | 318 |
| S98_00753 | 24.6 | 16.4 | 7.0 | 31.7 | 3.5 | 215.0 | 2.7 | 0.2 | 0.3 | -13.22 | -2.1 | -8 | 0.7 | 305 |
| S98_00754 | 59.5 | 43.3 | 6.8 | 64.0 | 6.0 | 190.0 | 238.0 | 0.2 | 0.3 | -12.29 | -2.9 | -16 | 1.2 | 229 |
| S98_00759 | 35.3 | 24.1 | 6.8 | 68.0 | 4.2 | 217.0 | 129.0 | 2.9 | 0.3 | -13.03 | -2.1 | -13 | 0.3 | 244 |
| S98_00762 | 36.7 | 22.7 | 6.9 | 70.5 | 3.7 | 268.0 | 74.0 | 0.5 | 0.3 | -9.12 | -1.9 | -12 | 3.1 | 195 |
| S99_00395 | 34.1 | 46.1 | 7.2 | 23.9 | 13.0 | 348.0 | 20.2 | 3.2 | 1.8 | -19.2 | -0.7 | -11 | 0.8 | 12 |
| S99_00396 | 20.2 | 12.9 | 6.8 | 20.4 | 2.2 | 171.8 | 1.7 | 0.2 | 0.5 | -11.2 | -2.9 | -14 | 2.3 | 262 |
| S99_00397 | 33.6 | 42.9 | 7.4 | 29.5 | 8.2 | 366.0 | 17.5 | 0.2 | 3.3 | -13.1 | -1.7 | -19 | 2.2 | 15 |
| S99_00398 | 34.7 | 62.0 | 7.2 | 104.0 | 14.3 | 414.0 | 140.0 | 0.7 | 4.4 | -19.2 | -1.9 | -17 | 4.4 | 11 |
| S99_00399 | 34.9 | 79.9 | 7.4 | 333.0 | 19.7 | 644.0 | 426.0 | 0.6 | 6.6 | -23.6 | -3 | -21 | 5.3 | 11 |
| S99_00400 | 22.0 | 12.0 | 6.8 | 23.5 | 2.6 | 174.4 | 1.8 | 0.2 | 0.5 | -13 | -2.6 | -14 | 0.2 | 296 |
| S99_00401 | 34.0 | 40.3 | 6.9 | 24.9 | 11.5 | 342.0 | 16.6 | 0.3 | 0.5 | -17.9 | -1.7 | -15 | 1.6 | 9 |
| S99_00402 | 22.0 | 31.4 | 6.9 | 23.3 | 6.3 | 316.0 | 7.7 | 0.3 | 0.5 | -16.1 | -2.1 | -21 | 1.7 | 14 |
| S99_00404 | 153.0 | 95.3 | 6.7 | 432.0 | 9.4 | 181.6 | 1050.0 | 68.2 | 0.5 | -12.9 | -3 | -17 | 0.9 | 253 |
| S99_00412 | 57.2 | 44.9 | 6.8 | 84.6 | 41.3 | 446.0 | 99.5 | 34.4 | 0.5 | -15.3 | -3.4 | -29 | 1.4 | 30 |
| S99_00416 | 25.0 | 16.1 | 6.9 | 49.0 | 4.9 | 248.0 | 17.6 | 0.2 | 0.5 | -15.6 | -3.3 | -21 | <0.1 | 224 |